Mitigation of Explosive Blast Effects on Vehicle Floorboard

Robert Benedetti
Advised by Dr. William Fourney

Department of Mechanical Engineering
University of Maryland
College Park, MD 20742
July 2008

Abstract

Title of Thesis:Mitigation of Explosive Blast Effects on Vehicle Floorboard

Thesis Directed By: Professor William Fourney

Department of Mechanical Engineering

This thesis investigates methods for mitigating the blast effects on the floorboard of passenger vehicles due to the detonation of explosives buried in water saturated sand underneath vehicles. The effects on floorboard acceleration of adding a vehicle hull, several types of floorboard bracing, the use of foam to fill the gap between the floorboard and hull, and the use of foam to isolate the floorboard from the hull. In addition, several tests have been conducted to examine how the distance of the floorboard from the ground affects the acceleration of the floorboard after the detonation. Testing showed that the addition of a hull to a vehicle, the hulls geometry, bracing of the floorboard, and increasing ground clearance all are able to help reduce floorboard accelerations. However, floorboard bracing had the potential to make accelerations much higher it is hit by the hull during testing. Foam filling between the hull and floorboard as well as a foam frame to isolate the floorboard from the hull did not have positive results. The primary method of investigation is differentiating a velocity profile found with the use of bar magnet velocity gages on the small scale model floorboard. Several other possible methods of investigation are discussed.

Mitigation of Explosive Blast Effects on Vehicle Floorboard

by

Robert Benedetti

Thesis submitted to the Faculty of the Graduate School of the
University of Maryland, College Park in partial fulfillment
of the requirements for the degree of
Master of Science
2008

Advisory Committee:

Professor William Fourney, Chair
Professor Henry Haslach, Jr.
Professor Teng Li

Acknowledgements

First, I would like to thank Dr. Fourney for allowing me the opportunity to study under his guidance. I could not have asked for an advisor with more trust and patience as I learned the research process.

Funding for this project was supplied by the Office of Naval Research, Mr. Lee Mastroianni and the US Army, TARDEC, Mr. Richard Goetze and Mr. David Fox. Thank you all for providing the resources for this project.

I would like to thank Dr. Haslach and Dr. Li for taking the time to read my thesis and sit on my committee.

I also want to thank Uli Leiste and Les Taylor for their continual guidance in both research matters and life outside the lab.

I would like to thank Dr. Goodings for her input during research meetings.

I would like the thank Captain Dennis Doyle, USMC and my fellow graduate students Sasha Tsarev, Damien Bretall, Chi Wang, Kevin Genson, and Silas Nesson for the tips they provided from their own experiences which helped make graduate school go more smooth for me.

I am extremely grateful to Dana Colegrove, Joshcha Neumann, Thomas Welker, Dominik Weinlein, Cory Peterson, Scott Yamada, Dimitri Jung, and Suat Drekovic. The testing required for this thesis would not have been possible without the efforts of these undergraduate assistants and German exchange students working in the Dynamic Effects Lab. My work was made easier and more enjoyable from all of your company.

I would like to thank Howie Grossenbacher, Russ Wood, and Edd Cole for allowing me to use their machine shops for making test equipment and for their patience in teaching me how to properly use the resources in their shops.

I would like to thank the Mechanical Engineering staff at the Univeristy of Maryland for all the help they have given me over the past year, especially Amarildo Damata and Fitz Walker.

I would like to thank Mr. Mike Laukaitis, Dr. Bruce Baloian, Matthew Vaughan, and Fred Sandusky for their encouragement throughout my entire educational experience.

Finally, I would like to thank my parents for their encouragement and for making education a reality for me.

Dedication

This thesis is dedicated to the brave men and women who take up arms so that their fellow Americans can continue this lifestyle we are free to enjoy. Especially, those United States Marines who have been processed through OSO, College Park.

Table of Contents

Table of Figures

Table of Tables

Ch 1: Introduction

1.1 Overview

This thesis describes research conducted at the Dynamic Effects Laboratory at the Clark School of Engineering at the University of Maryland, College Park. The purpose of this research is to use small scale testing to investigate several methods to mitigate the acceleration experienced by the floorboard of a hulled vehicle after the detonation of an explosive charge buried in water saturated sand beneath the vehicle. This subject is of interest to the designers of armored vehicles, such as the Mine Resistant Ambush Protected (MRAP) vehicles currently being designed for service in the fleet.

The mitigation effects investigated in this thesis include the effect of the hull itself, hull geometry, several bracing systems to support the floorboard, the use of foam to fill the gap between the floorboard and hull, and the use of a compliant foam frame to isolate the floorboard from the hull. The scope of this thesis is limited such that both the floorboard and hull of the vehicle are deformed without fracture.

As of 5 April 2008, 2198 of the 3559 hostile deaths and 21,306 of the 31,590 troops wounded in action by hostile action during Operations Enduring Freedom and Iraqi Freedom were from explosive devices, such as IED's and Mines [1.1]. With a large amount of troop casualties and injuries resulting from explosive attacks, it is of great interest for the military to have vehicles designed to minimize the risk from these attacks. Small scale testing provides a quick, economical, and relatively safe method to run many tests for gathering the necessary data to design these vehicles.

1.2 Scaling

There are several models to scale explosive effects. These models include the cube-root scaling models based on mass and energy which are derived from dimensional analysis and ignore gravitational effects, models based on dimensional analysis which include gravity, and empirically justified modifications of the above methods [1.2-4]. The scaling used throughout this thesis and in the Dynamic Effects lab in general, is the cube-root scaling method based on the mass of the charge. Previous testing in the Dynamic Effects Laboratory has shown that the cube-root scaling method provides sufficient accuracy in predicting full scale effects from small scale testing [1.5-6, 1.9].

The scaling model used is defined by the following:

$$SF = \left(\frac{mass_{Full-Scale}}{mass_{Small-Scale}} \right)^{1/3} = \frac{length_{full-scale}}{lenth_{small-scale}} = \frac{time_{full-scale}}{time_{small-scale}} \qquad \text{eq. 1.1}$$

Where SF is the scaling factor, which is 13.14 throughout this thesis, was chosen because it was used for related testing by a previous graduate student in the Dynamic Effects Laboratory [1.8]. Originally, 13.14 was chosen as a scaling factor because it corresponded to stock aluminum sheet which was available at the local supply store and made a reasonable scale for modeling the vehicles being investegated.

The small scale thicknesses of the floorboard and hull are 0.020 in and 0.090 in, respectively. These correspond to 0.26 and 1.2 in full scale thicknesses, respectively. The small scale distance from the surface of the sand to the top of the charge and to the bottom

of the model floorboard are 0.30 in and 3.19 in, respectively. This corresponds to 3.9 in and 42 in, respectively, for a 5 lb charge. Several tests have stand off distance (SoD) values of 1.75 in and 2.55 in, which correspond to 23.0 in and 33.5 in, respectively. The SoD is the distance from the bottom of the floorboard to the top of the sand's surface. While the larger floorboard heights are larger than expected in actual vehicles, it allowed for the high ground clearance needed to investigate extreme geometries of the hull. The small scale mine contains 1.0 g of explosive, which corresponds to 2269 g (5 lb) of explosive in full scale.

1.3 Explosive Loading

Because this thesis considers the effects of explosives buried in sand underneath vehicles, it is valuable to first understand previous work on target loading in similar situations. When the explosive is detonated, there are three types of loading that a target can undergo: stress wave, ejected soil, and air blast [1.9]. The stress wave loading becomes insignificant because of the low impedance of air compared to the impedance of saturated sand [1.5].

When the buried charge is detonated, soil and hot gas are ejected from the sand bed creating a crater. The soil is ejected at supersonic speeds and accounts for a significant portion of the impulse on a plate above the sand bed. The ejected sand applies a large pressure to the target over a short interval of time. The ejected sand, the resulting crater, and the target can form a sort of enclosure around the high pressure explosive product which continues to load the target in the form of the air blast mentioned above. This air blast acts over a longer period of time and accounts for the remaining impulse imparted to the target [1.9].

Several mitigation methods are investigated in this thesis to reduce the acceleration of the vehicle's floorboard. The effects of such mitigation methods as adding a hull to a vehicle, changing the vehicle's hull geometry, and supporting the floorboard with bracing are investigated. Other methods looked at include attempts to use foam filling between the hull and floorboard in order to absorb as much of the loading as possible and the use of foam to isolate the floorboard from the shock experienced in the vehicle's hull. In addition to this, the effects of the height of the vehicle off the ground are briefly examined.

Ch 2: Research Equipment

2.1 Explosive Charge

The charges used for all tests are made by inserting an RP-87 Exploding Bridge Wire (EBW) detonator into Deta Sheet. Deta Sheet is a plasticized sheet explosive consisting of 63% pentaerythritol tetranitrate (PETN), a very stable high explosive, by mass. Each test uses 1.48 g of Deta Sheet, which contains 0.93 g of explosive. It is pressed into a cylindrical Delrin plastic charge casing with an inner diameter of 14.8 mm, height of 6.5 mm, and wall thickness of 0.9 mm.

The RP-87 is manufactured by Teledyne RISI (P/N 167-9643). It contains 26 mg of PETN and 43 mg RDX, a commonly used military explosive referred to as Cyclonite. It is inserted about 1/16 in into the Deta Sheet and covered with epoxy to hold it in place. The dimensions of the RP-87 and the explosive train can be found in Figures 2.1 and 2.2, respectively; the firing parameters can be found in Table 2.1, which were obtained from the manufacturer's website [2.1]. The fully assembled charge can be seen in Figure 2.3.

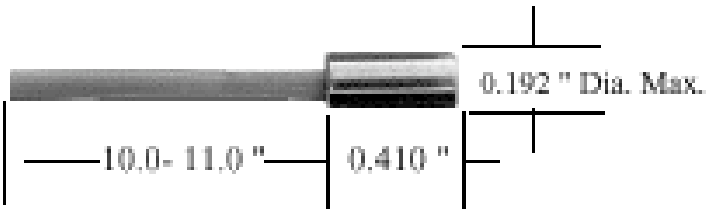

Figure 2. 1: RP-87 Dimensions

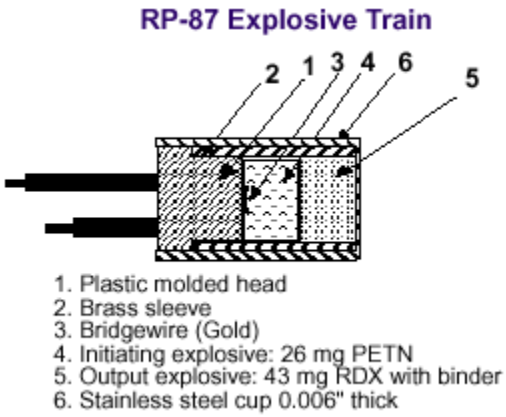

Figure 2. 2: RP-87 Explosive Train

RP-87 Firing Parameters	
Threshold Burst Current:	210 amps
Threshold Voltage:	Approx. 500 volts
Threshold Voltage Std. Deviation:	75 volts maximum
Function Time:	1.95 µsec. typical
Function Time Simultaneity Standard Deviation:	0.125 µsec Max.

Table 2.1 RP-87 Firing Parameters

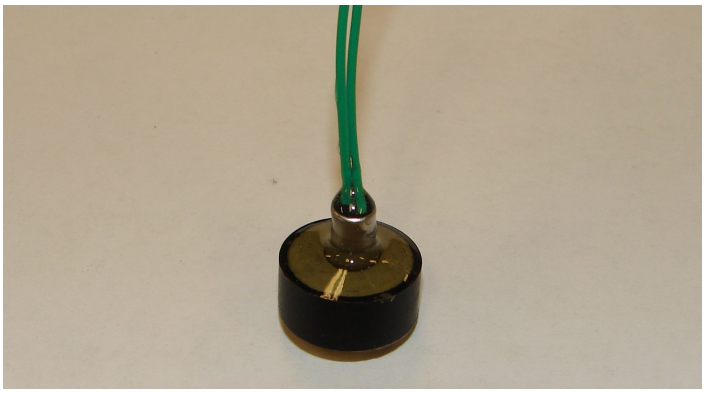

Figure 2.3: Explosive Charge

2.2 FS-17 EBW Firing System

The firing system used to detonate the charge is the FS-17 EBW firing system, manufactured by Reynolds Industries Inc. The system consists of a control unit (P/N 167-8917) and a firing module (P/N 167-8371). The unit, which can be seen in Figure 2.4, is battery operated and provides a 4000 Volt electrical spike which induces detonation of the charge [2.2]. The trigger mechanism, which can be seen on the far right in Figure 2.4, allows the camera and oscilloscope used for collecting data to be triggered in sync with the detonation. Using the firing system ensures that the charge will not be prematurely detonated, which could cause injury to workers in the lab.

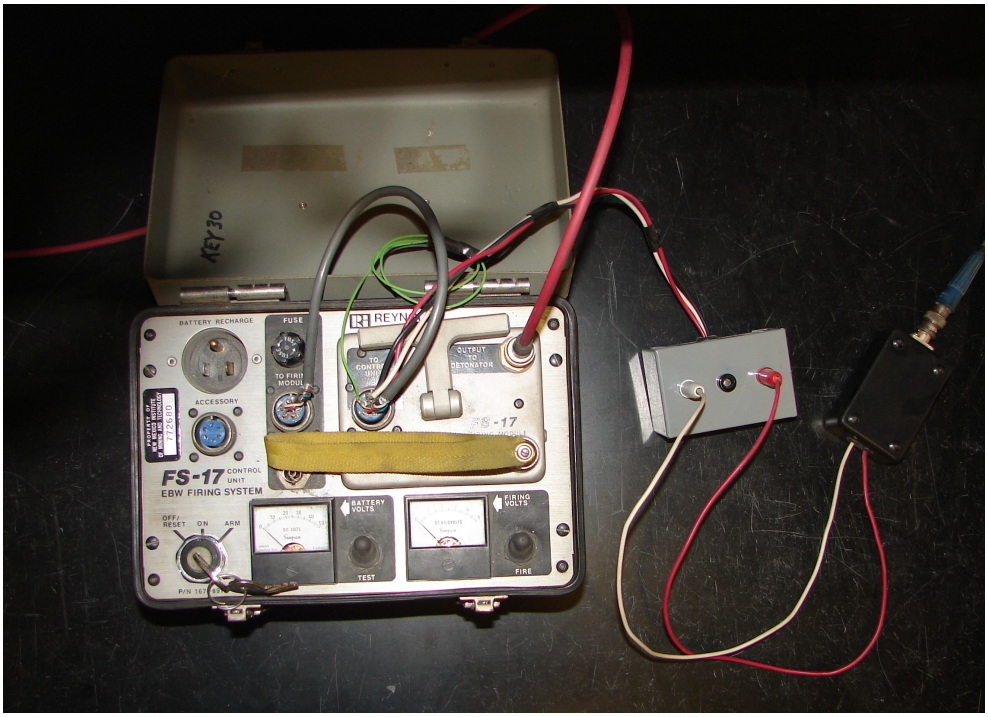

Figure 2.4: Firing System

2.3 Dummy Charge

In order to make sure the firing system is working correctly and both the oscilloscope and camera are being triggered at the correct time, a dummy charge is used. This is constructed by running two wires through a graphite block which is inserted into an aluminum tube. When the firing system is working correctly, it generates a 4000 volt electric pulse which causes an arc across the approximately 1/8 in air gap between the two wires. If the triggering mechanism is working correctly, the camera and oscilloscope will be triggered in time to read the voltage spike on the oscilloscope and see the arc in the video. The dummy charge can be seen in Fi gure 2.5.

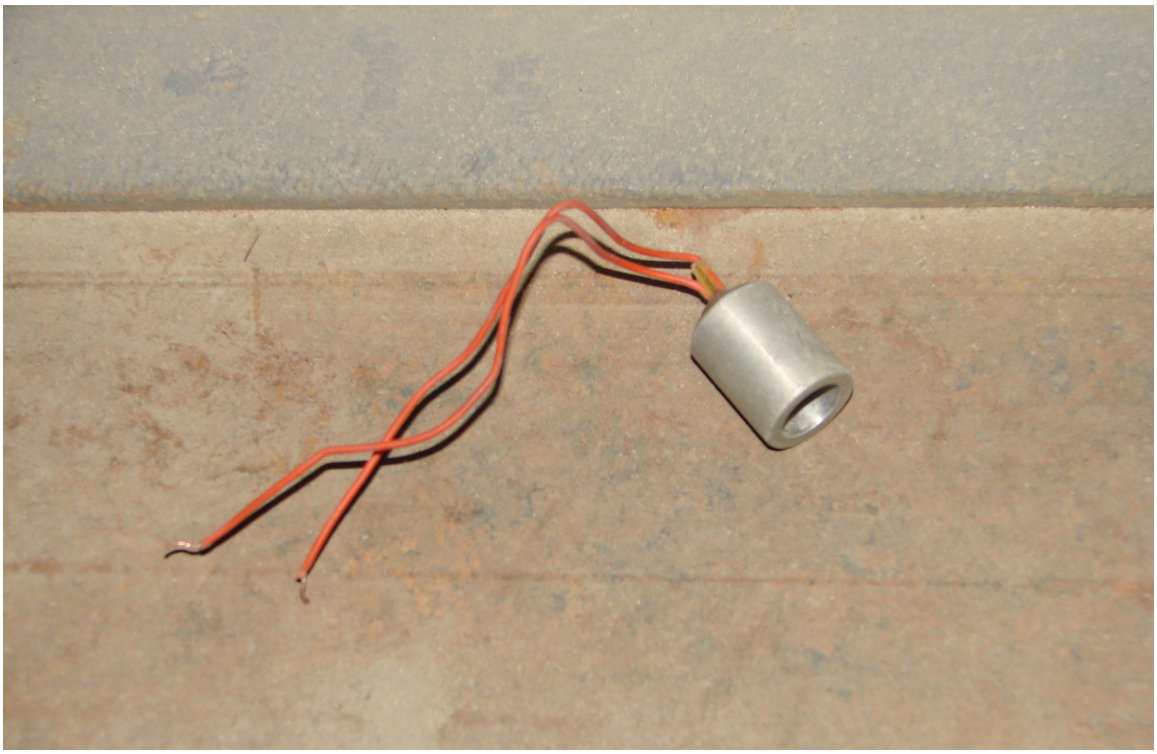

Figure 2.5: Dummy Charge

2.4 Sand Pit

The explosives tests are conducted in the sand pit, located in the subbasement of the laboratory. The pit, which can be seen in Figure 2.6, is a steel box 5 foot square by two feet deep. It has a water saturation control system that fills the box with water from the bottom, as can be seen in Figure 2.6. The system consists of a column which fills up with water that is then piped to the bottom of the box. This provides even water saturation of the sand. The bottom of the pit contains a mesh underneath a layer of coarse gravel which prevents sand from contaminating the water saturation system. On top of the gravel is the Home Depot's HD-2 sand.

Figure 2.6: Sand Pit

2.5 Vehicle Model

Each test models the hull and floorboard of a vehicle. As is typical of actual vehicles, aluminum is used to construct the model. The floorboard is made of 0.020 in thick 6061-T6 Al sheet metal. The hull is made of 0.090 in thick 6061-T6 Al sheet metal. These correspond to a 0.26 in thick floorboard and a 1.18 in thick hull in full scale. The two components are separated by an aluminum frame. The frame is constructed from 1 in by ½ in aluminum bar. It is welded into a rectangular frame 14 in x 16 in the outer dimensions, which can be seen in Figure 2.7. On top of the floorboard is a second frame of the same dimensions as the first frame. The floorboard, hull, and frames are fastened to one another by eighteen 3/8 in stainless steel bolts, as shown in Figure 2.8.

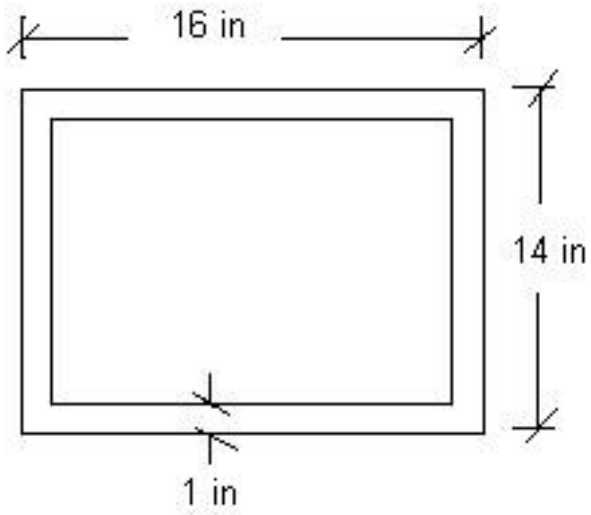

Figure 2.7: Frame Geometry

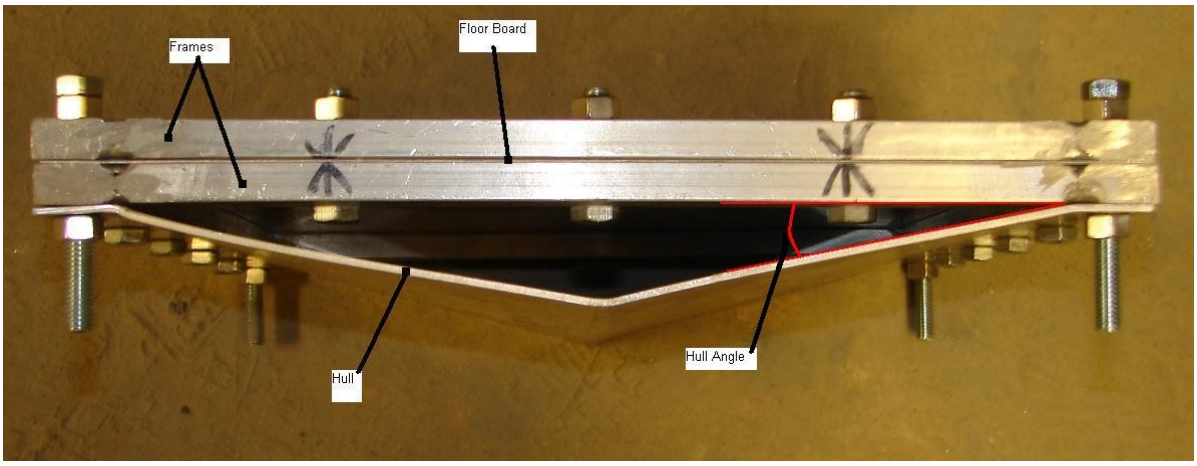

Figure 2.8: Vehicle Model Assembly

The floorboard is always made of a flat sheet. The top of the floorboard is painted white in order to prevent glare from overexposing the video footage of experiments. The hull is bent using a hand sheet metal break. Wedges of the correct angles are used to ensure the precision of the bend and repeatability of the hull geometry. The frames are used as templates when drilling holes through the floorboard and hull to guarantee that everything fits together properly.

Several hull geometries are tested in this paper. The geometry is specified by the angle between the bottom frame and the portion of the hull going from the frame to the bottom bend of the hull, as seen in Figure 2.8. This angle is referred to as the hull angle throughout this thesis.

Several additional mitigation methods are used for some of the tests. For tests with floorboard bracing, the braces are made from the same aluminum stock—6061-T6—as the floorboard is made. For any tests requiring foam, the foam was always taken from the same sheet. A quasi-static compressive stress-strain test for the foam was conducted and

the results can be seen in Figure 2.9. The curve was obtained using the Universal Testing Machine at the University of Maryland. The foam was chosen out of several varieties tested because it showed a significant amount of strain for low pressure before it began to require large pressure to compress further. The foam was used in an attempt to absorb the blast effects from the explosive.

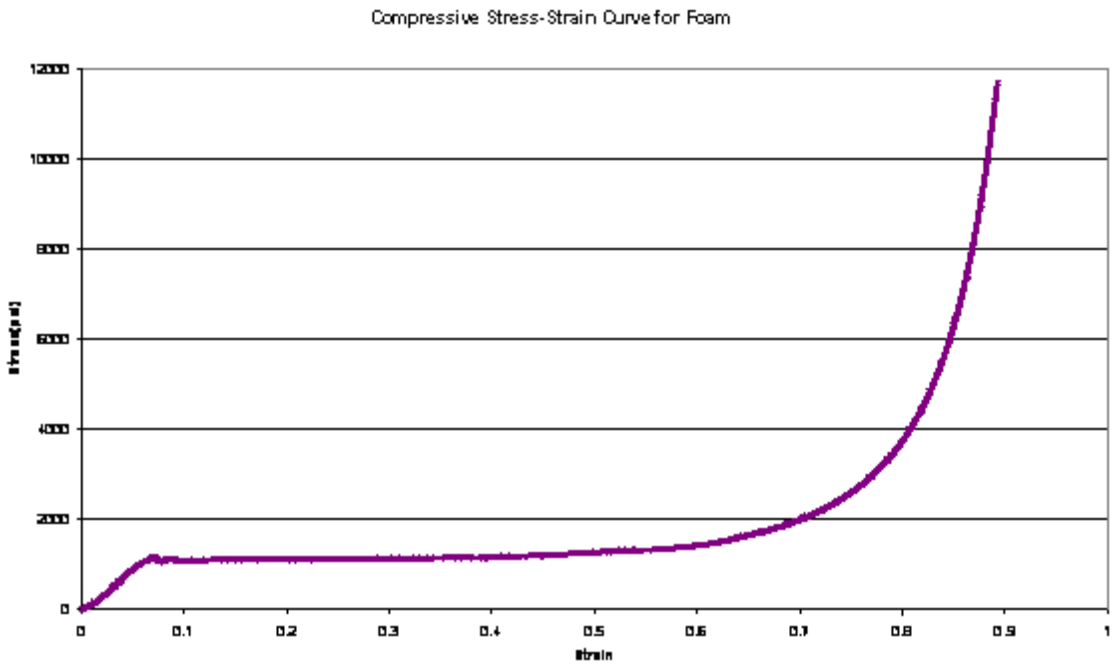

Figure 2. 9: Quasi-static compressive stress-strain curve for foam used in testing

2.6 Velocity Gages

A velocity gage was developed so that the velocity vs. time curves could be differentiated to determine the acceleration of the floorboard during experiments. Similar gages have been used in the past by other researchers [2.3]. The gage works by Faraday's Law of Induction. It is made up of a round Alnico bar magnet and a coil which breaks the lines of flux from the magnet. Alnico magnets work well because the magnets are very polarized, which allows for a linear relationship between induced voltage and velocity [2.3]. The magnet is purchased from McMaster Carr (P/N 5852k11) and is 1/8 in diameter by 4 in long. The coil is 4 in long and is made of thin copper wire wound within a lathe turned channel on a polycarbonate tube. This tubing, which is bought from McMaster Carr (P/N 8585K53) has a 5/8 in outer diameter and a 3/8 in inner diameter. The coil can be seen in Figure 2.10. The tubing is approximately ½ in longer than the coil on either end of it. Epoxy is used to coat the coil, to help prevent deformation of the coil other than that of the tubing. However, camera resolution is not high enough to confirm this assumption.

During an experiment, the magnet is suspended from above the coil and allowed to penetrate the coil from 1 in to 1.5 in, depending on the specific gage's range of linearity (which will be discussed in the following chapter). Epoxy is used to adhere the coil to the floorboard during the experiments. Figure 2.11 shows the assembled gage. As the floorboard moves, the coil is displaced over the magnet and the gage records the velocity of this displacement.

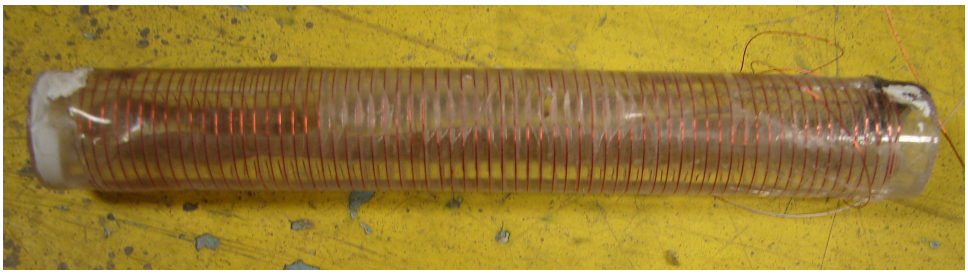

Figure 2.10: Velocity Coil

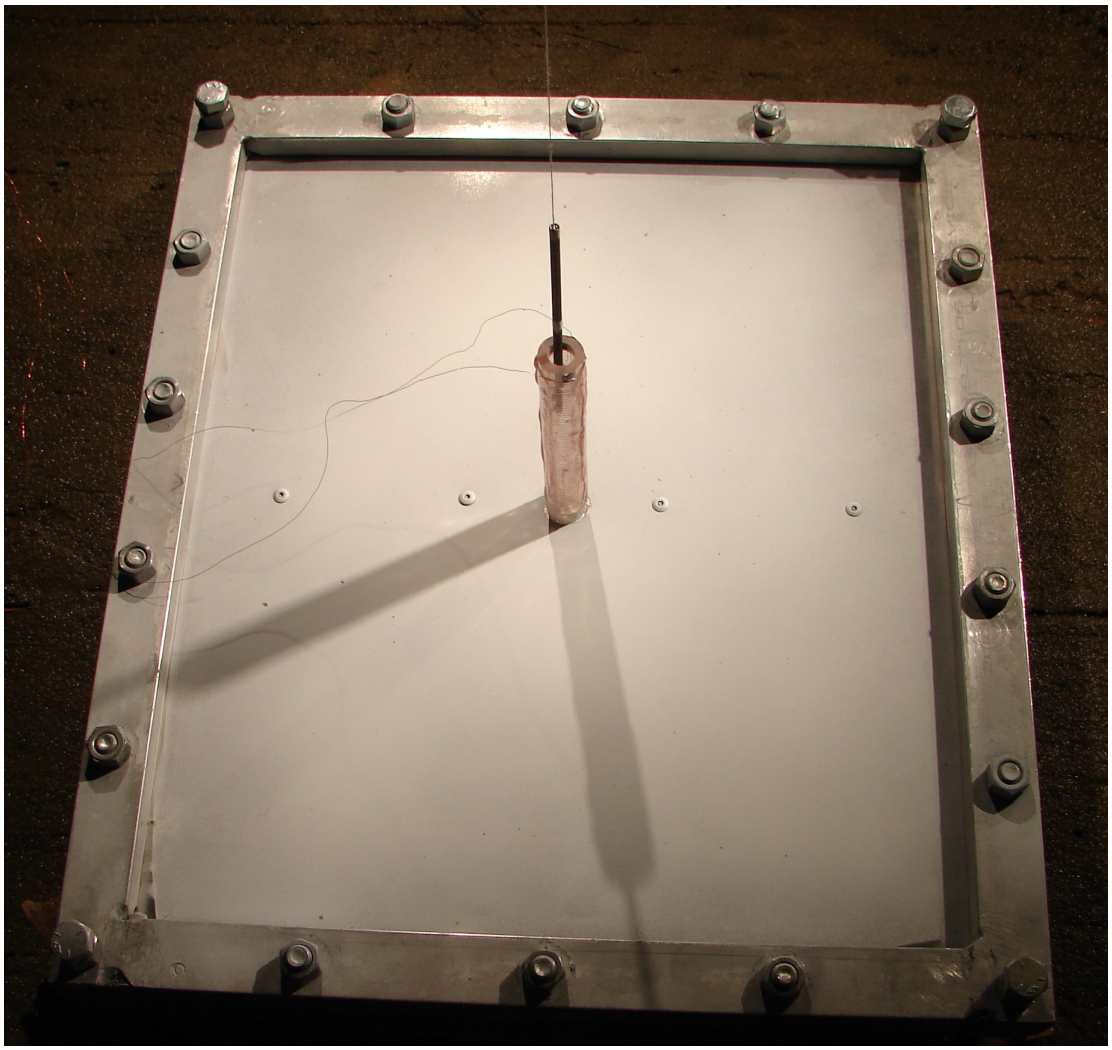

Figure 2.11: Velocity gage in preparation of experiment

2.7 Lecroy 9314AM Oscilloscope

Data from the velocity gage is collected via the Lecroy 9314AM oscilloscope. This scope has the ability to record at a maximum sampling rate of 400 MHz simultaneously on four channels, which provides the ability to look at data at several different resolutions. The oscilloscope can be connected to the trigger mechanism on the firing system, which assures that the data from experiments will be properly collected. It also simplifies the process of comparing data because it eliminates the human factor by automatically syncing velocity profiles according to charge detonation time. The oscilloscope can be seen in Figure 2.12.

Figure 2.12: Lecroy 9314AM

2.8 Phantom v7.2 High Speed Camera

The Phantom v7.2 high speed camera is used in order to calibrate the velocity gages and provide visual evidence of what is happening during explosive experiments. The camera has a 800 x 600 pixel monochrome sensor. Depending on the resolution set for the recording, the camera can record at a maximum speed of 190,476 pictures per second (pps) with exposure times as small as 1 t s. Typical settings during the explosive experiments in this paper are 48 x 256 pixel resolution recording at 81,632 pps with 5 s s exposure time. Full manufacturer specifications of the camera can be found in Appendix B. The camera was used with a Nikon Nikkor f/1.2 50 mm lens, both of which can be seen in Figure 2.13.

Figure 2.13: Phantom v7.2 and Nikon Nikkor f/1.2

2.9 Lighting

In order to provide the intense lighting required to use the high speed camera, several 250W North Star halogen lamps with goosenecks are clamped to the sand pit. The lamp can be seen in Figure 2.14 [2.4].

Figure 2.14: North Star Lamp

Ch 3: Test Procedures

3.1 Test Overview

A schematic showing the test setup can be seen in Figure 3.1. The velocity gage is attached to the middle of the model's floorboard, which is directly above the buried charge. The Lecroy 9314AM oscilloscope is used to collect the gage data. The lead wires from the gage to the scope must be placed so that they have slack and are not tangled, which prevents them from breaking during the test. The camera is used to verify the gage data. The firing system is used to detonate the charge and trigger the camera and oscilloscope. This allows the data to be collected during the desired time period and facilitates the syncing of the camera and gage data.

The stand off distance (SoD) is defined as the distance from the bottom of the floorboard to the top of the saturated sand. Unless specified, the SoD for every test in this thesis is 3.19 in. The depth of burial (DoB) is defined as the distance from the top of the sand to the top of the explosive charge. For all tests in this thesis, the DoB is 0.30 in.

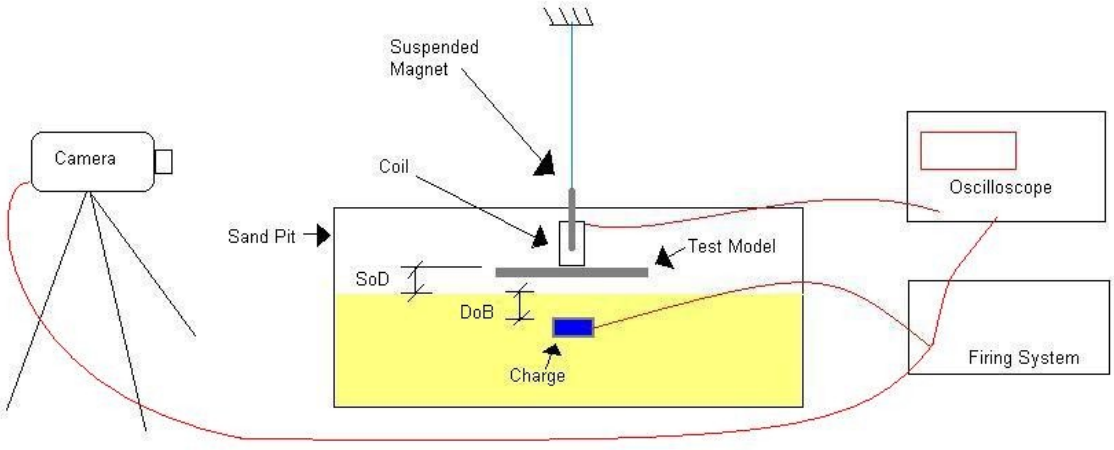

Figure 3.1: Schematic of test setup (not to scale)

3.2 Velocity Gage Calibration

The velocity gage works on Faraday's Law of Induction. The gage is constructed by placing an electrical conducting coil on the center of the floorboard, where the highest acceleration is expected. A magnet is then suspended in the middle of the coil. The construction can be seen in Figure 3.2. As the target moves, the coil passes over the magnet, causing a change in the magnetic flux through the coil. This induces a voltage which is recorded by an oscilloscope. The high-speed camera is used to visually confirm what is recorded by the velocity gage.

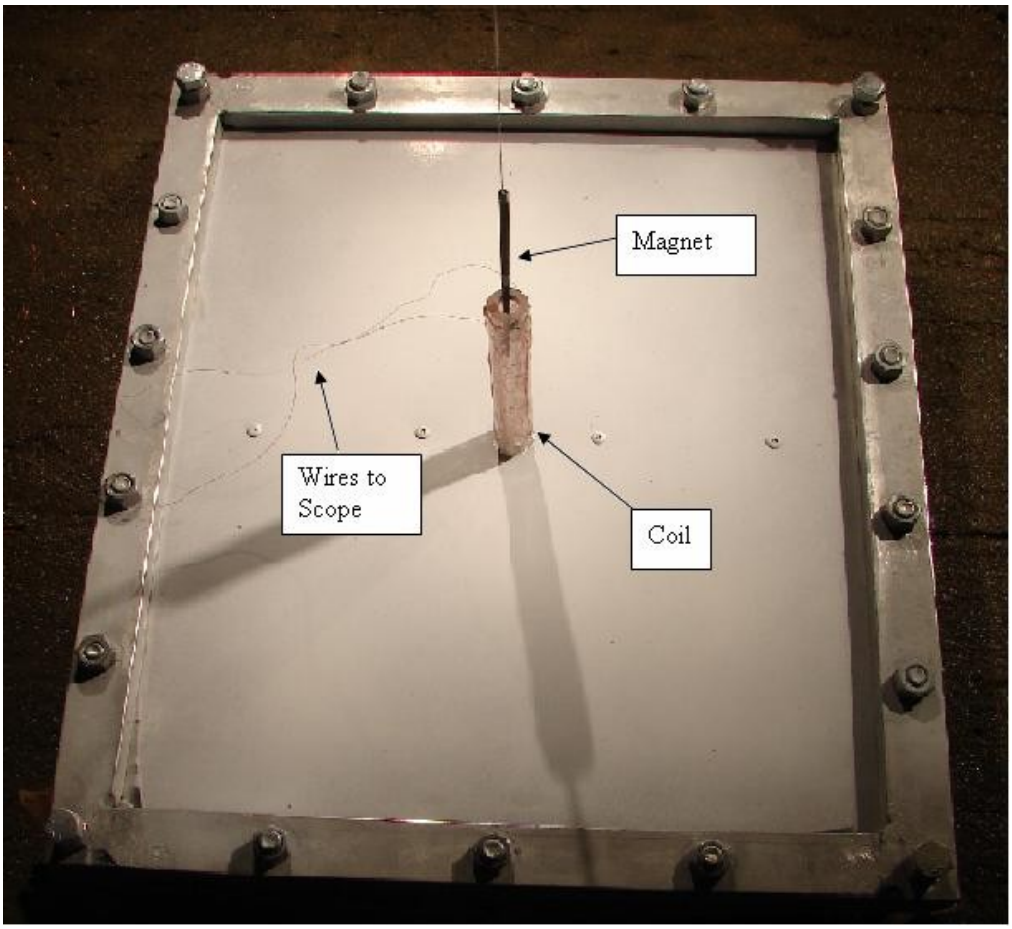

Figure 3.2: Top view of velocity gage on test model

Because of the destructive nature of the experiments, testing requires multiple velocity gages to be used. The magnets are often destroyed by being broken during an impact. The coils lead wires break such that they can not be repaired or the coil itself can be broken. If the lead wire breaks, it can be repaired in most cases.

Each time that a new velocity gage needs to be used, drop tests are conducted to calibrate it. Two assumptions are needed for this calibration. The first is that the coil responds to the motion of a magnet through it by inducing a voltage which is proportional to the time rate of change in magnetic flux passing through the interior of the coil, according to Faraday's Law of Induction.

The second assumption is that there exists some linear region where velocity of the magnet relative to the coil is proportional to the induced voltage mentioned above. This constant of proportionality, which we will refer to from here on out as the *calibration factor*, needs to be determined for calibrating the velocity gage. The linear region where the calibration factor can be used to determine velocity occurs when all lines of magnetic flux which break through the side of the coil (i.e.—sweep from inside the coil through the side of it) have entered the top of the coil, but none have exited the bottom. According to our first assumption, each line of magnetic flux induces some voltage multiplied by the number of loops it passes through. In the linear region, the sums of these effects add to give the calibration factor, C. Therefore, the velocity can be deduced from the voltage from the following equation:

$$v = CV \qquad \text{eq. 3.1}$$

where v is velocity, C is the calibration factor, and V is the induced voltage.

The easiest way to determine this calibration factor is to conduct drop tests for each gage before it is used in an experiment. The coil is wound onto a long polycarbonate tube which will serve as the drop tube before the coil is cut from it. The equation above can be integrated over time to reveal that:

$$C = \frac{\Delta x}{\int V dt} \qquad \text{eq. 3.1}$$

where Δx is the distance the magnet travels through the coil during the time period of the integration in the numerator. The equation is evaluated with data from triggering a high speed camera and an oscilloscope during the drop. The oscilloscope data within the linear region is numerically integrated to obtain the denominator. An example of the data from the oscilloscope is contained in Figure 3.3. The distance that the magnet travels (the numerator) can be determined from the high speed camera video. The timing on the camera and oscilloscope is synced by using the point when the magnet and coil ends are aligned. This can be clearly seen on the camera data and can be identified on the oscilloscope data when the gage output returns to zero.

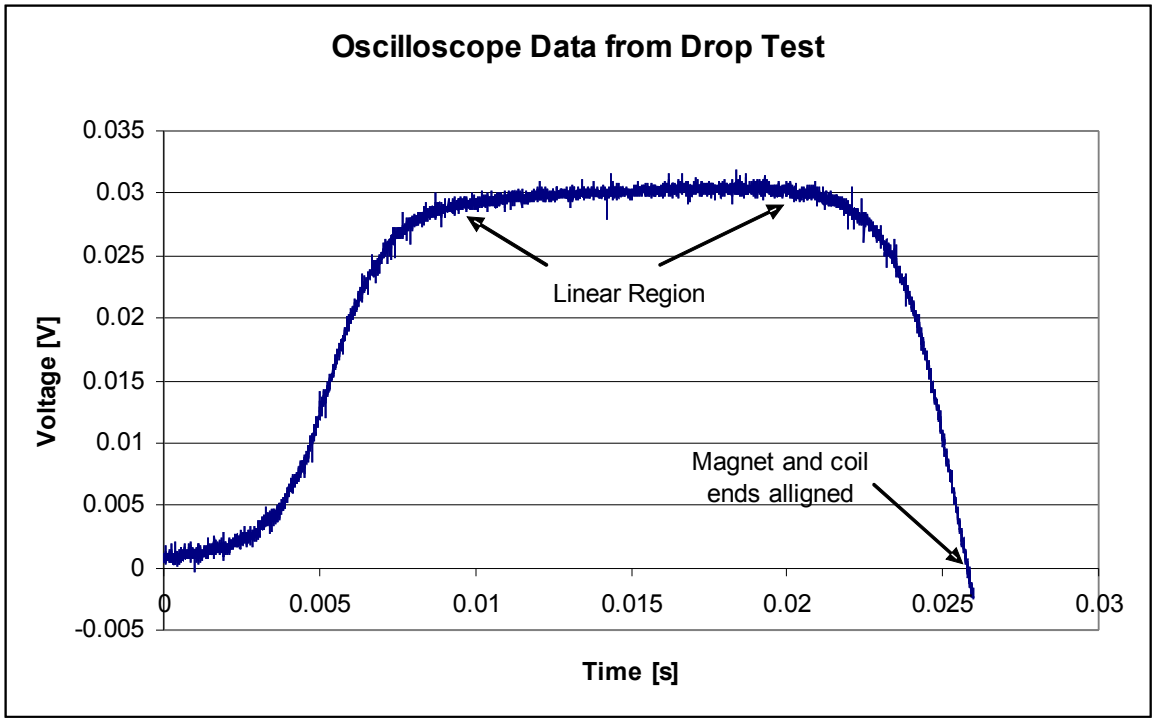

Figure 3.3: Drop test data sample

The results from several of these drops are averaged to determine the calibration factor. The calibration factors from individual drops for a coil-magnet system show standard deviations of approximately 1%-3% of their average. Several coils were calibrated in a similar manner using several drop heights. The standard deviation of the calibration factors were of the same magnitude as above, confirming the calibration factor is not velocity dependant. Further confirmation comes from numerically integrating the velocity coil data from an explosive test and comparing it to the displacement data from the same test gathered using high-speed photography. Figure 3.4 shows an example of this from a 13 deg hull test with no bracing or foam.

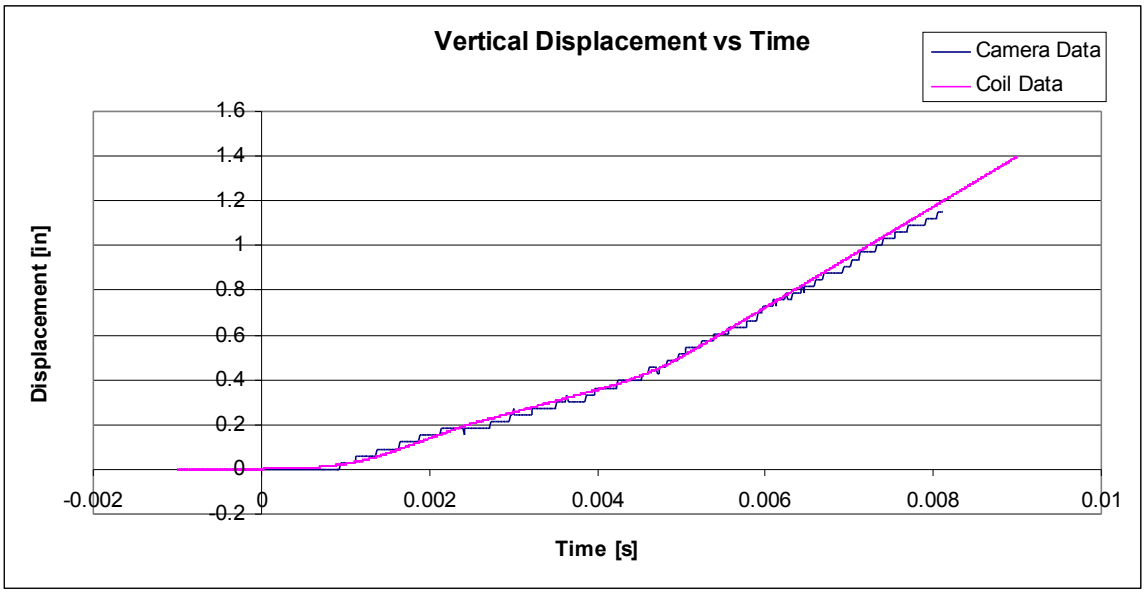

Figure 3.4: Vertical displacement data for 13 deg hull with no bracing using high-speed camera and velocity gage data

3.3 Model Construction

The vehicle model is described in section 2.5. This section describes the construction of the model.

The material for the floorboard and hull are ordered cut to proper dimensions. If the model has a nonzero hull angle, a hand sheet metal bending break is used to bend it. Aluminum wedges cut to the appropriate angles are used to ensure repeatability in the hull geometries. The hulls are bent to the appropriate angle lengthwise through the center of the hull with 1 in flanges bent flat on the edge of the hull to attach it to the frame.

The floorboard, hull, and frame are then fastened together with C-clamps in the same orientation as they will be for the explosive testing. The frame serves as a template for drilling the bolt holes through the floorboard and hull on a drill press. After this is complete, the clamps are removed and the model is bolted together.

Several tests use bracing on the floorboard. Two types of braces were used. The first is a brace with an L shaped cross section, which is a 1 in strip of 0.02 in thick 6061-T6 Al bent to 90 deg through its center making 2 perpendicular 0.5 in thick sections. The second type of brace is the U shaped cross sectioned brace which is cut from a similar strip of Aluminum with two 90 deg bends making a 0.5 in. section which will be normal to the floorboard after assembly and two 0.25 in thick sections which are at both ends of the previous section and will be parallel to the floorboard during assembly. This forms the U shape for which the brace is named. After the braces are shaped, they are attached to the bottom of the floorboard with 1/8 in rivets. The rivets are put in 1.5 in and 4.5 in from

center on braces running short ways across the floorboard and 2 in and 5 in on braces running long ways across the floorboard. Figure 4.19 shows an L brace after being hit by a hull during an explosive test.

For tests requiring foam mitigation, the foam is cut to proper dimensions using a hot-wire foam cutter. If necessary, additional detail is added to the geometry using sand paper or a saw to ensure a close fit between the foam filler and the natural shape of the space between the floorboard and hull. When the foam is used to fill the gap between the floorboard and the hull, it is simply cut to fit snuggly between the two and is held in place during assembly by its close tolerance to the gap size. When the foam mitigation is a foam brace, it is used to replace the brace in-between the floorboard and hull.

At this point, the model is assembled. If the model uses aluminum framing, it is bolted together. If the model uses foam framing, a bead of epoxy on the top and bottom of the foam frame is used to fasten the floorboard and hull on opposite sides of the foam frame. A steel frame with the same dimensions as the aluminum and foam frames is then attached to the top side of the floorboard using epoxy. This gives the model a similar weight to those using aluminum framing.

After the model is assembled, the velocity gage is attached to the center of the top of the floorboard using 5-minute epoxy. The floorboard is first roughened up where the gage will be placed using sand paper to help with the adhesion. Finally, the top of the floorboard is spray painted flat white in order to reduce glare in the high-speed video of the test. The velocity gage is covered with paper or tape to prevent paint from coating it, so that the magnet can be seen through the coil during testing. If the magnet is in motion when

velocity readings are being recorded from the gage, the readings are not accurate. The paint is allowed to cover a thin ring at the base of the coil. This makes it easier to see when the velocity gage breaks free from the floorboard during testing, making the data no longer reflective of the floorboard acceleration. Figure 3.5 shows an assembled model before being painted.

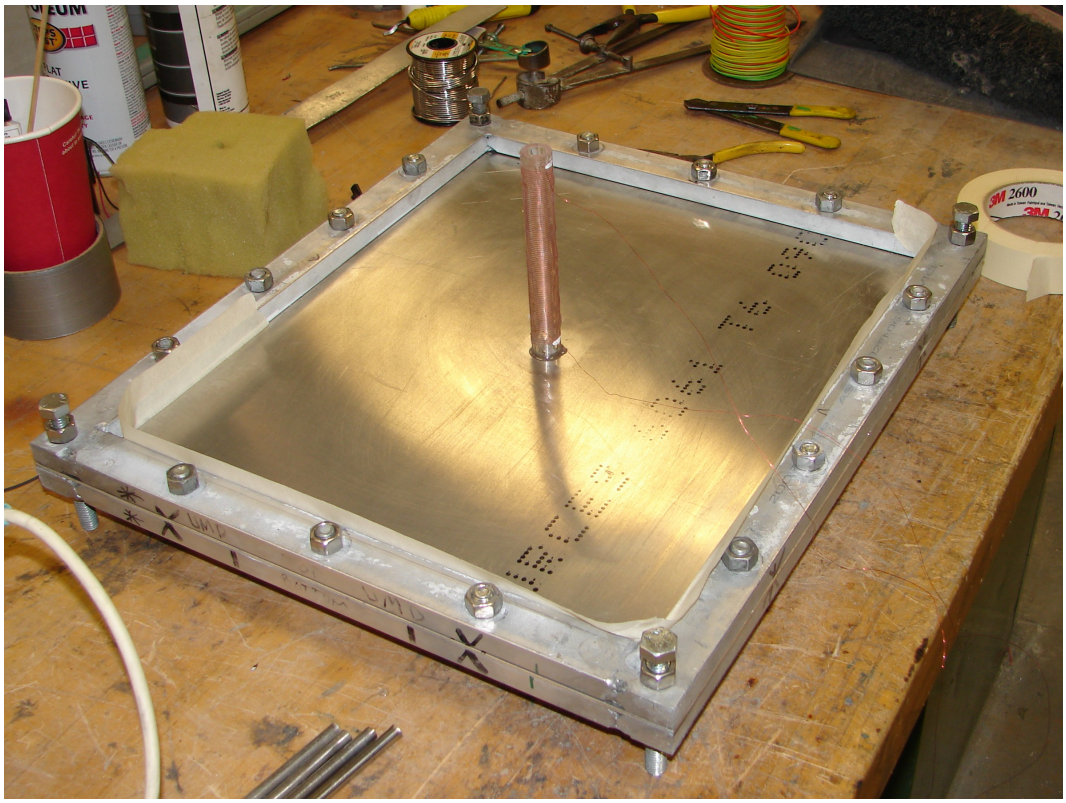

Figure 3.5: Assembled model before being painted

3.4 Test Setup

It is important to setup the tests similarly each time to ensure that testing conditions are consistent so the data can result in confident conclusions. This section discusses how the tests are set up and analyzed.

3.4.1 Sand Pit and Model Preparation

Each test requires controlling conditions as closely as possible. To ensure that the test bed is the same in each test a specific process is followed. The first step is to mix the sand in the sand pit. This is done with hand shovels. While mixing the sand, any debris such as wires from previous tests, is removed from the sand pit. Sand is then built up over one half of the pit. Using a cinder block, the sand on the built up half of the pit is compressed. A leveling tool is then used to scrape across the half of the sand pit where sand was built up and compressed. When the sand bed is leveled, a small hand shovel is used to dig a trench around the leveled half of the bed. This will allow the water saturation level to be easily monitored later. A photo of a leveled test bed with the scraping tool can be seen in Figure 3.6.

Figure 3.6: Leveled test bed with leveling tool

Once the test bed is prepared, the explosive charge must be buried. An indentation of the charge is made in the sand which serves as a guide for where to bury the charge. The charge must be placed so that the model, when placed above it, will not be too close to the edge of the scraped part of the sand bed where it is not strong enough to support the model's weight. A small charge sized hole is dug where the indent was made with a trench out of its side to hold the lead wires connecting the charge to the detonator. The charge is buried so that the top of it is 0.30 in from the top of the sand bed (DoB=0.30 in). The charge must fit snug into its position to ensure that it will not shift when sand is filled on top of it. Using a digital caliper, the DoB is checked in five places to ensure the charge is buried accurately and its surface is parallel to the sand bed. The lead wires are held down

with small V shaped spikes to ensure they are not pulled out of the sand which can affect the charges DoB.

Before covering the charge with sand, two perpendicular lines are scored in the sand bed, which cross each other at the center of the charge. The lines are discontinuous around a few inch radius centered at the charge because previous testing in the Dynamic Effects Laboratory has shown that the scored lines can affect the properties of the dome of sand coming up after detonation. These lines provide the means to later center the test model above the charge. They will cross the model in between each of its corners. A photo of the scored lines can be seen in Figure 3.7. Finally, the charge is covered with sand, which is compacted and leveled.

Figure 3.7: Buried charge with scored lines for centering test model

At this point, water is let into the sand pit using the saturation control system discussed in section 2.4. Water is allowed to come into the pit until it is flush with the top of the sand bed without flowing on top of it causing puddles. This ensures that the sand is fully saturated with water, which previous testing in the Dynamic Effects Laboratory showed was the worst case scenario for explosive pressures [1.9].

Once the sand is saturated, the model is centered on the charge and adjusted to the appropriate SoD. The model is not set up until after the sand is saturated because otherwise it can sink into the sand when it is saturated, which will cause an incorrect SoD if not corrected for. Wooden blocks are placed on the sand under the long corner bolts of the

model which prevent the model from sinking. The model is centered according to the previously scored lines. Using digital calipers, the SoD is checked at all corners. Figure 3.8 shows a model centered and at the correct SoD.

Figure 3.8: Centered model before testing

Once the model is setup, braces are connected to the side of the sand pit which serve as platforms for a 2x4 which runs over the model to suspend the velocity gage magnet. The braces are used to set the 2x4 high enough that the impact on the magnet and coil is minimized when the charge is detonated, which greatly improves the lifetime of the gages. The magnet is suspended by string into the center of the coil at the appropriate depth,

according to the linear region discussed above, to maximize valid measurement time while ensuring that the first readings are accurate. Figure 3.9 shows the velocity gage setup before a test.

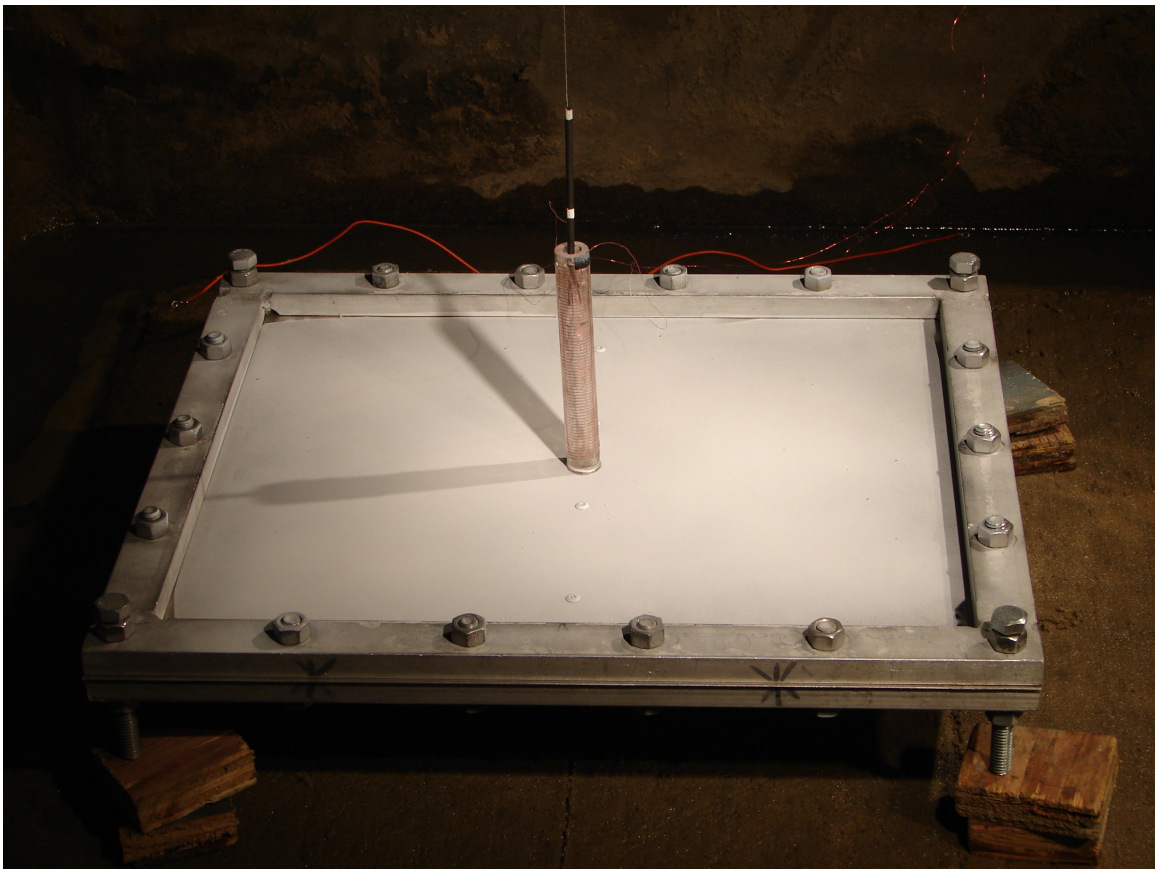

Figure 3.9: Velocity gage setup before testing

3.4.2 Data Collection Equipment Setup

Once the sand pit is ready, the data gathering equipment must be set. The gooseneck lamps are placed on the side of the sand pit to provide lighting for the high-speed camera. The camera is generally adjusted so that about half an inch below the coil and above the magnet can be seen. A small amount of space is allowed on either side of the gage. This minimizes the necessary camera resolution, which maximizes the possible frame rate. Typical camera settings are about 48x256 pixel resolution, which allows for 81,632 frames per second at an exposure time of 5 x

camera is used to confirm the data collected from the velocity gage. Figure 3.10 shows one frame of the video footage before a test. Occasionally, a larger resolution is used to allow the entire model to be seen. This significantly reduces the frame rate, which in turn increases the inter-frame period.

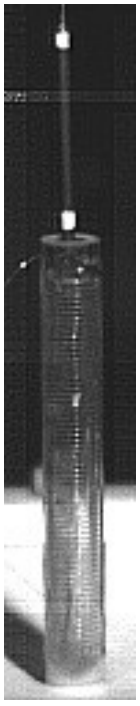

Figure 3.10: One frame from high-speed video before test

In order to collect data from the velocity gage, the oscilloscope must be connected to it and the scope must be set properly. The temporal resolution is maximized on the oscilloscope by setting it so that all data as the magnet of the velocity gage moves through the coil is collected. Ideally, the oscilloscope will stop collecting data shortly after this. The resolution of the velocity data is also maximized by adjusting the scope settings to as small of a voltage per division as possible. Because the oscilloscope has four channels, the data is collected on all four, which have different settings, and the one with the highest resolution and all necessary data is analyzed. Because the test results cannot be perfectly predicted, educated guesses must be used for determining the scope settings in each test based on previous results and calibration factor of the gage being used in the specific test. Typically, 5-20 ms must be recorded. The voltage settings can vary greatly depending on the gage used and test conducted.

As mentioned above, both the oscilloscope and the camera are set to trigger when the charge is detonated. This is done by splitting the wire from the trigger mechanism of the detonator and allows data to be easily synced when the test is analyzed. Figure 3.11 shows the testing room before a test.

Figure 3.11: Testing room before test

3.4.3 Charge Detonation

Once the test is fully prepared, the charge must be detonated. People in the surrounding labs are informed that tests are about to be conducted. Care must be taken to ensure that data is collected properly and in a safe manner. The equipment is checked one final time to make sure there is not an unreasonable amount of noise interfering with the oscilloscope or that any equipment has triggered prematurely. Once all the equipment has been checked, a countdown is made and the firing system is used to detonate the charge.

3.5 Test Analysis

After data is collected, it must be post processed and analyzed. The Lecroy Scope Explorer software is used to convert the oscilloscope data from trc files into text files which can be imported into an Excel spreadsheet. The raw data from the scope returns voltage as a function of time. Using the calibration factor discussed above, the voltage data can be transformed into velocity data.

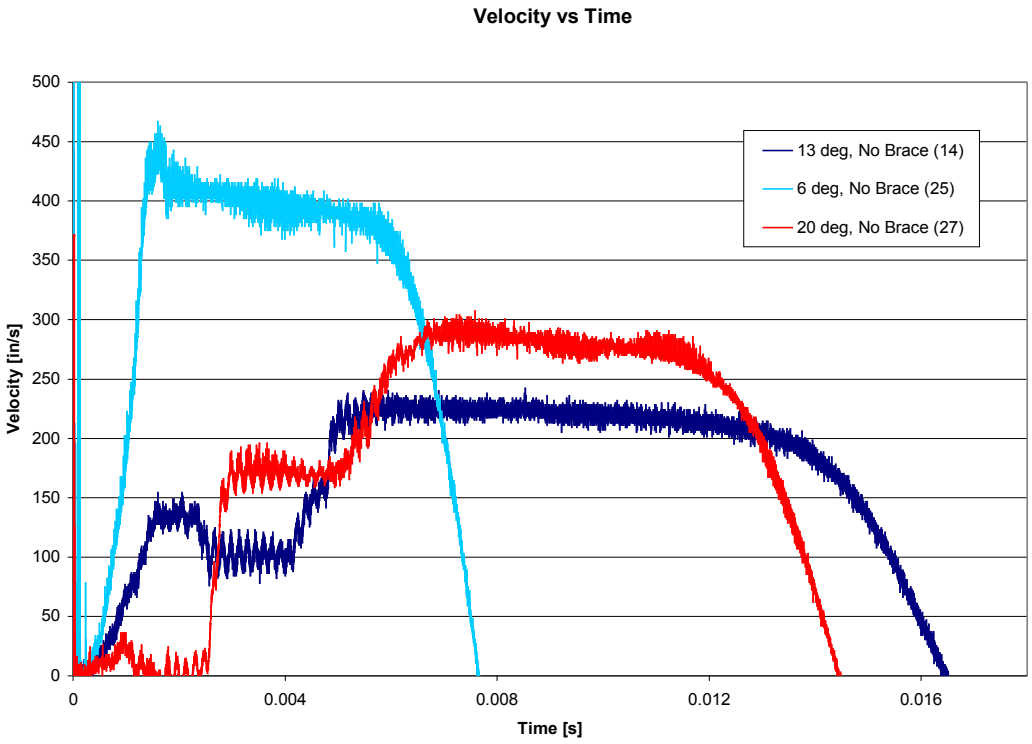

Figure 3.12: Typical velocity curves from velocity gages

Figure 3.12 shows typical waveforms of the measured voltage multiplied by the calibration factor. The initial spike at time zero is a voltage spike from the triggering mechanism and does not represent a velocity. The following inclines on the waveforms are real and are differentiated to obtain the floorboard acceleration. On both the 13 deg and 20 deg hulls,

there are regions where velocity is nearly constant. Those regions are where the gage has come off of the floorboard and is hit by it a second or third time. This velocity data is real, but represents the gage and not the floorboard, so that it is not useful for data collection. In all of the tests, there is a long region of constant nearly constant velocity for which there is no following positive derivative. This region occurs because the velocity coil has come off of the floorboard and is not hit by it again. This region is not useful for data collection for the same reason stated above. Finally, all of the waveforms have sudden drops in velocity where they enter the negative region. This is caused when the gage leaves its linear region. When velocity reads zero, the coil ends are flush with the magnet ends, as discussed in the coil calibration section. These regions are shown on a typical waveform in Figure 3.13.

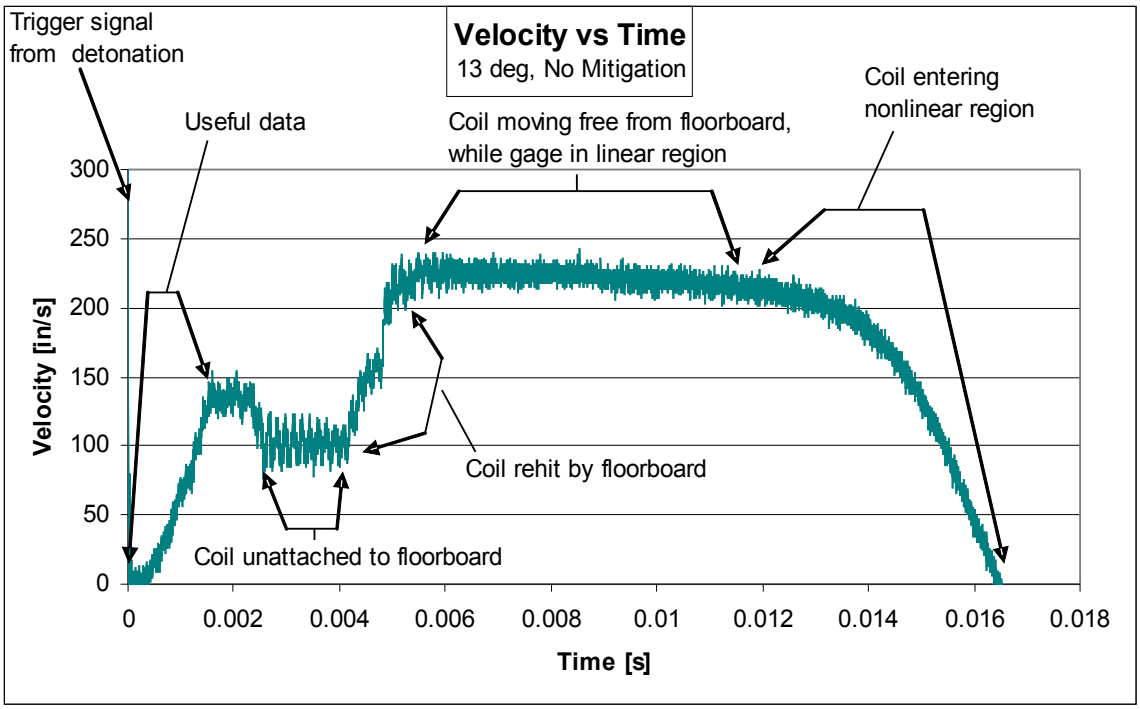

Figure 3.13: Typical waveform with regions marked

As mentioned above, the useful region for data collection is the first positive increase in velocity. This incline, or some section of it with maximum acceleration, has a curve fit to

it in Excel which can then be differentiated to obtain maximum acceleration of the floorboard. For most curves, this can be done with a linear curve fit. However, some curves required a nonlinear curve fit. Figure 3.14 shows an example of a linear curve fit graph in Excel.

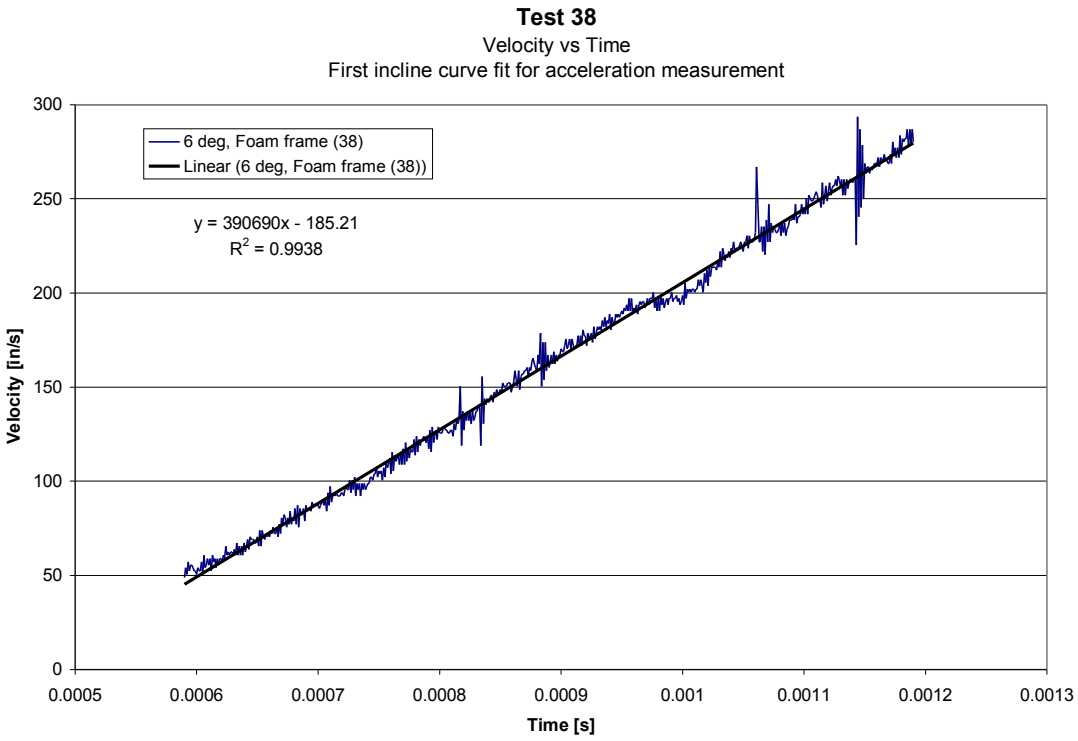

Figure 3.14: Linear curve fit for velocity gage test to obtain acceleration

Ch 4: Results

The results discussed in this chapter were obtained using the velocity gage, as discussed in Chapter 3. Sections 4.1-7 discuss tests at SoD of 3.19 in. Section 4.8 considers the effects of changing the SoD. Figure 4.1 shows what a full waveform looks like after being multiplied by the calibration factor. The linear region, which the gage has been calibrated for starts at the beginning of the waveform and ends when the dependent variable begins dropping quickly, which occurs at approximately 10 to 12 ms in the test shown. This generally allows between 1 to 2 inches of displacement before the gage is out of usable range.

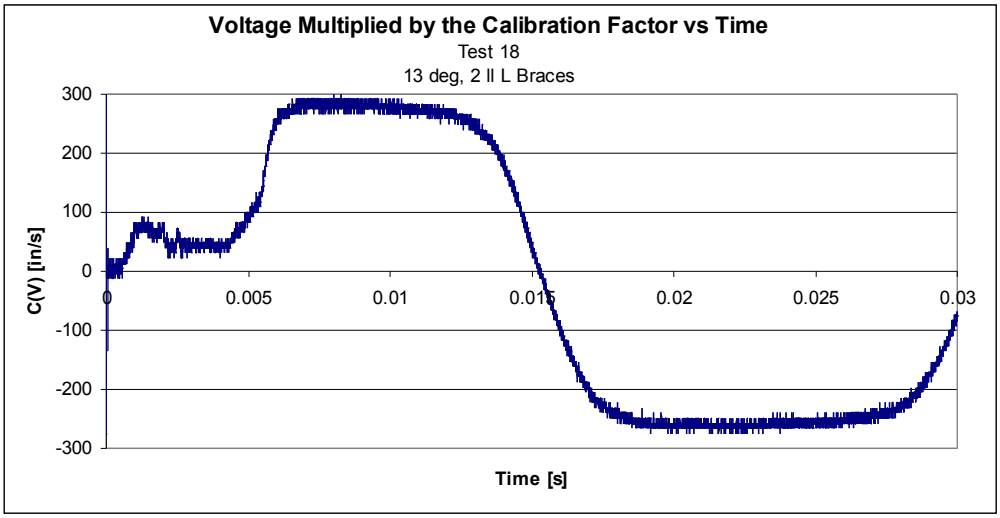

Figure 4.1: Typical waveform showing voltage multiplied by calibration factor versus time

Figure 4.2 shows just the first incline of another test, which is the useful part of the test for gathering data on the plate acceleration. This section is significantly smaller than would be expected from the calibrated linear region because the gage breaks free from the floorboard and moves independently. At that point, data collection would no longer reflect a history of the Floorboard. This occurs when the velocity of the floorboard slows down quicker

than the gage attached to it, and the tension in the epoxy becomes to great for the epoxy to hold the two together.

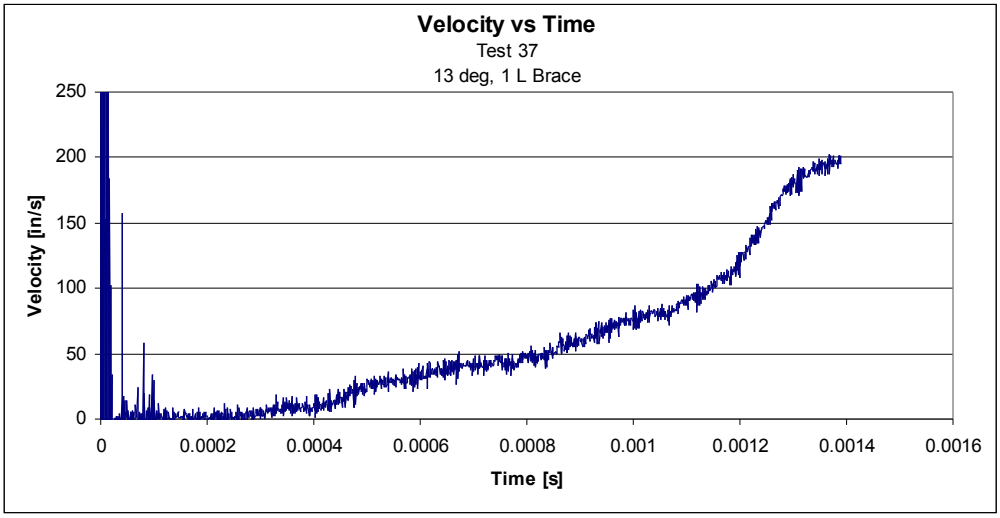

Figure 4.2: Velocity versus time profile, as used to analyze tests

4.1 Repeatability

One concern when analyzing the data in this series was whether the results were repeatable. As can be seen in figures below, the results of experiments conducted for given conditions are similar. The velocity profiles tent to be very similar, but acceleration values can vary significantly due to small changes in the profiles.

Figure 4.3 shows three repeats of tests with 0 degree hulls and no mitigation. Figure 4.4 shows the remaining repeated tests, which are for angled hulls with no mitigation methods. The angled hull adds an additional complexity to the setup which accounts for the less repeatable behavior in these tests. Table 4.1 shows how the maximum accelerations from the repeated tests compare.

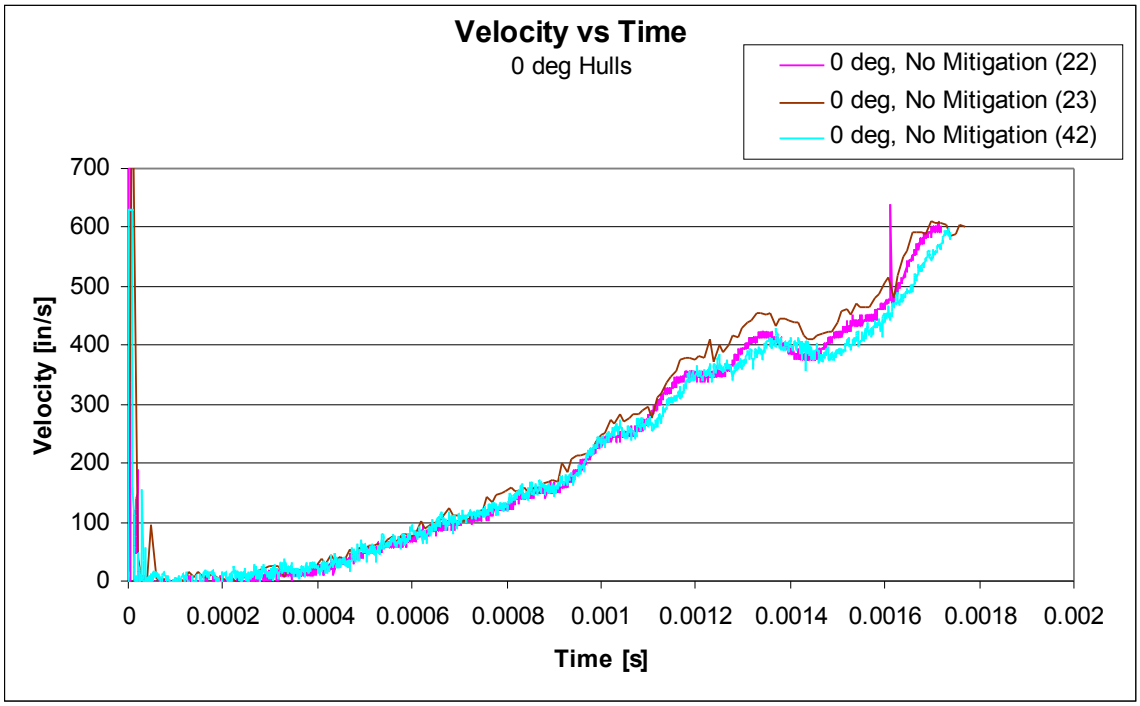

Figure 4.3: Velocity versus time profiles for three repeated tests with 0 degree hull and no mitigation

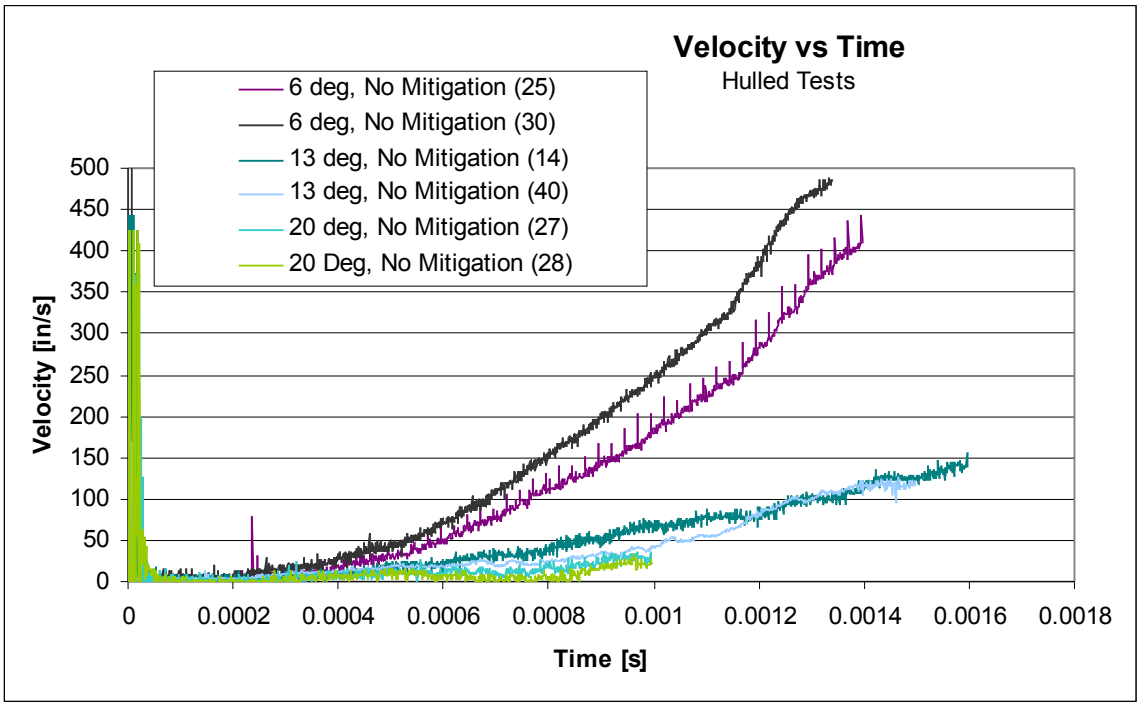

Figure 4.4: Repeated tests for angled hulls with no mitigation

Repeated Tests (SoD=3.19 in)		Small Scale	Full Scale
Test #	Hull Angle [deg]	Acceleration [g's]	Acceleration [g's]
22	0	4268	325
23	0	3693	281
42	0	3556	271
25	6	1936	147
30	6	2641	201
14	13	384	29
40	13	1037	79
27	20	721	55
28	20	414	32

Table 4. 1: Accelerations from repeated tests

4.2 Overview of Test Data

Below is a summary of all data with a 3.19 in SoD used in this thesis. Section 4.8 discuses several tests which had different SoD. Figure 4.5 shows velocity profiles and Figures 4.6-7 show the maximum acceleration data from these tests. Table 4.2 contains the maximum accelerations for each of these tests. Note that throughout this thesis, if a testing condition has repeated tests, the acceleration reported is the average of them all. The acceleration for the individual tests of a repeated series can be found in Table 4.1 and Appendix A.

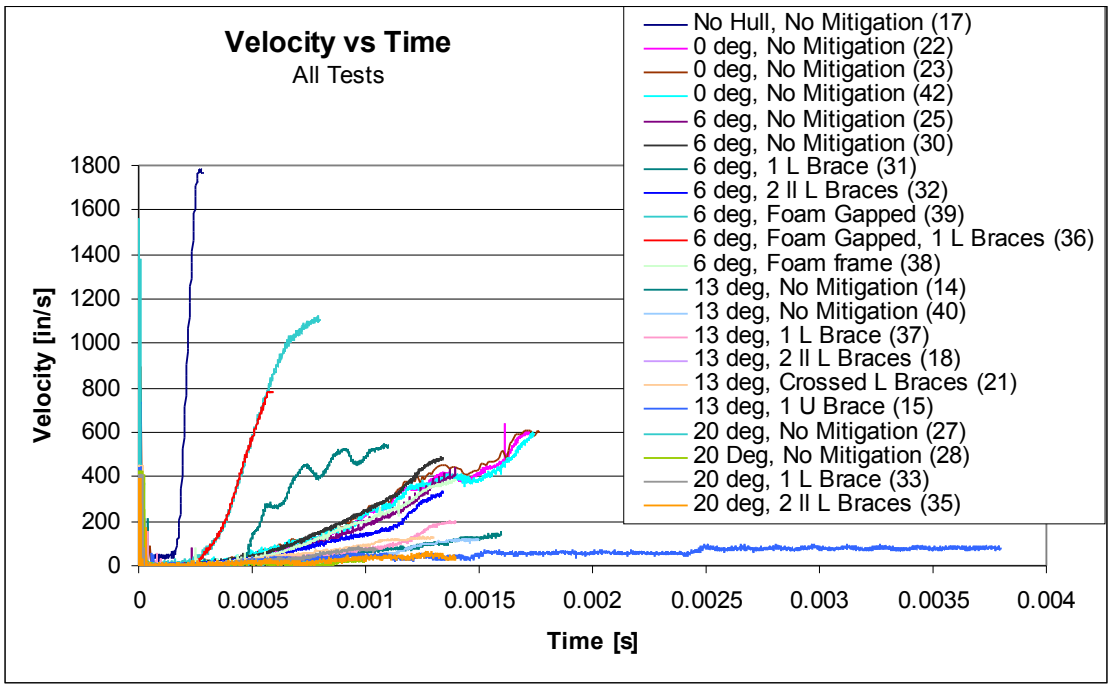

Figure 4.5: Velocity Profiles from all tests with SoD of 3.19 in

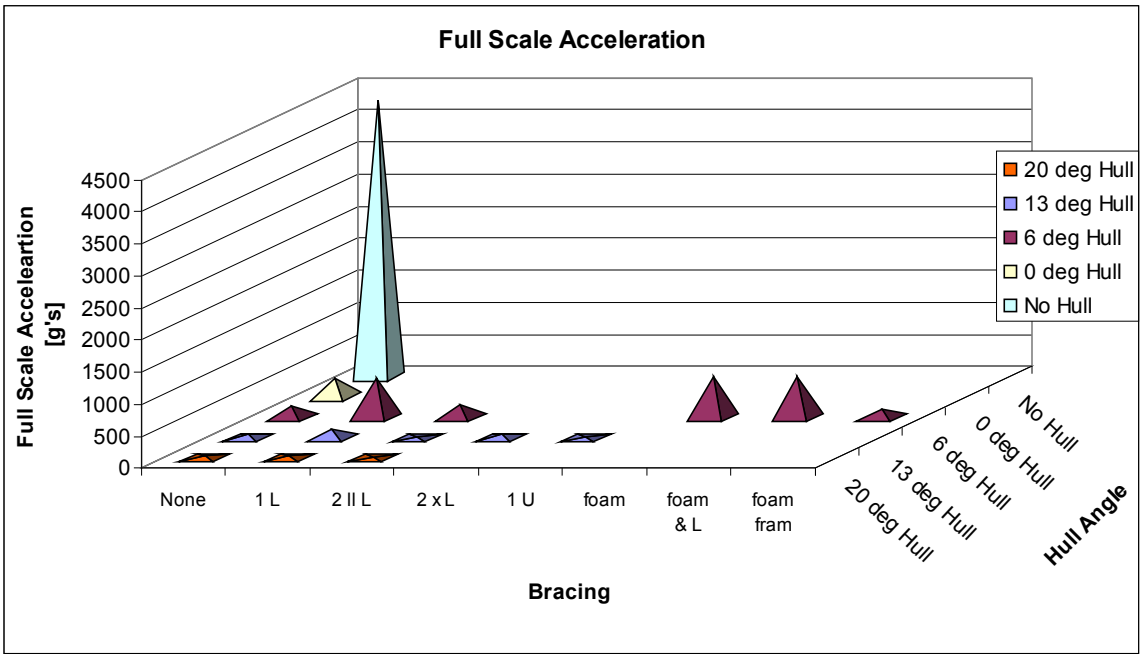

Figure 4.6: Maximum accelerations from all tests

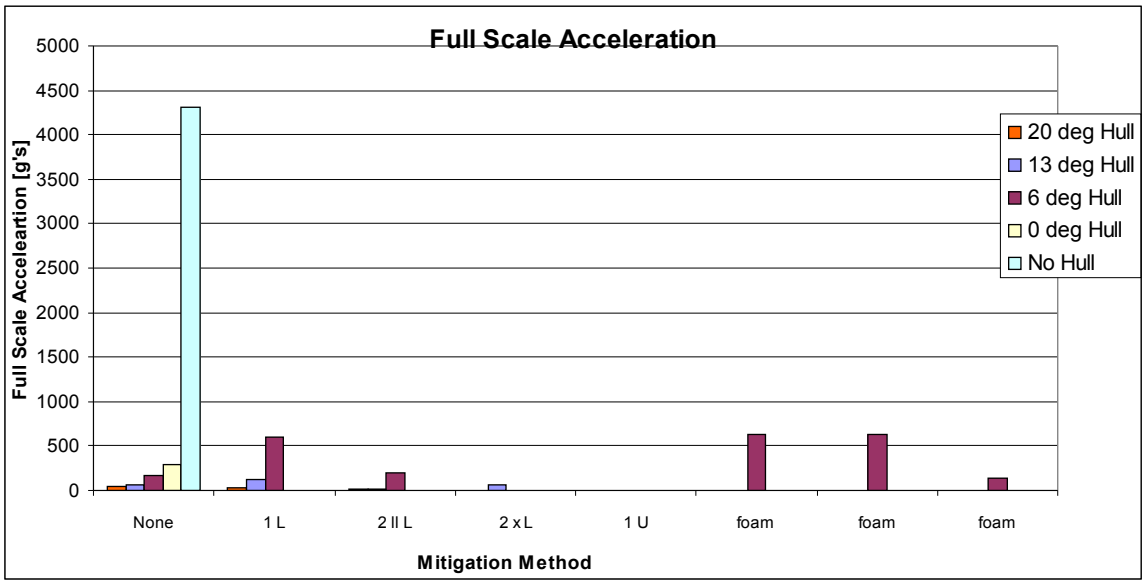

Figure 4.7: Maximum accelerations from all tests

Acceleration Values (SoD = 3.19 in)					Small Scale	Full Scale
Test #	Conditions	Hull Angle	# Braces	Foam	Acceleration [g's]	Acceleration [g's]
17	No Hull, No Mitigation	N/A	0	None	56646	4311
22	0 deg, No Mitigation	0	0	None	4268	325
23	0 deg, No Mitigation	0	0	None	3693	281
42	0 deg, No Mitigation	0	0	None	3556	271
25	6 deg, No Mitigation	6	0	None	1936	147
30	6 deg, No Mitigation	6	0	None	2641	201
31	6 deg, 1 L Brace	6	1	None	7926	603
32	6 deg, 2 ll L Braces	6	2ll	None	2651	202
39	6 deg, Foam Gapped	6	0	Gap	8314	633
36	6 deg, 1 L Brace, Foam Gapped	6	1	Gap	8188	623
38	6 deg, Foam Frame	6	0	Frame	1835	140
14	13 deg, No Mitigation	13	0	None	384	29
40	13 deg, No Mitigation	13	0	None	1037	79
37	13 deg, 1 L Brace	13	1	None	1625	124
18	13 deg, 2 ll L Braces	13	2ll	None	292	22
21	13 deg, 2 x L Braces	13	2x	None	813	62
15	13 deg, 1 U Brace	13	1 U	None	63	5
27	20 deg, No Mitigation	20	0	None	721	55
28	20 deg, No Mitigation	20	0	None	414	32
33	20 deg, 1 L Brace	20	1	None	449	34
35	20 deg, 2 ll L Braces	20	2	None	274	21

Table 4. 2: Accelerations from all tests with 3.19 in SoD

Figures 4.10-11 show the test results for hulled tests, which are easier to compare without the no hull test dominating them. While maximum accelerations of tests are reported in this section, more in depth look at the tests are required in order to understand what is happening. Some tests show similar maximum accelerations, but experience these accelerations for different time periods, which results in different target behavior. The rest of this chapter addresses this further analysis.

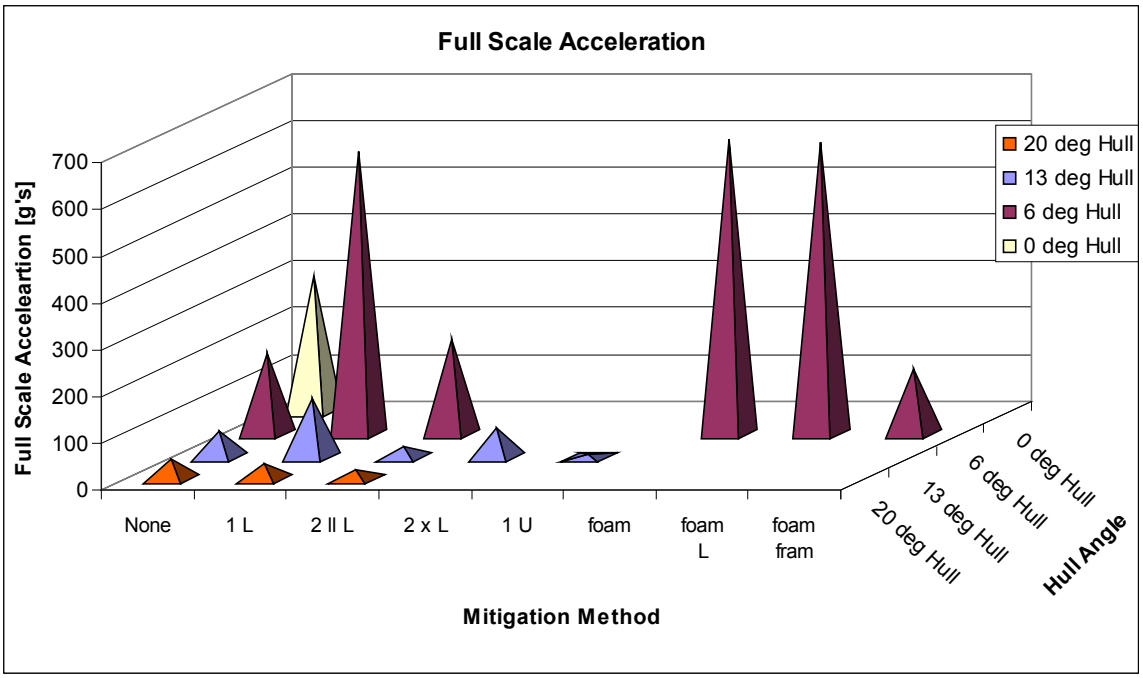

Figure 4.8: Maximum accelerations from hulled tests

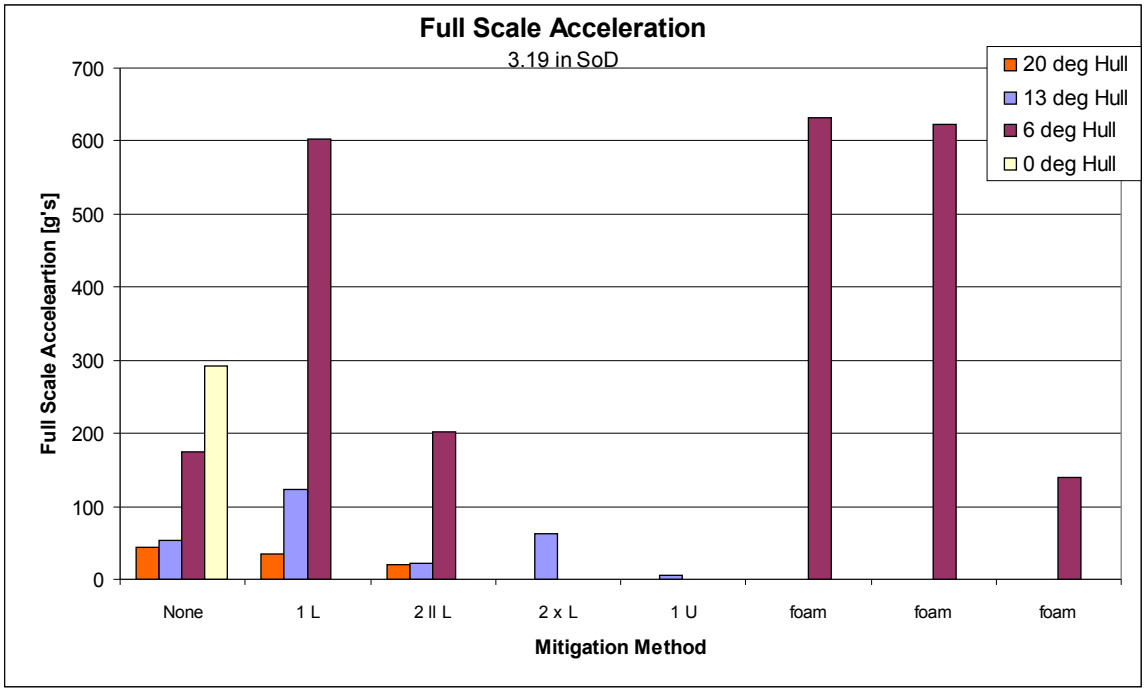

Figure 4.9: Maximum accelerations from hulled tests

4.3 Effect of Adding a Hull to a Vehicle

Figure 4.10 shows the accelerations for all tests with no mitigation method other than the hull geometry. It is apparent from this and the velocity profiles in Figure 4.5 that having a hull greatly reduces the maximum acceleration of the floorboard. Table 4.2 shows that adding a flat hull to the model reduces the acceleration by about 4000 g's compared to a test with no hull. The acceleration from the test with no hull is 14.8 times greater than the highest acceleration from the hulled tests with no other mitigation method. It is 6.8 times greater than the 3.19 in test with the second highest acceleration reported in the thesis (test 39 with 6 degree hull and foam filled gap). More evidence of the mitigation effects of a hull will be presented in section 4.8, which discusses several tests at various stand off distances.

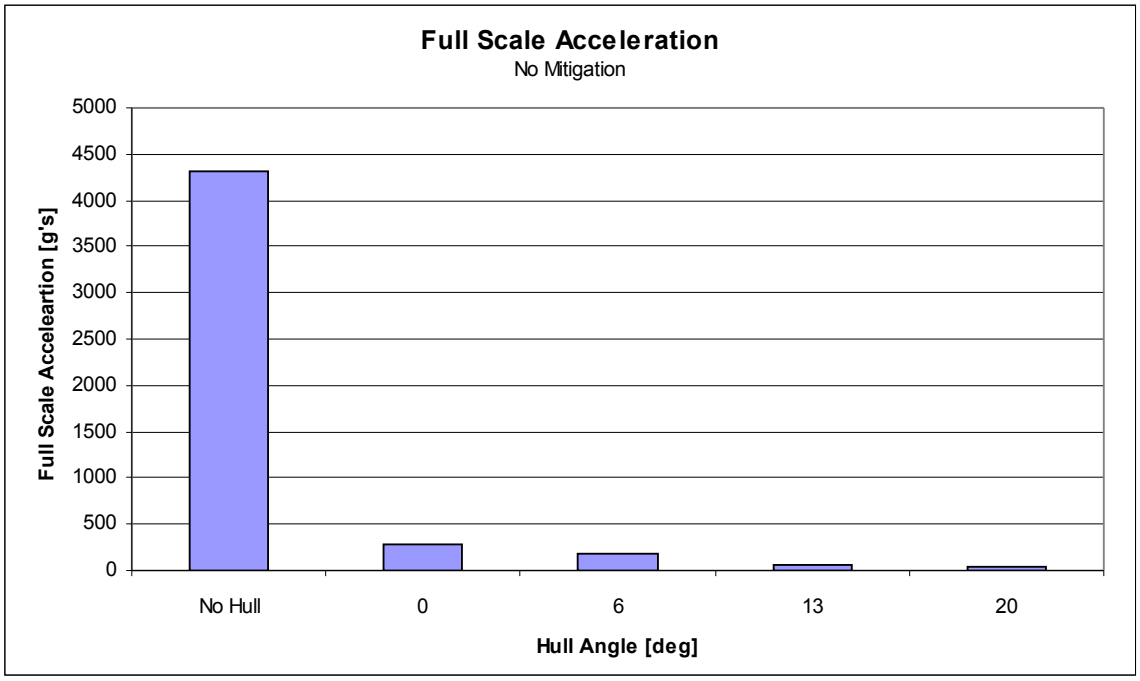

Figure 4. 10: Plot of acceleration versus hull angle showing the mitigation effect of having a vehicle hull

4.4 Effects of the Hull Angle

The primary mitigation method investigated was the hull geometry. Previous impulse testing resulted in a minimum impulse on hulls with a 13 degree angle [4.1]. For this reason, hulls with 0, 6, 13, and 20 degree angles were tested, to determine the effects of changing the hull angle.

4.4.1 Tests with No Bracing

Figure 4.11 shows a representative sample of how the velocity profiles look for the angles tested. As mentioned above, the mitigation effect of adding a hull can be readily seen on the graph. It can also be seen that the 0 and 6 degree hulls show similar behavior to each other while the 13 and 20 degree hulls show similar behavior to each other. The remaining profiles for the tests discussed in this section can be found in Figures 3-4.

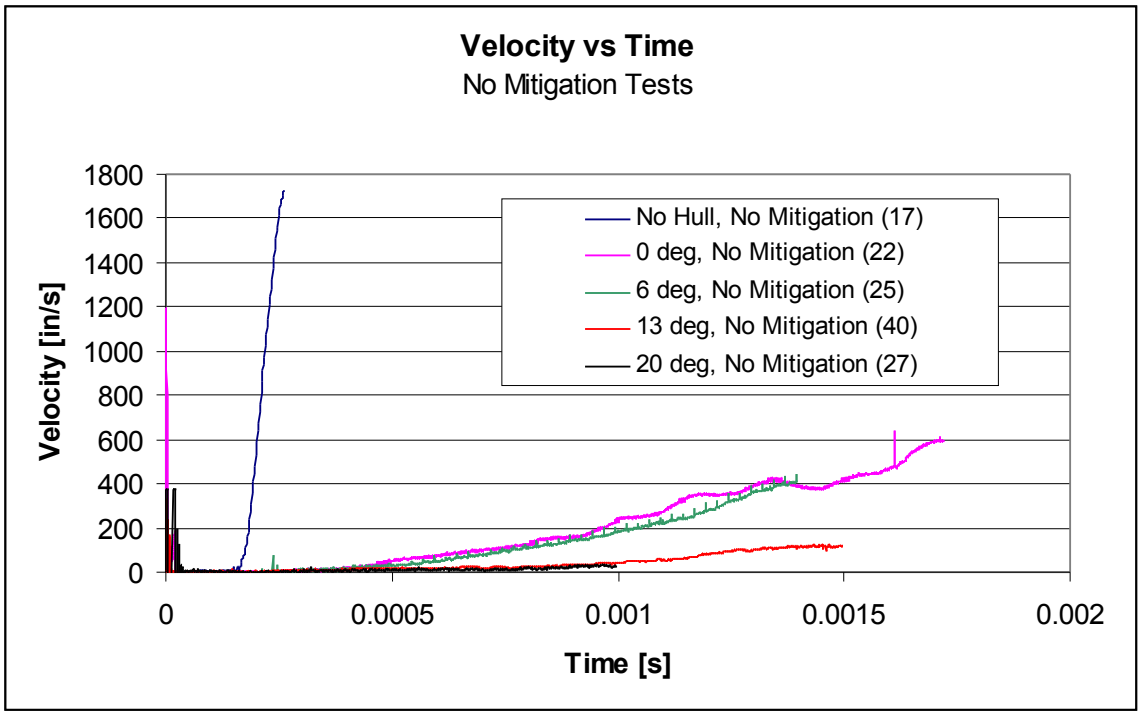

Figure 4.11: Representative sample of velocity profile for different hull geometry

Figure 4.12 shows the maximum accelerations from tests with no bracing or foam as a function of hull angle. As the hull angle is increased the acceleration is decreased. However, the mitigation benefit from increasing the hull from 13 degree to 20 degree is marginal in comparison to the increase from a flat hull to a 6 degree hull and from a 6 degree hull to a 13 degree hull. For most of the velocity histories recorded, the flat hull and 6 degree hull tests look very similar. From Figure 4.11, it should be noted that while the flat hull has a significantly higher maximum acceleration than the 6 degree hull, this occurs for a short period of time. This sudden acceleration can be attributed to the added momentum transfer from the hull being closer to the floorboard before the hull hits the floorboard.

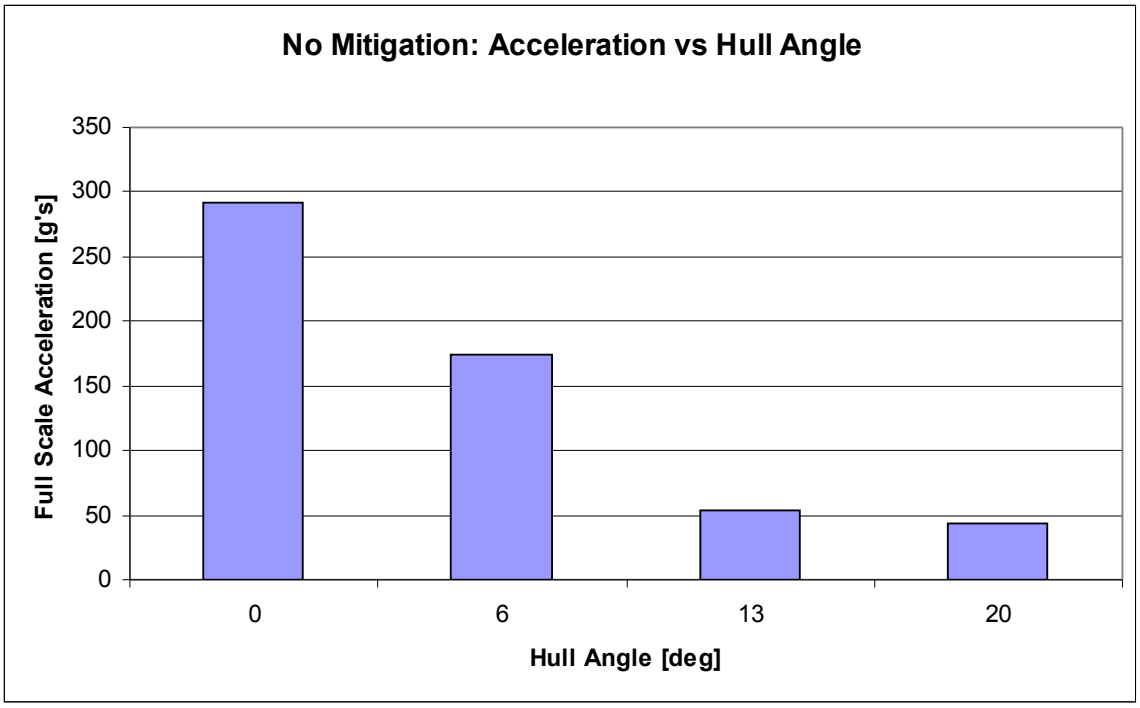

Figure 4.12: Full scale acceleration versus hull angle for no mitigation method

4.4.2 Tests with 1 L Brace

Figure 4.13 shows the maximum accelerations from tests with 1 L brace as a function of hull angle. For the 1 L brace tests, the 13 degree hull showed a significantly higher acceleration than the 20 degree hull with 1 L brace. It also showed a larger acceleration than the 13 degree hulls with no mitigation and two parallel L braces. This is because the brace was impacted by the hull. This can clearly be seen by the sudden change in velocity at approximately 11 ms in Figure 4.14, which contains the single L brace test velocity profiles. Similarly, the 6 degree tests show higher accelerations for both the 1 L brace and the two parallel L braces tests than the 6 degree with no brace tests, because in both cases the braces were hit by the hull, as seen in Fig 4.16.

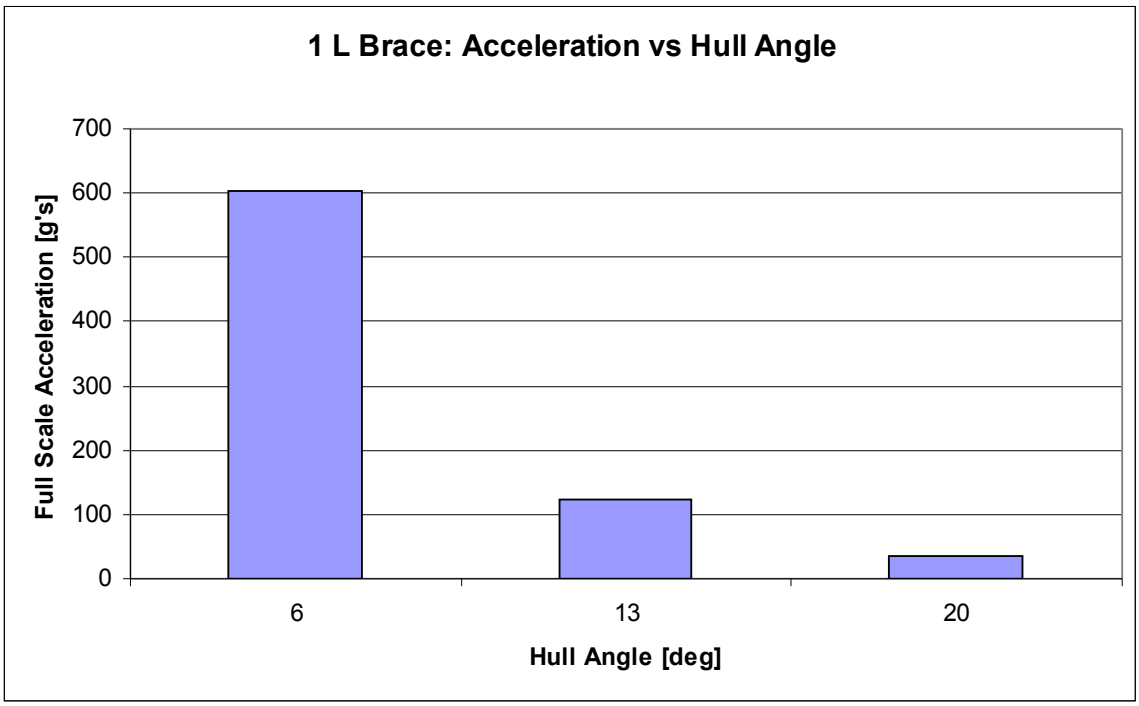

Figure 4.13: Full Scale acceleration versus hull angle for 1 L brace mitigation method

Figure 4.14 shows the velocity profile for the tests with 1 L brace. The first 0.4 ms of the floorboard responses look similar. At this point the 6 degree hull begins to be accelerated slightly more than the other hulls. Just before 0.5 ms, the brace of the 6 degree hull test is hit by the hull, as marked on the graph, which causes a significant acceleration of the floorboard.

Similarly to the no mitigation tests, the 13 degree hull behaves like the 20 degree hull except that it acts over a longer time period. Around 1.1 ms, the 13 degree hull hits the brace, which causes the significant acceleration that can be seen in Figure 4.14. As can be seen in Figure 4.13, the accelerations when bracing is hit by the hull are large compared with those when the hull does not hit the brace or floorboard. This is caused by the stress wave which is induced in the brace and transmitted into the floorboard.

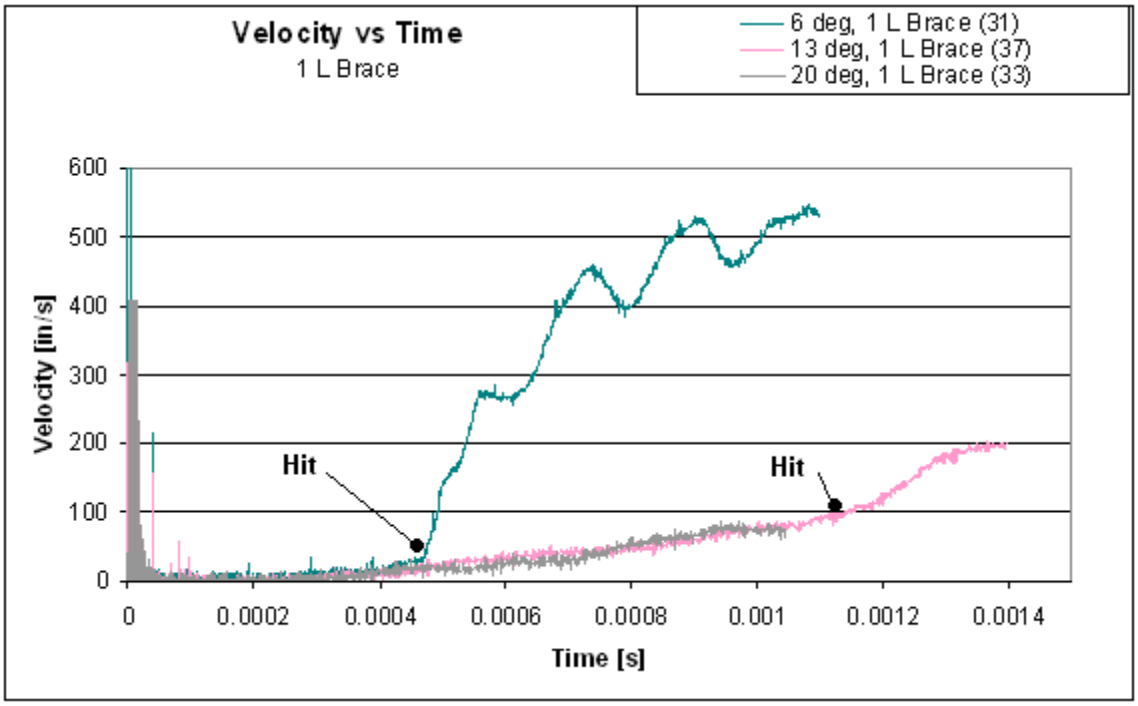

Figure 4.14: Velocity profile for tests with 1 L brace

4.4.3 Tests with Two Parallel L Braces

Figure 4.15 shows the maximum accelerations versus hull angle for tests with 2 parallel L braces. The general trend is that as the angle of the hull is increased, the maximum observed acceleration of the floorboard is decreased. The acceleration of the test with the 6 degree hull is significantly higher than tests with the 13 degree and 20 degree hulls: 9.1 and 9.7 times as high, respectively. The decrease in acceleration from the 13 degree to 20 degree hulled tests, 22 to 21 g's, however, this not significant enough to declare the 20 degree hull more effective than the 13 degree hull when 2 parallel L braces are used to brace the floorboard.

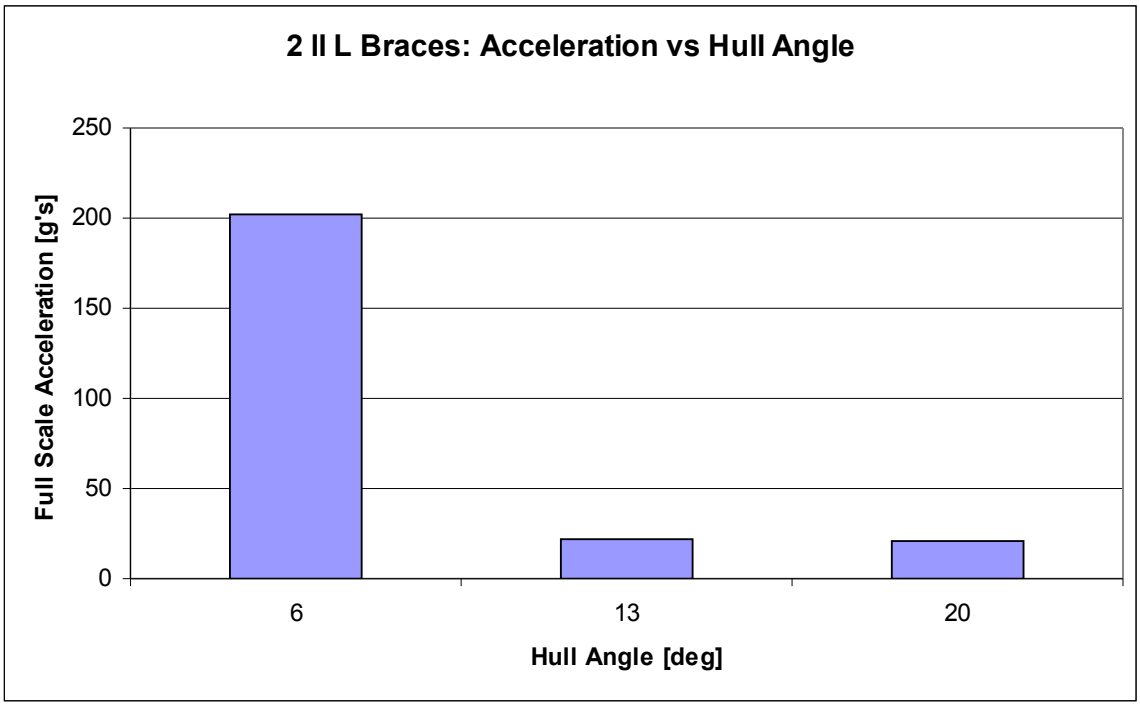

Figure 4.15: Full Scale acceleration versus hull angle for 2 parallel L braces mitigation method

Figure 4.16 shows the velocity profiles from the tests with 2 parallel L braces. Again the 6 degree hull begins to distinguish itself from the 13 degree and 20 degree hulls at approximately 0.3 ms. It continues to be accelerated at a higher rate than these tests until

about 1.1 ms when the hull hits either the floorboard or the brace, at which point the floorboard experiences a significantly higher acceleration than in the other tests. It is unclear whether it is the floorboard or the braces that are hit by the hull.

The velocity profiles of the 13 degree and 20 degree hulls are again similar to each other. They are distinguished from previous tests with fewer braces because the velocity gage breaks free from the 20 degree hull later in this test than the 13 degree hull, suggesting the 13 degree hull rebounded earlier than the 20 degree hull. The 13 degree hull is accelerated at a slightly higher rate, which is consistent with this conclusion.

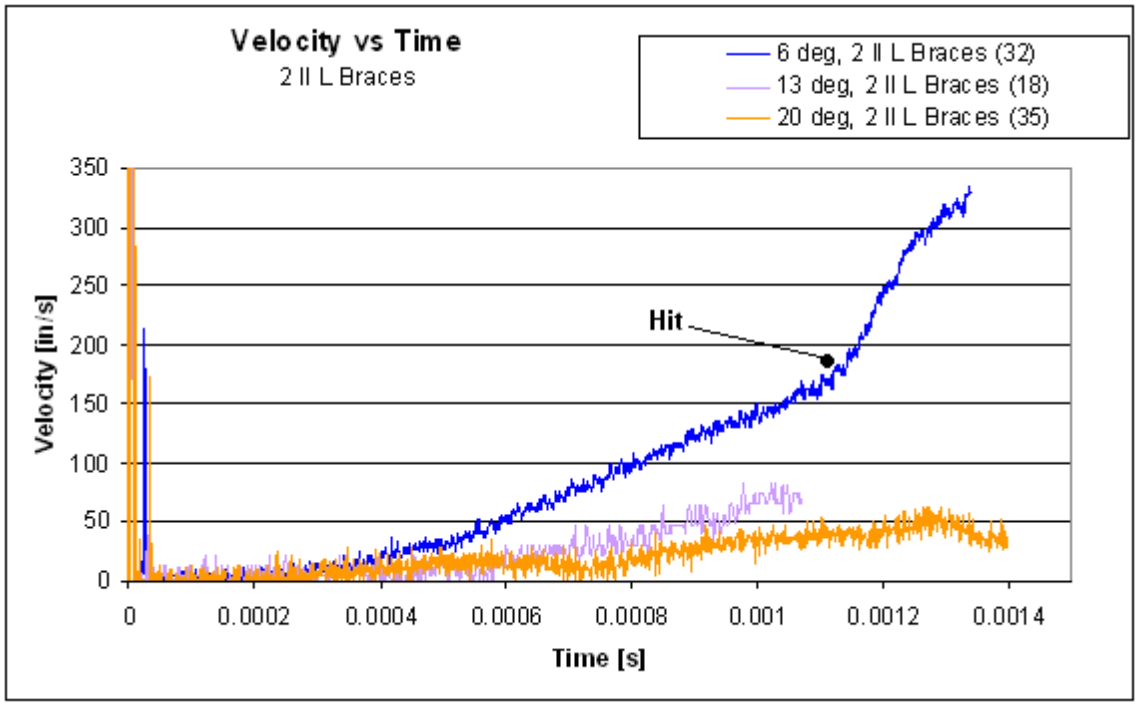

Figure 4.16: Velocity profiles for 2 parallel L braces tests

4.4.4 Summary of Effects of Hull Angle

From the velocity profiles and their calculated accelerations above, it is clear that increasing the hull angle results in better mitigation of the explosive effects. Generally,

there is a large decrease in measured acceleration of the 13 degree hull tests compared to the 6 degree hulls. The differences in acceleration from the 13 degree to 20 degree hulls are marginal in comparison. When designing a vehicle, there must be a tradeoff between ground clearance and blast mitigation. As the hull angle is increased, more of the blast impulse can be deflected, but the ground clearance is decreased.

4.5 Effects of Bracing

The tests in Section 4.4 can be looked at while holding the hull angle constant to investigate the effects of different bracing systems. In addition to these core tests, two additional types of bracing are presented for 13 degree hulls: 2 crossed L braces and 1 U brace, which were described in chapter 3. It is important to test how bracing affects blast mitigation because all real vehicles will require some type of bracing to support their floorboard. The hope is to design it so that it helps blast mitigation as well as general floor support.

4.5.1 Effects of Bracing on 6 degree Hulled Models

Figure 4.17 shows the acceleration versus the number of L braces for tests with 6 degree hulls. The tests with bracing show higher accelerations than the test with no bracing. In both cases the high acceleration is caused by the bracing being hit by the hull. The test with a single L brace resulted in an acceleration of 603 g's, 3.5 times larger than the average of the tests with no bracing. The test with two parallel L braces resulted in an acceleration of 202 g's, 1.2 times larger than the test with no bracing. The reason that the test with a single brace results in a much larger acceleration than the test with two braces is that the single brace is directly between the charge and the gage. This causes the single brace to be hit significantly harder than the two braces, and the stress wave to be transferred directly into the area of the floorboard with the gage. The two braces are hit at a later time than the single brace and with less floorboard momentum, and the stress wave must travel through several inches of the floorboard before reaching the gage.

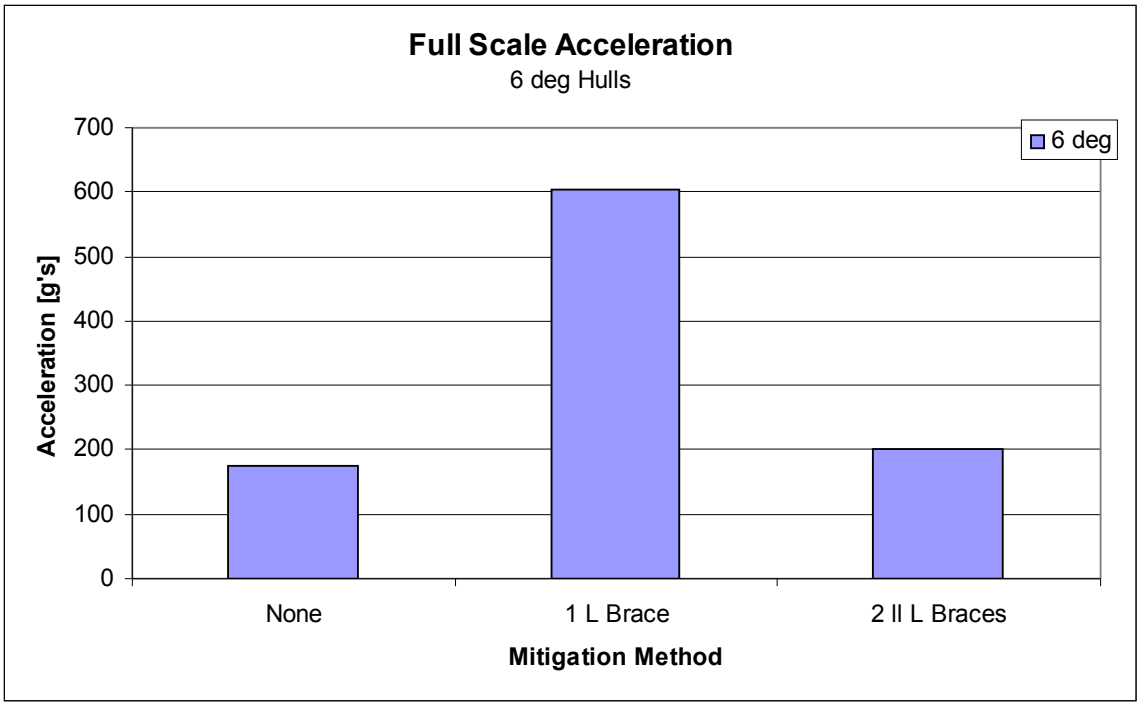

Figure 4.17: Acceleration versus bracing method for 6 degree hulled tests

Figure 4.18 shows the velocity profiles for the tests with 6 degree hulls. Note that there are two tests with no mitigation reported. For the first 0.5 ms, the profiles cannot be easily distinguished. At this time, the hull from the test with one L brace strikes the brace causing the sudden increase in velocity which causes an acceleration nearly 3.5 times greater than the average of the tests with no mitigation. The test with 2 parallel braces seems to perform better than the tests with no mitigation until approximately 1.1 ms, when the braces are hit by the hull. These braces are not hit nearly as violently as the single brace, due to them not being directly above the explosive charge. It is apparent from both the velocity profiles and the plastic deformation of the bracing after a test if a brace is hit by the hull or not, as can be seen in Figures 4.18 and 4.19. Examination of both the velocity

profile and the severity of the plastic deformation suggests how violently the brace was impacted by the hull.

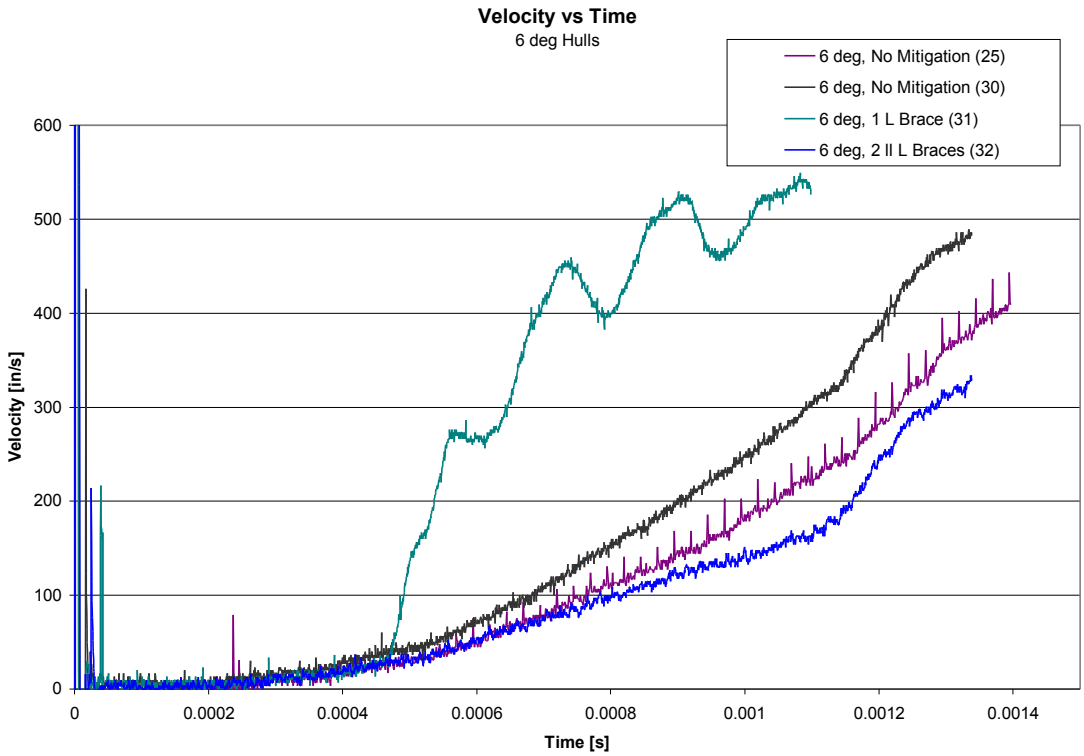

Figure 4.18: Velocity profiles for tests with 6 degree hulls

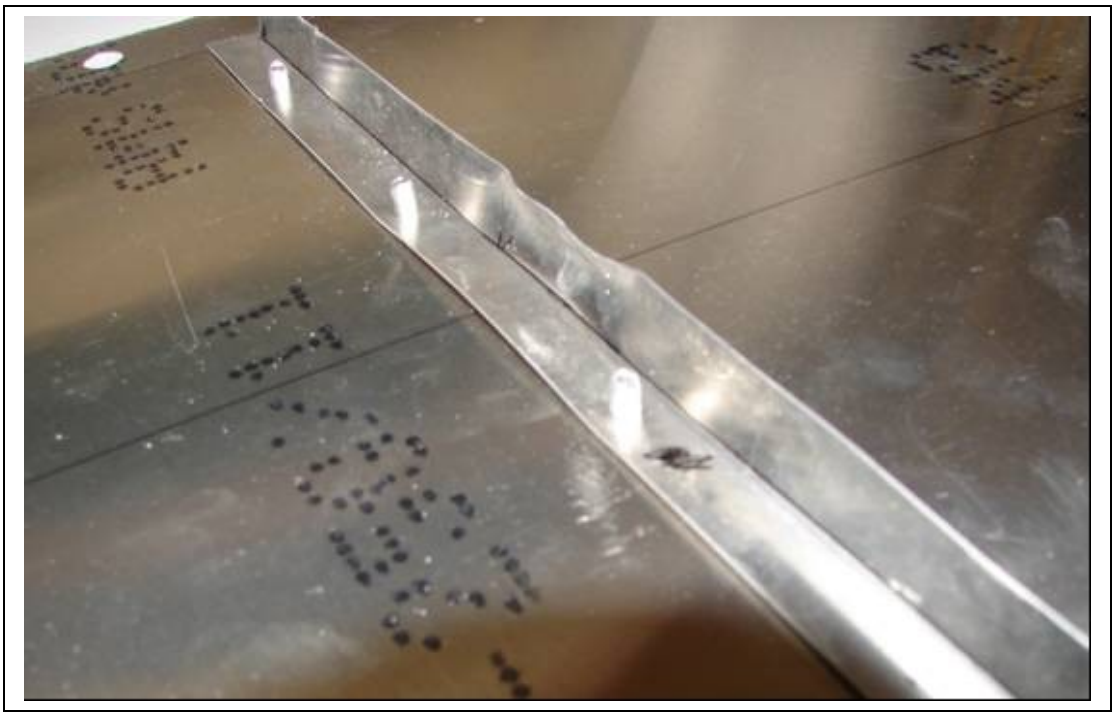

Figure 4.19: Plastic deformation of L brace from test 31 (1 L brace, 6 degree hull)

Tests 25 and 30 in Figure 4.18 show the possible variation in tests with repeated conditions. The cause for the variation is most likely due to the random magnitude variations of the forcing function on the target at constant distance from the explosive's center. These arise from the imperfections in the environment between the charge and target. Previous testing in the Dynamic Effects Laboratory has shown significant pressure variations at gages on points on a target which are symmetrically positioned around the detonated charge. Figure 4.20 shows a frame from a high speed video taken in the Dynamic Effects Laboratory showing the 'fingers' of high pressure spikes of sand from a charge buried at the same depth as those in this thesis that have hit a rubber target. If one of these high pressure spikes hits directly on the edge where the target hull is bent, it could account for the higher acceleration seen in test 30 than in test 25, when the spike may have hit off center to the edge, allowing more of the impulse to be deflected.

Figure 4.20: High pressure 'fingers' from the explosive detonation of Detasheet buried at 0.30 in shows how complicated a forcing function on a target can be

4.5.2 Effects of Bracing on 13 degree Hulled Models

Figure 4.21 shows the maximum acceleration versus bracing type for tests with 13 degree hulls. Notice that in addition to the three basic tests which are conducted for all angled hulls, there are two additional tests in this series: 2 perpendicular L braces and 1 U brace. Both the additional bracing methods were described in Chapter 3.

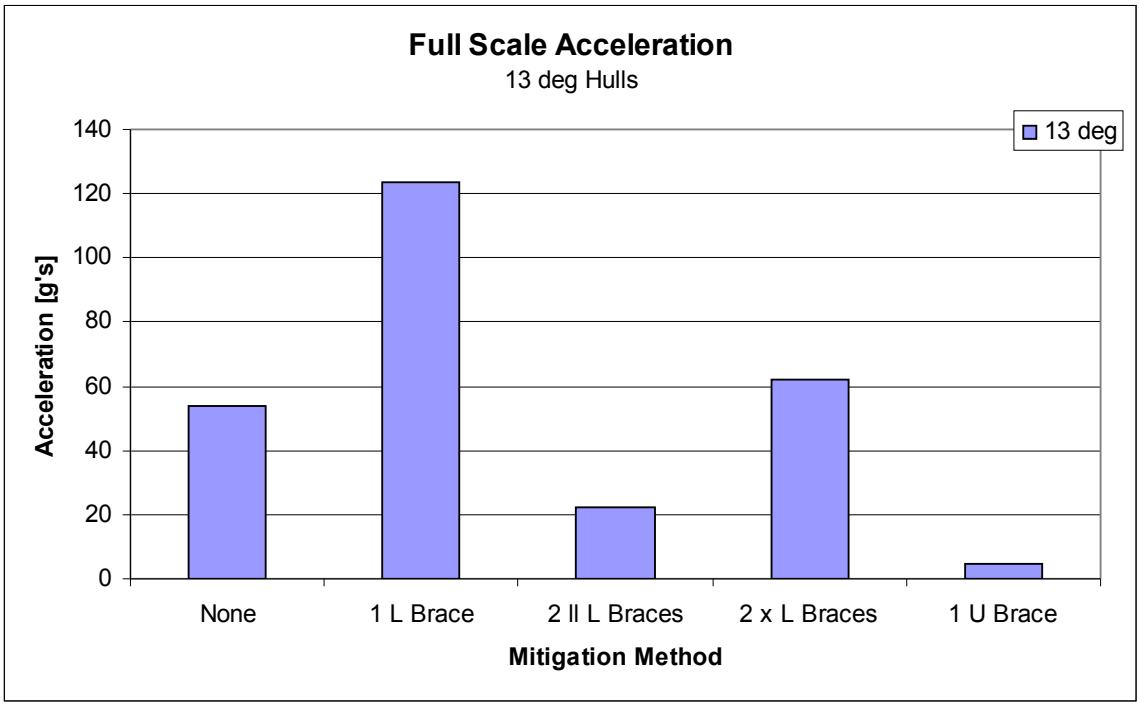

Figure 4.21: Maximum acceleration versus bracing method for 13 degree hulls

The single L brace in this test shows similar behavior to that observed in the 6 degree hulled tests because the hull hit the brace. However, from examination of both the velocity profile in figure 4.22 and the plastic deformation of the brace, the brace was not hit nearly as violently as the brace with the 6 degree hull. The test with 2 parallel L braces resulted in a 59% decrease in acceleration compared to the test with no bracing. Examination of the 2

parallel braces shows that one of the braces was hit by the hull during the test, however it was not hit until after the gage had broken from the floorboard and the data collection was not effected (Figure 4.23).

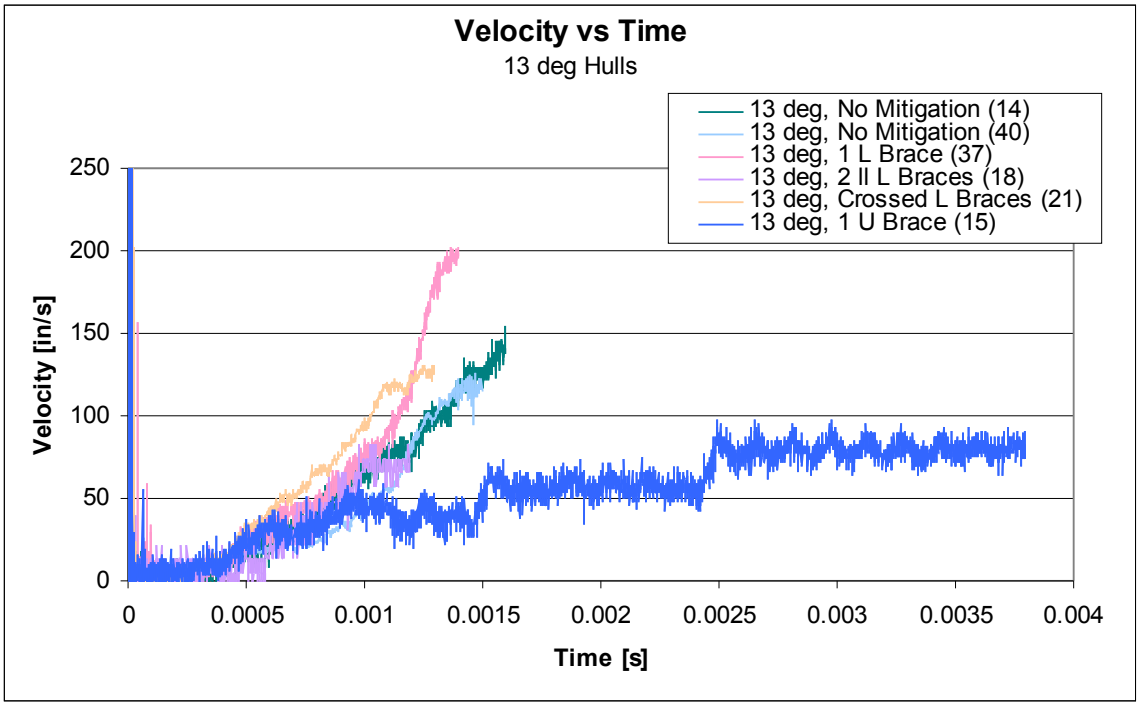

Figure 4.22: Velocity profiles for tests with 13 degree hulls

The test with 2 crossed L braces shows a larger acceleration than any of the test with a 13 degree hull besides the single L braced test. The reason for this is that it had a brace in the same location as the single L brace test, which again was hit by the hull. However, it is notable that this test still results in a 50% decrease in acceleration compared to the single L brace test. The acceleration of the crossed L braces was only 14% higher than the non-braced test with a 13 degree hull. This suggests that the added stiffness from the two braces could successfully mitigate the blast effect from an explosive.

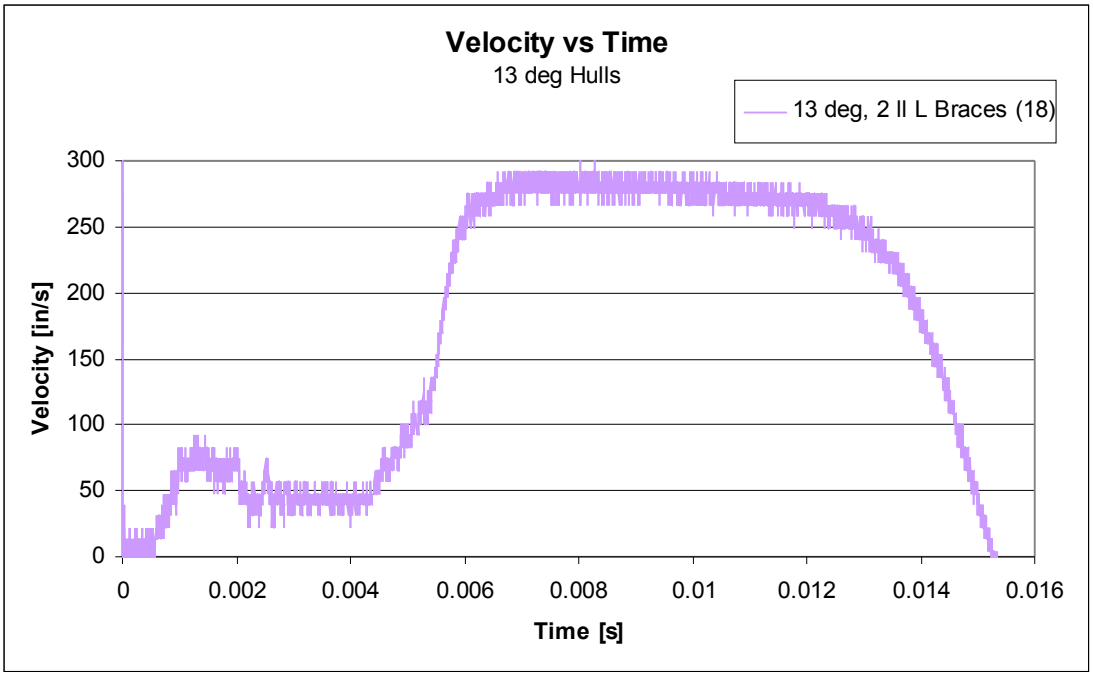

Figure 4.23: Velocity profile from 13 degree hull with 2 parallel braces shows the bracing was not hit by the hull during the initial acceleration

The test with a single U brace resulted in the lowest acceleration seen from any of the tests with 13 degree hulls. In fact, this test resulted in an acceleration 77% lower than the next lowest of any test in this thesis (20 degree hull with 2 parallel L braces). This can be accounted for because the moment of inertia of the U brace was 1.5 times higher than that of the L brace. Furthermore, because of its geometry, it was less likely to bend out of original form into one with a smaller moment of inertia during loading, which can further reduce the effectiveness of the L braces. However, it should be noted that if the entire waveform recorded from the test with the U brace is examined, the brace was not struck by the hull until after the velocity gage was broken off the floorboard, as seen in Figure 4.24. There was a very large acceleration of the floorboard after the U brace was hit. As discussed previously, the nearly constant 'velocity' portions of the graph occur when the

gage is free from the floorboard and the rapid decline of 'velocity' at the end of the waveform is when the gage has left its linear region and is no longer useful for collecting data.

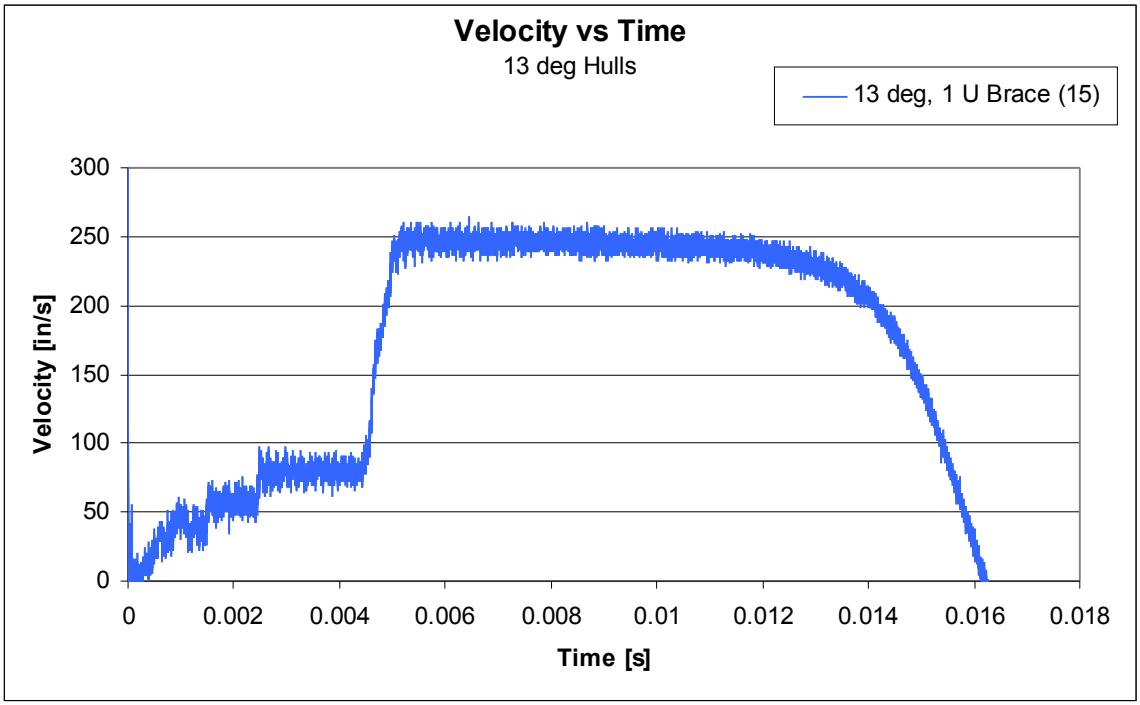

Figure 4.24: Induced voltage multiplied by the gage calibration factor versus time for the 13 degree hulled test with a U brace supporting the floorboard

4.5.3 Effects of Bracing on 20 degree Hulled Models

Figure 4.17 shows the acceleration as a function of bracing for tests with 20 degree hulls. This graph shows that as the number of braces used to reinforce the floorboard is increased, the maximum acceleration of the floorboard is decreased. Because neither the braces nor the floorboard are hit by the hull, this reinforces the idea that bracing the floorboard can be used effectively mitigate the effects of an explosive blast as experienced on the floorboard, provided that the hull does not make contact with the bracing. The single L brace reduces the acceleration compared to the non-braced test by 21%. The test with two parallel L braces reduces the acceleration compared to the test with no bracing by 52%. This is comparable to the 59% reduction seen in the tests with the 13 degree hulls.

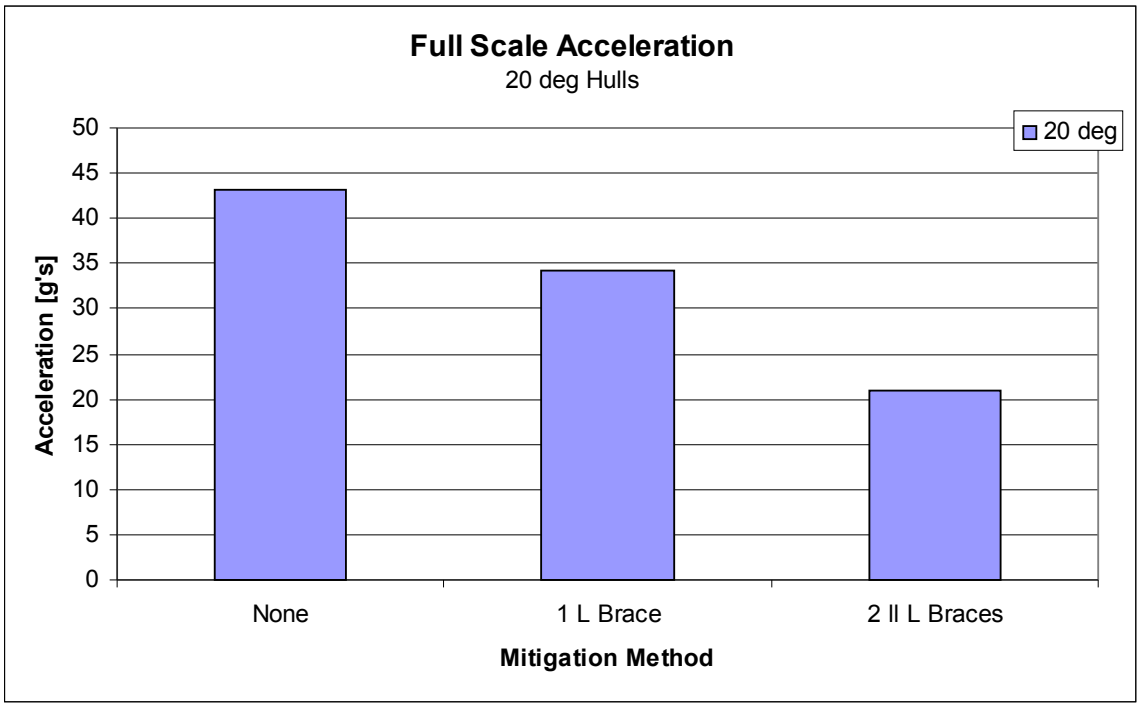

Figure 4.25: Acceleration versus bracing for 20 degree hulls

4.5.4 Summary of Mitigation Effects of Bracing

Testing shows that the use of bracing to support the floorboard of the target vehicle can reduce the acceleration of the floorboard in the vehicle caused by an explosive detonation underneath the vehicle. However, the bracing makes the acceleration worse if it is hit by the hull. Therefore, when designing bracing, one must take care to ensure that the risk of it being hit by the vehicle hull is minimized.

Increasing the moment of inertia of the brace, and strengthening it so that it does not easily bend out of original form can greatly reduce the acceleration of the floorboard. However, like before, if the brace is hit by the hull, the floorboard experiences a large acceleration. Therefore, a brace will be most effective if it has a high moment of inertia and a low profile, so as to minimize the risk of the brace being hit by the hull.

4.6 *Effects of Foam Filling Between Floorboard and Hull*

One method used to attempt to mitigate the acceleration caused by the explosive blast was to absorb the impulse delivered to the floorboard by filling the gap between the floorboard and hull with foam. All testing of this kind was done with 6 degree hulls, where the acceleration previously seen was worst. One test used foam to fill the gap between a hull and floorboard with no other mitigation method. A second test used the foam filling in addition to a single L brace, which was installed in the same way as the single L brace with no foam. The acceleration from these tests can be seen with the 6 degree hulled tests with no foam in Figure 4.26.

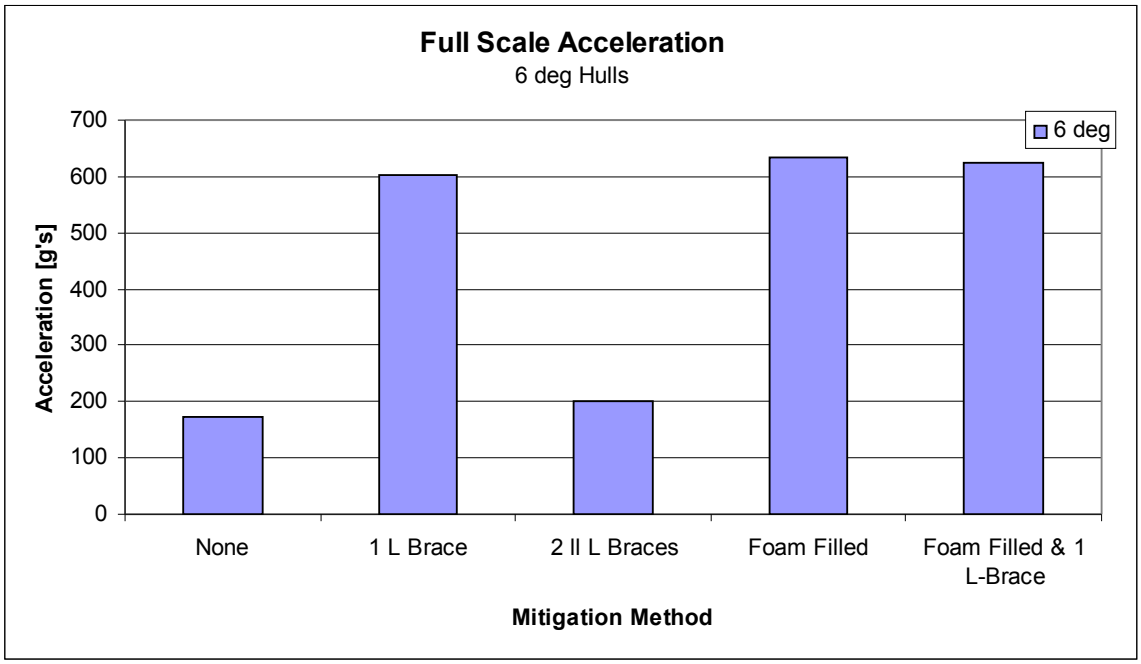

Figure 4.26: Acceleration from tests with 6 degree hulls

The maximum full scale acceleration from the foam filled test was 633 g's, which is a 4.9% increase over the test with a single L brace and no foam filling. The test with foam and an L brace resulted in a 623 g acceleration, which is a 3.3% increase compared to the single L

brace with no foam filling. What is most notable about the tests with foam filling the gap is that their velocity profiles (Figure 4.27) seem nearly identical to each other and show that the acceleration in these tests acted over a longer time period than for the single L brace with no foam. Note that at approximately 0.58 ms, the test with a foam filled gap and L brace exceeded the maximum range of the oscilloscope, so that the velocity profile was no longer able to be recorded after this time. The velocity profiles show that the foam, which it was hypothesized would absorb some of the energy from the blast, actually transmitted the energy very efficiently from the hull to the floorboard.

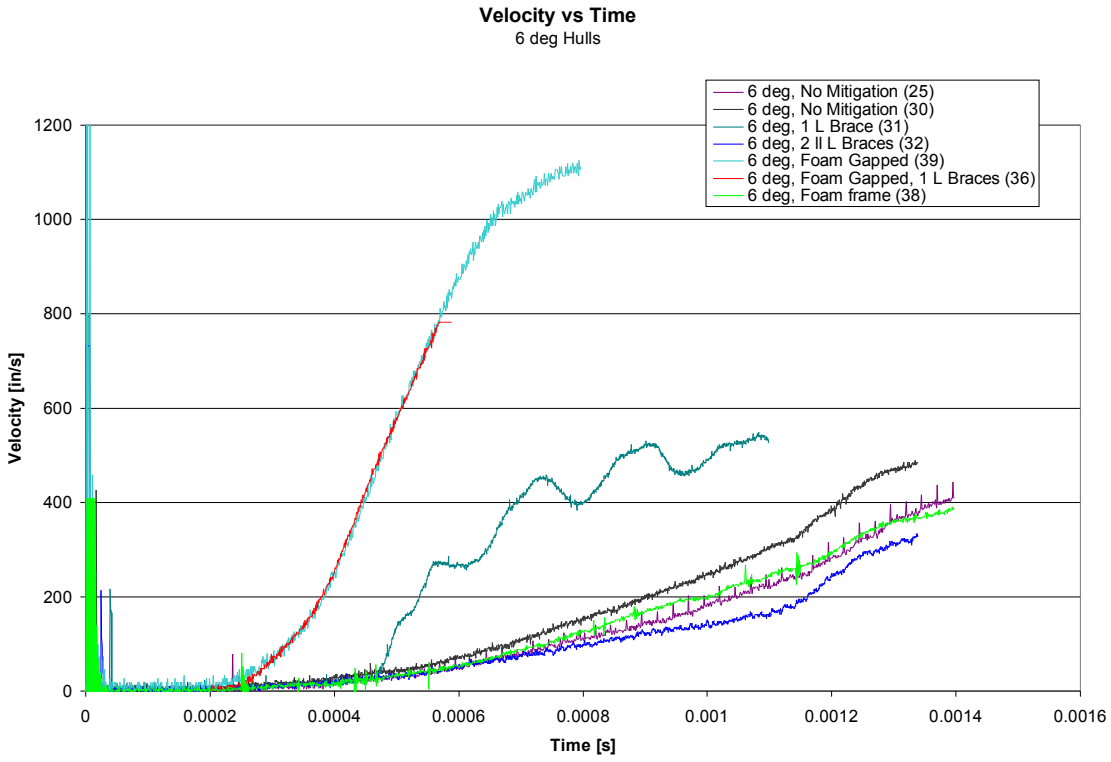

Figure 4.27: Velocity profiles for 6 degree hulls show that foam filling imposes a large acceleration on the floorboard for a sustained period of time

4.7 *The Effects of Using Foam Framing*

One method used to mitigate the acceleration of the floorboard from the explosive blast was building a foam frame to go in-between the floorboard and the hull. This frame had the same dimensions as the aluminum ones used in other tests, but the model was held together with epoxy instead of bolts, as discussed in chapter 3. The velocity profile and acceleration results from this testing condition can be seen along with the other tests with 6 degree hulls in Figures 4.27 and 4.28, respectively.

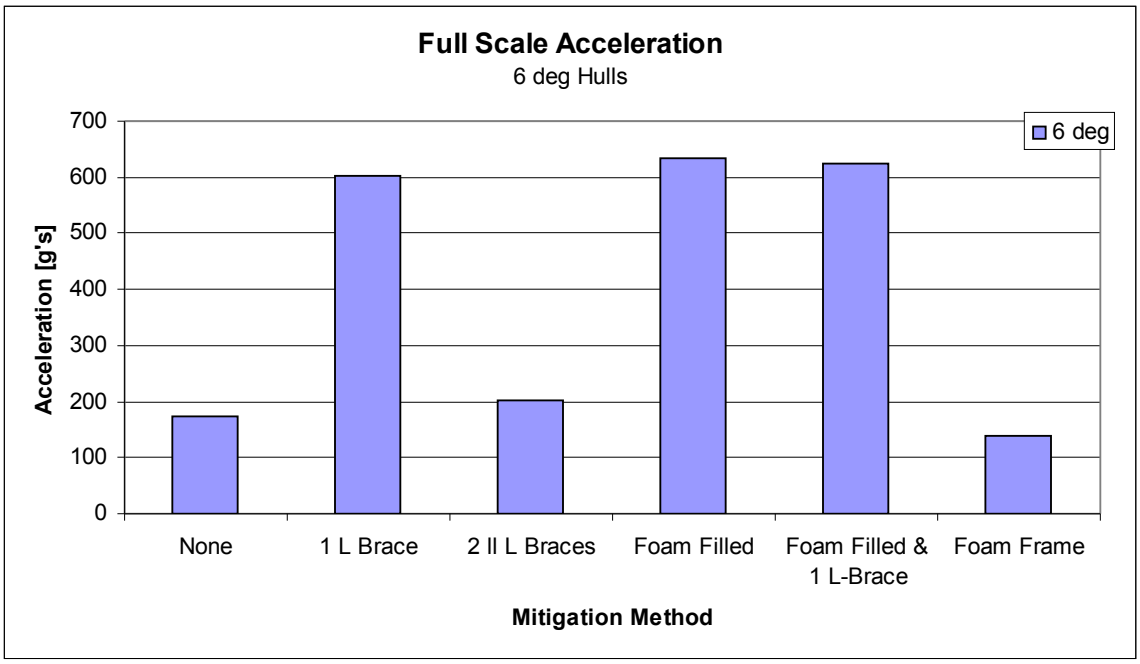

Figure 4.28: Full scale accelerations from tests with 6 degree hulls

The test with foam framing shows that this method does not improve the mitigation effects of the blast on the floorboard. From the velocity versus time graph, it easily seen that the profile from the foam frame lies in-between the two tests with aluminum framing. The acceleration from the foam framed test is 5.3% lower than the aluminum framed test in

which the floorboard was not hit by the hull, and 31% lower than the aluminum framed test in which the floorboard was hit by the hull. This suggests that the loading experienced first at the center of the floorboard is caused from compression of the material between the floorboard and hull, not from a stress wave traveling from the hull through the frame and into the floorboard. This can also be visually confirmed by the high-speed video because the gage begins to move before the floorboard around it, confirming that the loading of the floorboard occurs first at the point above the charge. If the loading were caused by a stress wave traveling from the hull through the aluminum frame and into the floorboard, then one would see deformation at the edges of the floorboard, near the frame, before the center of the floorboard.

4.8 *The Effects of Changing the Stand off Distance*

In addition to the tests discussed above, which all had a SoD of 3.19 in, several tests were conducted to examine how the SoD affects the floorboard acceleration. Figure 4.29 shows the accelerations recorded for all tests with like models and DoB's, but different SoD's. Table 4.3 shows the corresponding values.

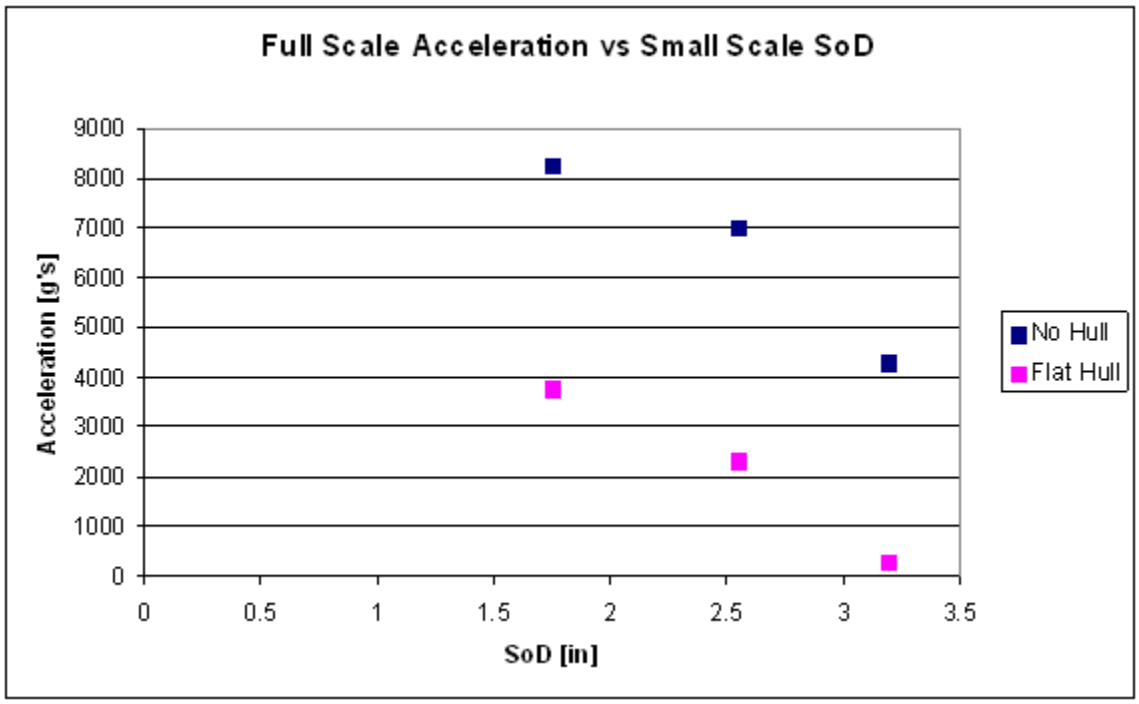

Figure 4.29: Full scale accelerations for tests with varying SoD

Acceleration Values (DoB=0.30 in)					Small Scaled	Full Scaled
Test #	Conditions	Hull Angle	# Braces	SoD [in]	Acceleration [g's]	Acceleration [g's]
12	No Hull	N/A	0	1.75	108529	8259
44	No Hull	N/A	0	2.55	92163	7014
17	No Hull	N/A	0	3.19	56646	4311
11	0 deg	0	0	1.75	49590	3774
43	0 deg	0	0	2.55	30551	2325
22,23,42	0 deg	0	0	3.19	3839	292

Table 4. 3: Full scale acceleration values for tests with different SoD values

The test series with no hull and with a 0 degree hull both show significant decreases in the floorboard acceleration as the stand off distance is increased. Increasing the SoD from 1.75 in to 2.55 in results in a 1246 g and 1449 g reduction of full scale acceleration for models with no hull and a flat hull, respectively. Similarly, increasing the SoD from 2.55 in to 3.19 in results in a 2703 g and 2033 g reduction of full scale acceleration.

Increasing the SoD had the second greatest mitigation effect investigated in this thesis. Adding a hull to the test had the greatest mitigation effect. At a SoD of 1.75, 2.55, and 3.19 the accelerations of the floorboards with flat hulls were reduced by 4485 g, 4689 g, and 4019 g, respectively, from tests with no hulls. These results agree with the results in section 4.3 on the effects of a hull for SoD of 3.19 in.

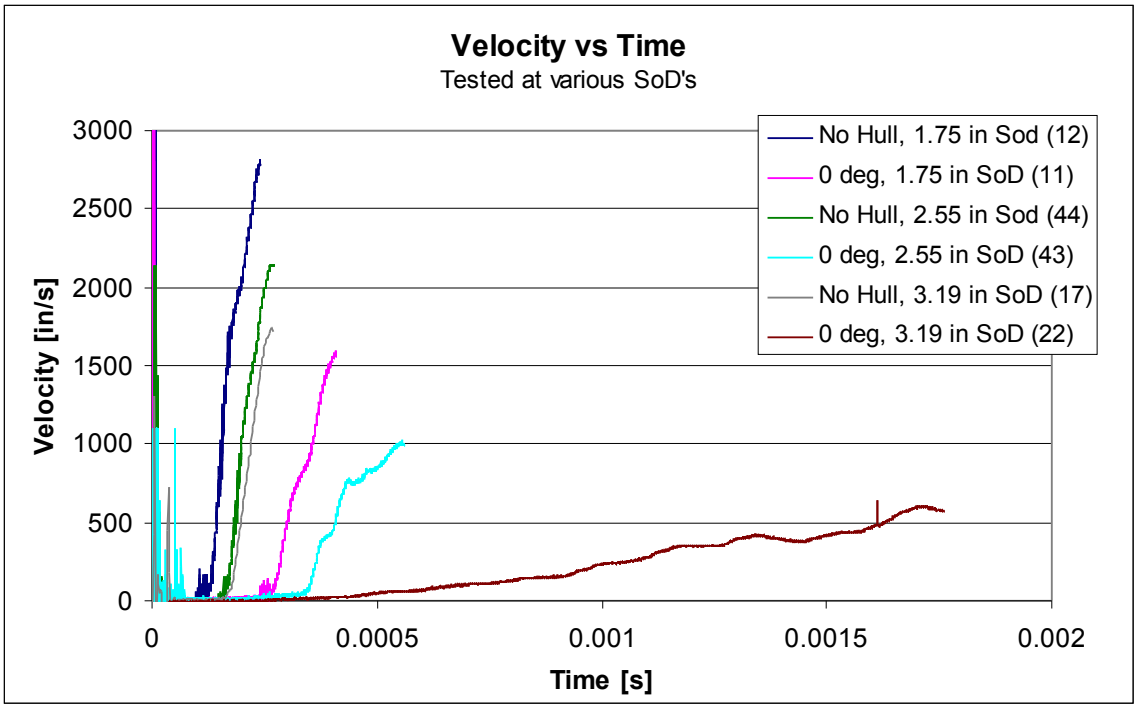

Figure 4.30: Velocity Profiles for tests conducted at various stand of distances

Figure 4.30 shows the velocity profiles for the tests conducted at various SoD's. The trends seen in the maximum acceleration distribution are confirmed by the velocity profiles. The test with no hull and a 1.75 in SoD produced the largest acceleration and for a more sustained period than the other tests with no hull. The test that combined a hull and 3.19 in SoD resulted in acceleration over a long period, but of a much smaller magnitude than all the other tests. The tests in this section show that when designing a vehicle susceptible to mine blasts, the best defense will include both a hull and as much ground clearance as possible.

Ch 5: Summary and Conclusions

This thesis discusses research done at the Dynamic Effects Laboratory in the Mechanical Engineering Department of the A. James Clark School of Engineering at the University of Maryland, College Park. The goal of the research was to investigate how various mitigation methods reduced the maximum acceleration of the floorboard of hulled vehicles when explosive charges buried in water saturated sand were detonated beneath them. Small scale testing was conducted, which used bar magnet velocity gages to measure the velocity as a function of time of the center of the floorboard, directly over the charge, where the acceleration was expected to be greatest. The velocity curve could then be differentiated in order to obtain acceleration values. Mitigation methods investigated include the use of a hull, various hull geometries, the used of bracing to support the floorboard, foam filling between the floorboard and hull, and the use of foam to isolate the shock in the hull from the floorboard. The effects of changing the vehicle stand off distance were also explored.

Analysis of the tests conducted showed that the two methods which most greatly reduced the acceleration of the vehicle floorboard are adding a hull to the vehicle and increasing the vehicle stand off distance. Increasing the vehicle stand off distance may cause additional problems such as making a vehicle more likely to tip over or causing difficulties for personnel to easily enter and exit the vehicle, but these effects were not investigated. Adding a hull would be relatively easier, however would likely decrease the vehicle's ground clearance. This could make the vehicle less mobile and be in conflict with the goal of increasing the stand off distance. Therefore, while adding a hull to a vehicle and

increasing the floorboard stand off distance can greatly mitigate mine blasts to a vehicle, a designer must carefully examine the various other effects which taking these actions might produce.

Making the vehicle hull into a V-shape, can deflect some of the blast pressures from a mine and reduce floorboard accelerations. The mitigation effects as the hull angle is increased are greater while the angle is small, but after the hull angle is about 13 deg, the effects of increasing it further are marginal. Angling the hull can also help mitigate the blast effects by increasing the space between the floorboard and hull, which makes the hull less likely to hit the floorboard, or some other material attached to it, causing large accelerations. Large hull angles significantly reduce the vehicle ground clearance. Furthermore, angling a hull is likely to increase the likelihood of a vehicle tipping over during a mine attack if the mine is off center of the vehicle. The likelihood of the vehicle tipping was not investigated in this thesis. Designers of vehicles can mitigate mine blasts with the use off a V-shaped hull, which will deflect blasts and minimize the risk of the hull hitting the floorboard. However, before implementing this into their design, they must consider factors such as necessary vehicle ground clearance or likelihood of the vehicle tipping over due to an attack.

The bracing system necessary to support the floorboard of the vehicle in ordinary use can be designed to also help minimize damage during a mine attack. The bracing system should have a large area moment of inertia about all axes so that it resists high floorboard accelerations and is unlikely to be bent. The bracing should be designed to be as low profile as possible, because, if it is hit by the hull, it will transmit a large amount of energy from to the floorboard causing very high accelerations.

The use of foam to fill the gap between the floorboard and hull had negative mitigation effects, both with and without floorboard reinforcement with bracing. The accelerations were comparable to those when the floorboard bracing was hit by the hull, but acted over a longer period of time. While some other materials might be able to absorb some of the pressures from an explosive blast, the foam used in this thesis greatly increased the damage during a mine blast.

The use of foam to isolate the floorboard from the shock in the hull during a mine blast attack did not reduce the floorboard acceleration. However, the foam used to isolate the floorboard was seen to transmit shock from the floorboard to the hull very well during the foam filling tests. Therefore, because the foam tested did not mitigate stress waves, it cannot be concluded that a more efficient system to isolate the floorboard from the hull will not produce positive mitigation effects.

Ch 6: Future Work

This chapter discusses future work which the Dynamic Effects lab can do to continue the work discussed in this thesis. Some of the discussed research methods have had preliminary work done already.

6.1 Expansion of the Test Matrix

In order to better understand potential mitigation methods, the amount of tests could be expanded by conducting tests with all the combinations of hulls, bracing, and foam filling and bracing. The tests which could be conducted to complete the matrix would include the foam filled and bracing tests for all angles that have not been conducted. Additional testing conditions could include additional hull angles and other geometries besides simple angles; different types of floorboard framing; different materials filling the gap between the floorboard and hull; and different methods to isolate the floorboard from the hull to reduce shock transmission. Besides changing the mitigation methods, testing could also be done with additional stand off distances and depths of burial.

The velocity gages could be improved by experimenting to determine how small the gages could be made before they became non-linear during testing. Decreasing the mass of the gages would make the tests less intrusive so that the data would be more accurate. This could quickly be done by shortening the coil lengths, because the gage always broke off the floorboard before the gage left the linear region (which is when the data is no longer describing the floorboard behavior). It is unlikely the velocity gages will continue being

used because two methods are currently being developed to gather more data in a less intrusive manner, as discussed below.

6.2 Data Filtering

In order to calculate acceleration vs. time curves, LabView digital filtering methods were used. Attempts were made to use high pass, band bass, band stop, and rolling average filters as well as curve fits to get velocity curves which could be differentiated to obtain acceleration curves over time. While these attempts showed promise, more work must be done in order to refine the method so large oscillations are not seen in the acceleration profiles, making them more accurately describe what is occurring with the target.

Figure 6.1 below shows a typical raw and filtered velocity profiles from Test 18. The raw data is in orange along with the processed data in black. Note that the abscissa shows time in seconds. The raw data was processed through a low pass filter followed by a 20 point rolling average. The filtered graph was shifted to center it more accurately with the raw data, and it appeared that the slope of the filtered data was lower than that of the raw data. The filtered data is still characterized by the oscillations which are apparent in the raw data. As can be seen in Figure 6.2, this causes significant oscillation in the resulting acceleration in time profile. Clearly, the raw data must be shielded better from noise and filtering attempts must be improved before the acceleration profiles will be useful for data analysis. As suggested when shifting the velocity profiles to be more uniform, the maximum acceleration from the filtered velocity (18 g's) was less than that from the raw data (22 g's).

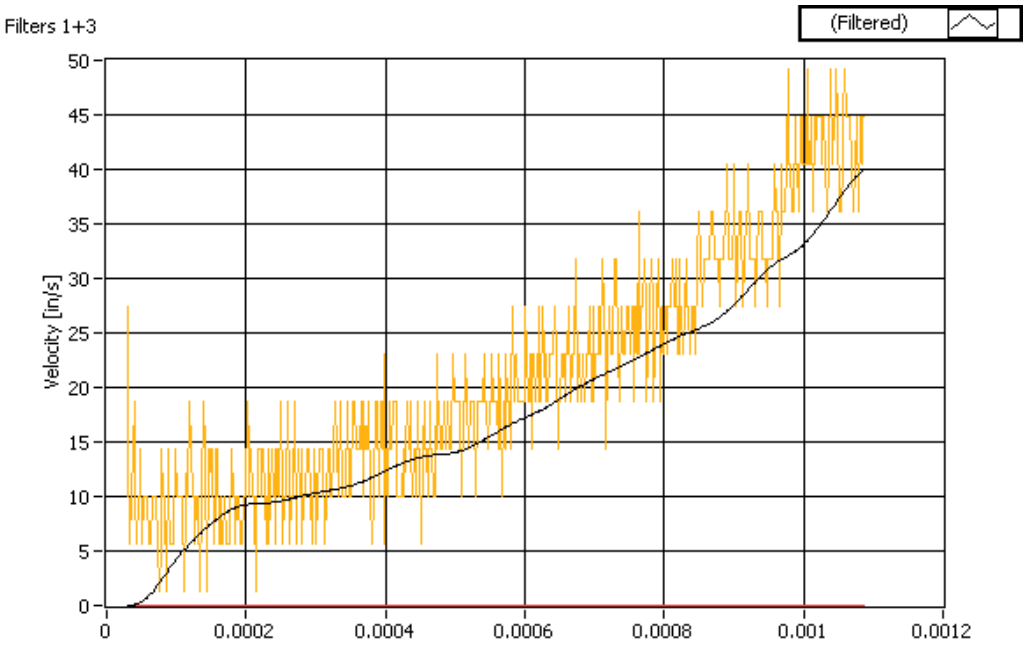

Figure 6. 1: Test 18 raw velocity (orange) and filtered velocity (black) profiles in time [s]

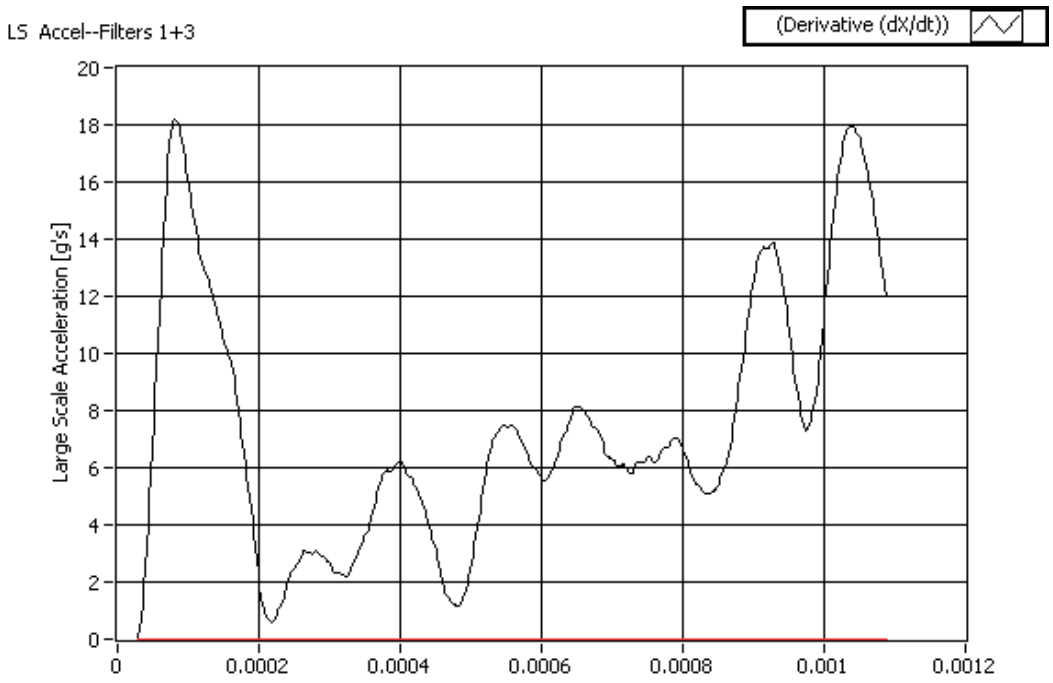

Figure 6.2: Test 18 full scale acceleration in time profile resulting from filtered velocity profile

6.3 Helmholtz Coil Velocity Gages

Currently, work is being done in the Dynamic Effects lab to develop a Helmholtz coil velocity gage which can be used to track similar data to that reported in this thesis. The Helmholtz coil velocity gages are advantageous to the velocity gages above because they are less intrusive and allow data to be collected from several points in a single test, making it possible to develop a mapping of the floorboard motion.

The Helmholtz gages work by electromagnetic induction, similarly to the above gages. Two coils are placed some distance from each other with a mutual axis. A constant voltage is applied to the two coils, which are attached in series to ensure the same current in both of them. Between the coils, there is a region with a relatively uniform magnetic field is induced with flux lines parallel to the coils' axis. This field strength can be predicted relatively accurately by analytical treatment [6.1] or by the use of a Tesla meter. Both of these methods show similar results when conducted in the Dynamic Effects lab. Figure 6.3 shows the analytical prediction for magnetic field strength in pink, which is based on the measured current through the coils and the resistance through the coils for each measurement. The corresponding measured field strengths are shown in blue.

A short length of wire is placed on the target so that it is perpendicular to both the magnetic field flux lines and the motion of the target after explosive detonation. Because the magnetic flux lines, the gage wire, and the gage motion are all mutually perpendicular, there is an induced motional emf given by:

$$\varepsilon = vlB$$

where v is the target velocity, l is the length of the gage wire, and B is the magnetic field strength.

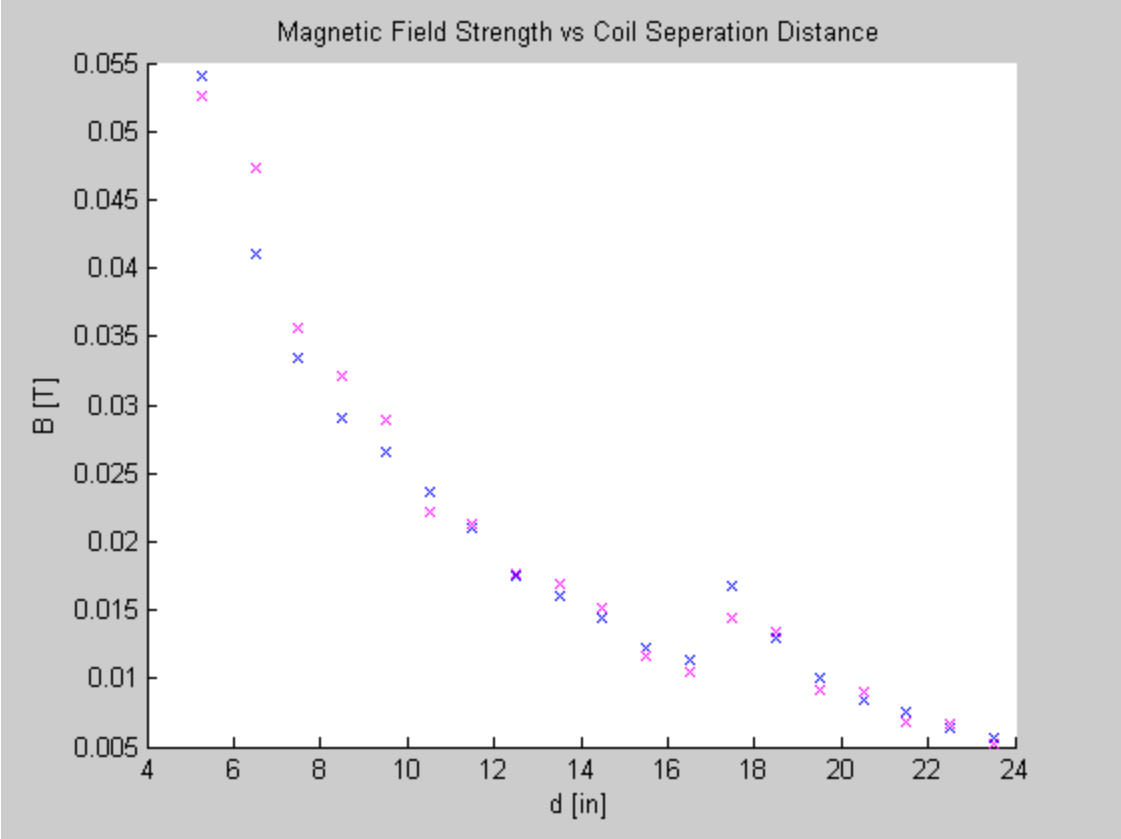

Figure 6. 3: Analytical (pink) and measured (blue) magnetic field strength vs coil separation distance

Because the only item in contact with the target is the length of wire and the leads going from it to the oscilloscope, this gage has a small enough mass that it will not significantly affect the behavior of the target. This ensures that the data collected is more accurate and allows for multiple gages to be attached at various locations of the target. Furthermore, it has been found that the gage will generally not separate from the target, which allows a much longer history to be taken than with the gages discussed in this thesis.

Tests with similar targets as the ones in this thesis have not successfully been completed. This is mainly due to the inability with current equipment to generate a strong enough magnetic field over a large enough region to conduct this test. However, several tests have been conducted with a 2 in x 2 in x 0.75 in aluminum block. Most of the tests have a zero SoD. These tests produce similar results to what is expected from the theory above, but will require additional efforts to become fully understood. A sample waveform from one of the calibration tests can be seen in Figure 6.4, below. The voltage drop seen after the initial spike seems to be due mainly to the lead wire spinning off axis so that the effective wire length, l, is shortened. At about 15 ms, the sudden voltage drop is due to the target hitting a stop near the top of the coils. Using high speed video footage, this timing has been verified. It was also seen that there was minimal lead wire movement before this time, and significant movement after the target hits the stop.

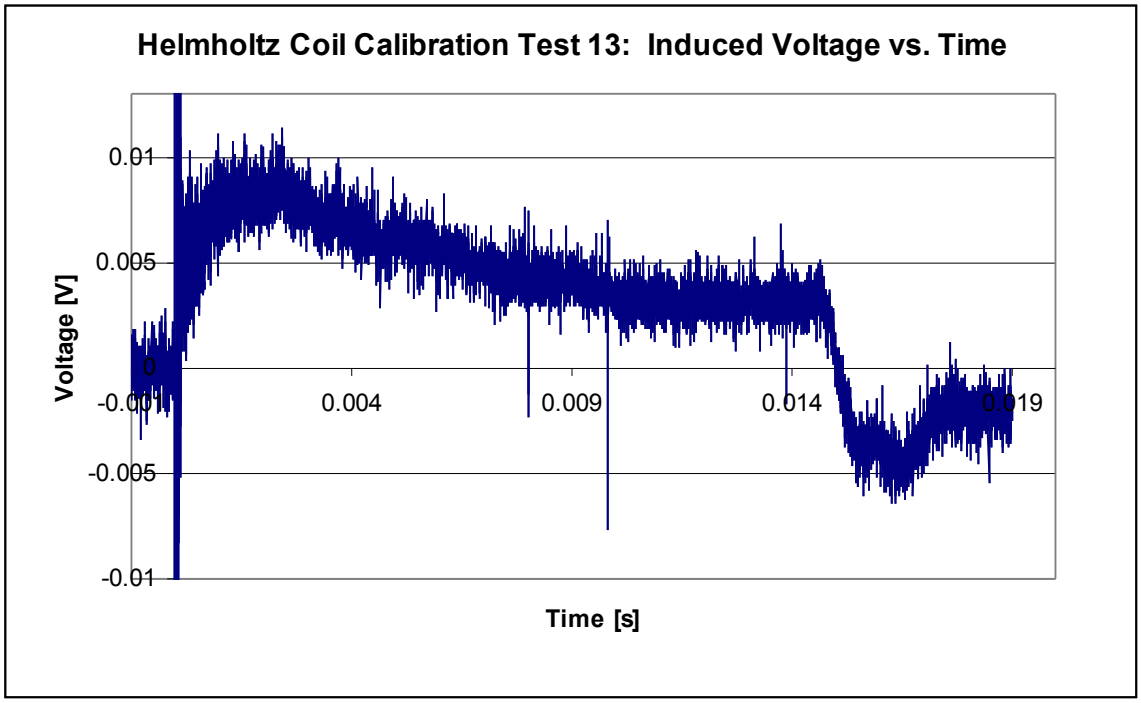

Figure 6.4: Induced voltage versus time for Helmholtz coil calibration test number 13

Some difficulties have been encountered while developing these gages. One difficulty has been generating a field strong enough to induce a usable voltage across the gage wire and making that field uniform over a large enough region so that the gage output is linear. One likely method to alleviate this problem will be to build larger coils with more loops than the one currently being tested. Another difficulty has been ensuring that the lead wires are parallel to the magnetic flux lines and that they move as little as possible, so that they will induce only negligible or predictable voltages. Camera footage has shown that this problem is minimal for the initial target motion, but becomes more significant at later times, which will make recording long histories of the target motion difficult. The induced voltage from the initial acceleration of the target in the calibration tests has been largely overwhelmed by the noise caused from the spark in the exploding bridge wire detonation. This means that the acceleration of the target cannot be obtained. When the larger targets are used, this will not be as much of a problem because there will be a larger time delay from when the charge is detonated until when the target begins moving.

6.4 Digital Image Correlation

A second method which is being explored involves digital image correlation using the Vic-3D software developed by Correlated Solutions. This method uses two high speed video cameras which can be synchronized so that each frame can be correlated from both cameras and a displacement in time mapping of the target can be calculated. This method gives a significantly higher number of data points than the Helmholtz velocity gages are capable of. Also, because it is using digital image correlation, there is no physical gage on the target, so that there is no interference with target behavior. The spatial resolution of

this method is better than manually tracking one point with one camera because the software allows for sub-pixel displacement detection. The difficulties associated with this method arise when the data must be differentiated to obtain acceleration. This is because displacement in time information is obtained, so that the data must be differentiated twice and also because the cameras can only be run at approximately 120,000 frames per second. In comparison, the oscilloscopes currently being used can sample at 400 MHz.

Appendix A: Test Data Used in Thesis

This appendix contains the test results from the tests discussed in the body of this text. Most of tests in this appendix have a SoD of 3.19 in and a DoB of 0.30 in. A note will be attached to any test with a different SoD (Tests 11, 12, 43, 44). Note that the test numbers correspond to the test numbers given for the entire mitigation method series. Those test numbers which do not show up either did not have conditions discussed in this thesis or did not provide useful data for some reason (equipment did not trigger correctly, charge did not fully detonate, etc.) Also note that the velocity profiles shown have been cutoff at the point where the coil breaks free from the floorboard, as discussed in Ch3. Some of the profiles have initial spikes which are noise resulting from the detonation, as discussed in Ch3.

The test conditions and accelerations from the tests are shown in Table A.1 and Figure A.1. Note that for test conditions with several tests, the acceleration is the average of listed tests. The individual values can be found below.

Acceleration Values (SoD=3.19 in, DoB=0.30 in)			3.19		Small Scaled	Full Scaled
Test #	Conditions	Hull Angle	# Braces	Foam	Acceleration [g's]	Acceleration [g's]
17	No Hull, No Mitigation	N/A	0	None	56646	4311
22,23,42	0 deg, No Mitigation	0	0	None	3839	292
25,30	6 deg, No Mitigation	6	0	None	2289	174
31	6 deg, 1 L Brace	6	1	None	7926	603
32	6 deg, 2 ll L Braces	6	2ll	None	2651	202
39	6 deg, Foam Gapped	6	0	Gap	8314	633
36	6 deg, 1 L Brace, Foam Gapped	6	1	Gap	8188	623
38	6 deg, Foam Frame	6	0	Frame	1835	140
14,40	13 deg, No Mitigation	13	0	None	711	54
37	13 deg, 1 L Brace	13	1	None	1625	124
18	13 deg, 2 ll L Braces	13	2ll	None	292	22
21	13 deg, 2 x L Braces	13	2x	None	813	62
15	13 deg, 1 U Brace	13	1	None	63	5
27,28	20 deg, No Mitigation	20	0	None	568	43
33	20 deg, 1 L Brace	20	1	None	449	34
35	20 deg, 2 ll L Braces	20	2	None	274	21
Acceleration Values (SoD=2.55 in, DoB=0.30 in)			1.75		**Small Scaled**	**Full Scaled**
Test #	Conditions	Hull Angle	# Braces	Foam	Acceleration [g's]	Acceleration [g's]
44	No Hull	N/A	0	2.55	92163	7014
43	0 deg	0	0	2.55	30551	2325
Acceleration Values (SoD=1.75 in, DoB=0.30 in)			1.75		**Small Scaled**	**Full Scaled**
Test #	Conditions	Hull Angle	# Braces	Foam	Acceleration [g's]	Acceleration [g's]
12	No Hull	N/A	0	1.75	108529	8259
11	0 deg	0	0	1.75	49590	3774

Table A. 1: Acceleration values from all tests

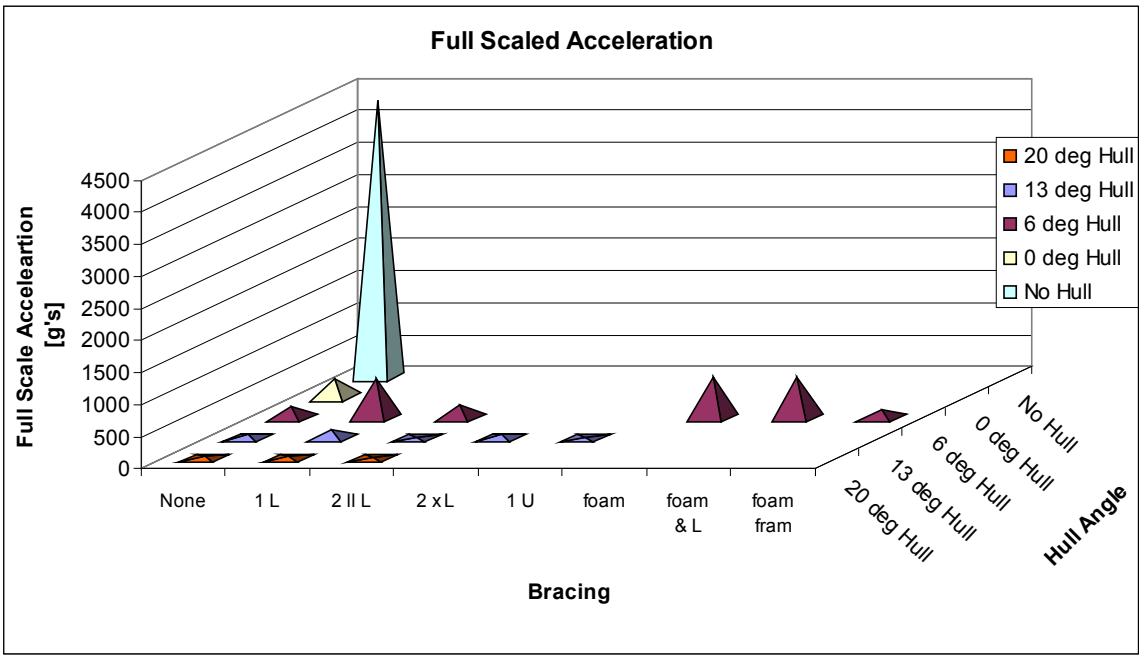

Figure A. 27: Acceleration plot for tests throughout thesis

Test 17: No Hull, No Mitigation

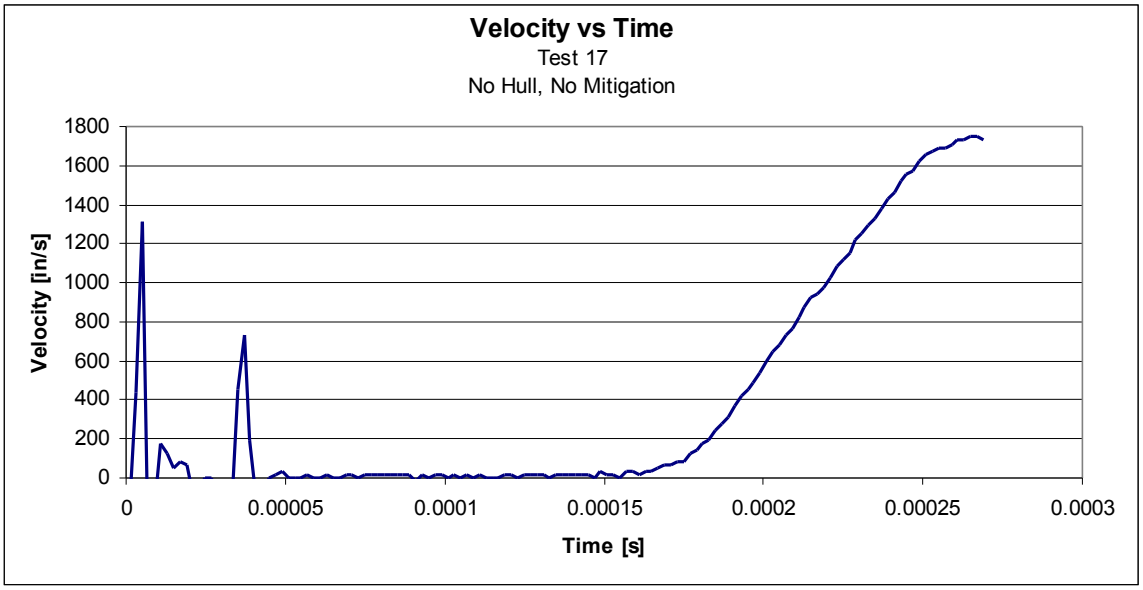

Figure A. 2: Test 17 velocity profile

SoD [in]	DoB [in]	Small Scale Acceleration [g's]	Full Scale Acceleration [g's]
3.19	0.30	56646	4311

Table A. 2: Test 17 conditions and acceleration

Test 22: 0 deg Hull, No Mitigation

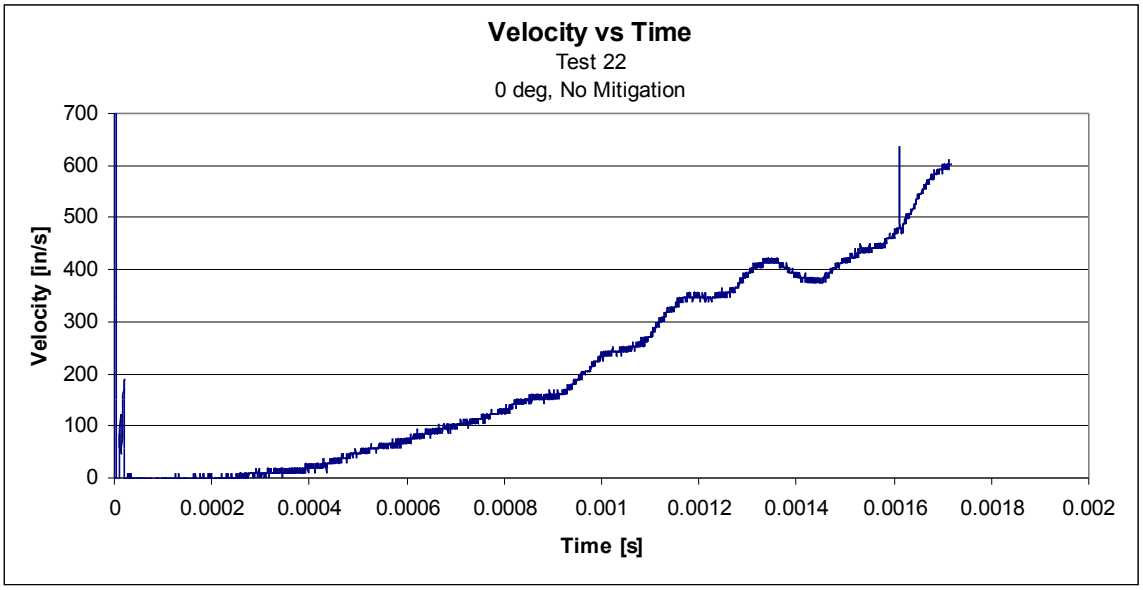

Figure A. 3: Test 22 velocity profile

SoD [in]	DoB [in]	Small Scale Acceleration [g's]	Full Scale Acceleration [g's]
3.19	0.30	4268	325

Table A. 3: Test 22 Accelerations

Test 23: 0 deg, No Mitigation

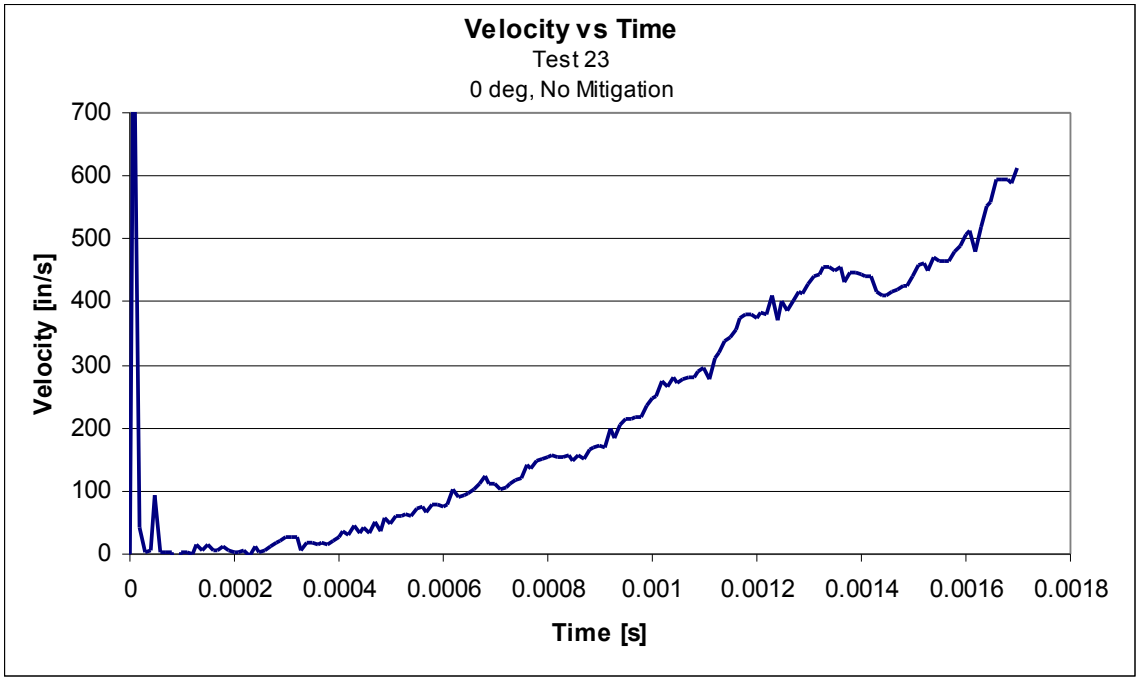

Figure A. 4: Test 23 velocity profile

SoD [in]	DoB [in]	Small Scale Acceleration [g's]	Full Scale Acceleration [g's]
3.19	0.30	3693	281

Table A.4: Test 23 conditions and acceleration

Test 42: 0 deg, No mitigation

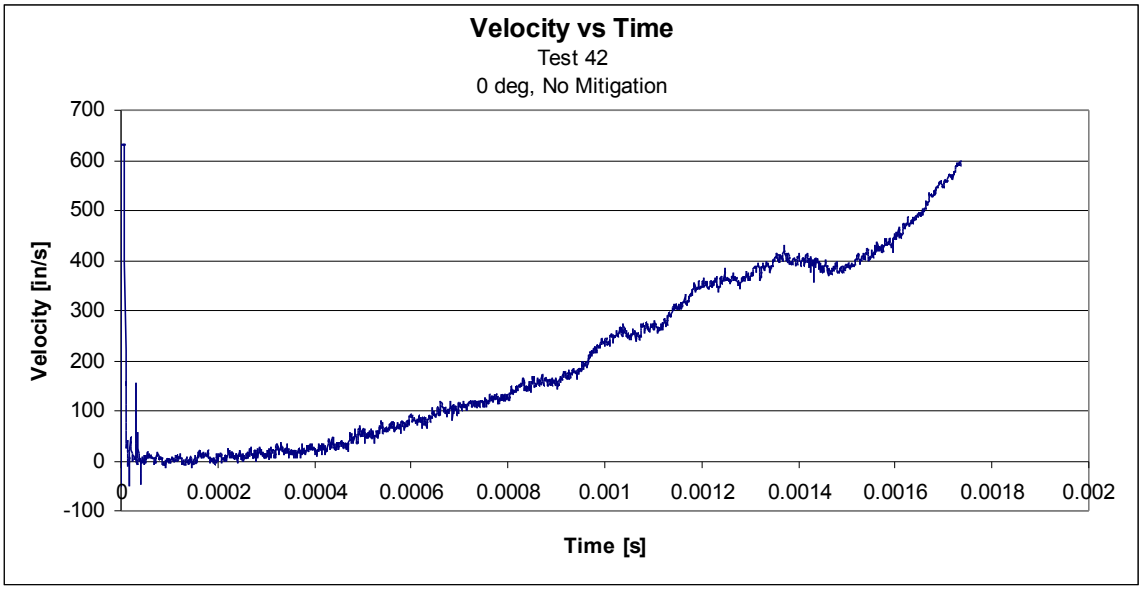

Figure A. 5: Test 42 velocity profile

SoD [in]	DoB [in]	Small Scale Acceleration [g's]	Full Scale Acceleration [g's]
3.19	0.30	3556	271

Table A.5: Test 42 conditions and acceleration

Test 25: 6 deg, No Mitigation

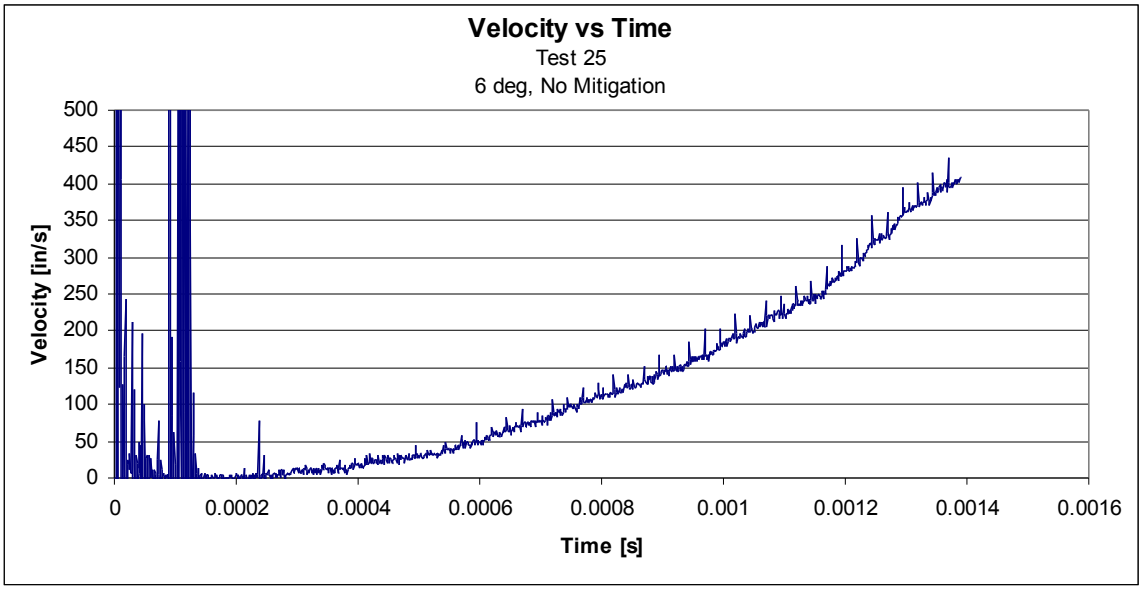

Figure A.6: Test 25 velocity profile

SoD [in]	DoB [in]	Small Scale Acceleration [g's]	Full Scale Acceleration [g's]
3.19	0.30	1936	147

Table A.6: Test 25 conditions and acceleration

Test 30: 6 deg, No Mitigation

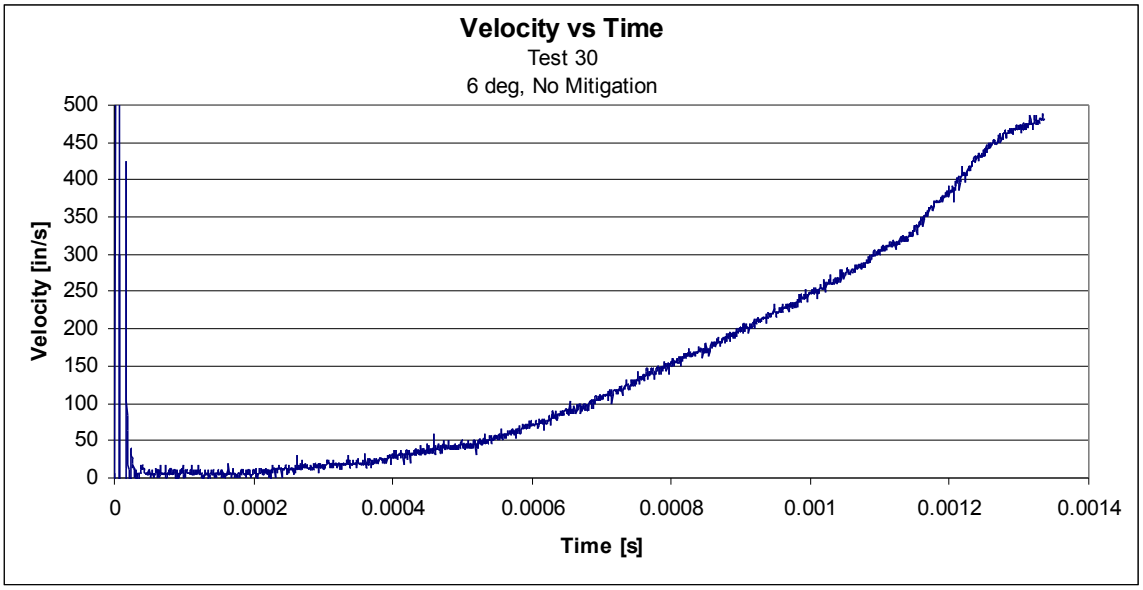

Figure A. 7: Test 30 velocity profile

SoD [in]	DoB [in]	Small Scale Acceleration [g's]	Full Scale Acceleration [g's]
3.19	0.30	2641	201

Table A.7: Test 30 conditions and acceleration

Test 31: 6 deg, 1 L Brace

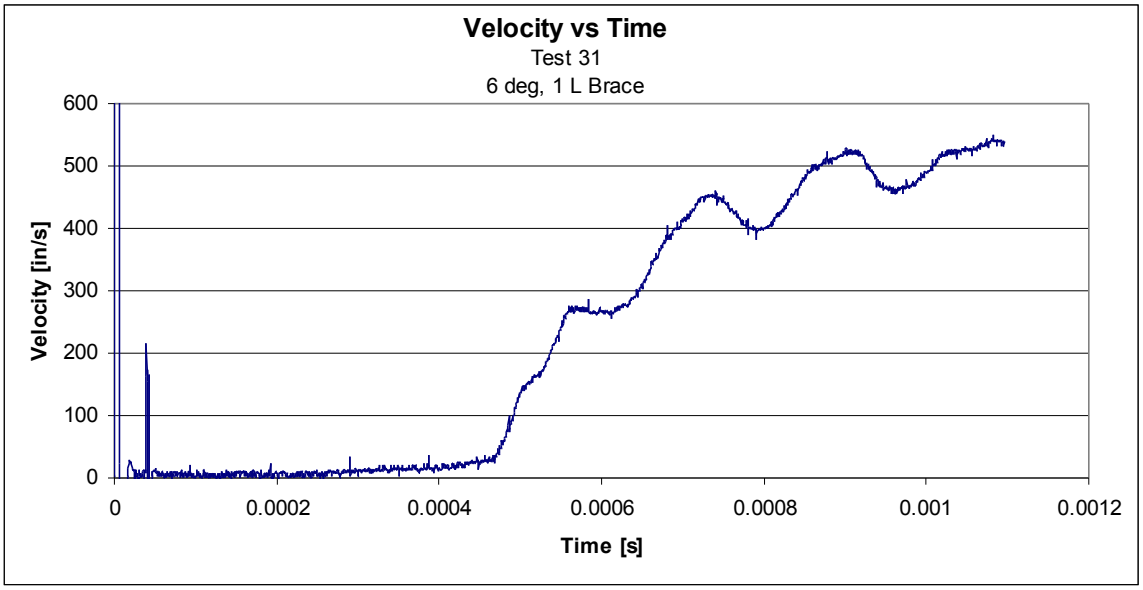

Figure A. 8: Test 31 velocity profile

SoD [in]	DoB [in]	Small Scale Acceleration [g's]	Full Scale Acceleration [g's]
3.19	0.30	7926	603

Table A.8: Test 31 conditions and acceleration

Test 32: 6 deg, 2 ll L Braces

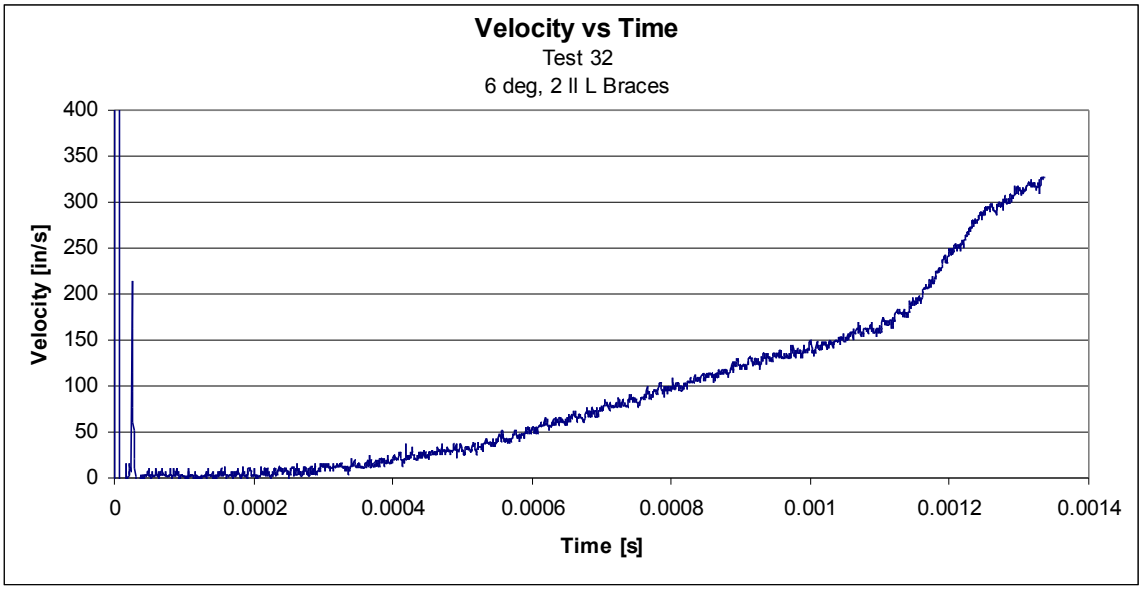

Figure A.9: Test 32 velocity profile

SoD [in]	DoB [in]	Small Scale Acceleration [g's]	Full Scale Acceleration [g's]
3.19	0.30	584 (before hull hits)	44
		2651	202

Table A.9: Test 32 conditions and acceleration

Table A.10 records two accelerations for Test 32. The first is from the less steep region in the graph above, the second is from the steeper region. The steep region occurs when the either the floorboard or braces were hit by the hull. Examination of the floorboard and braces show that they were both hit during the test, but it is unclear which one was hit first, causing the steep region. The higher acceleration is recorded in the text.

Test 39: 6 deg, Foam Gapped

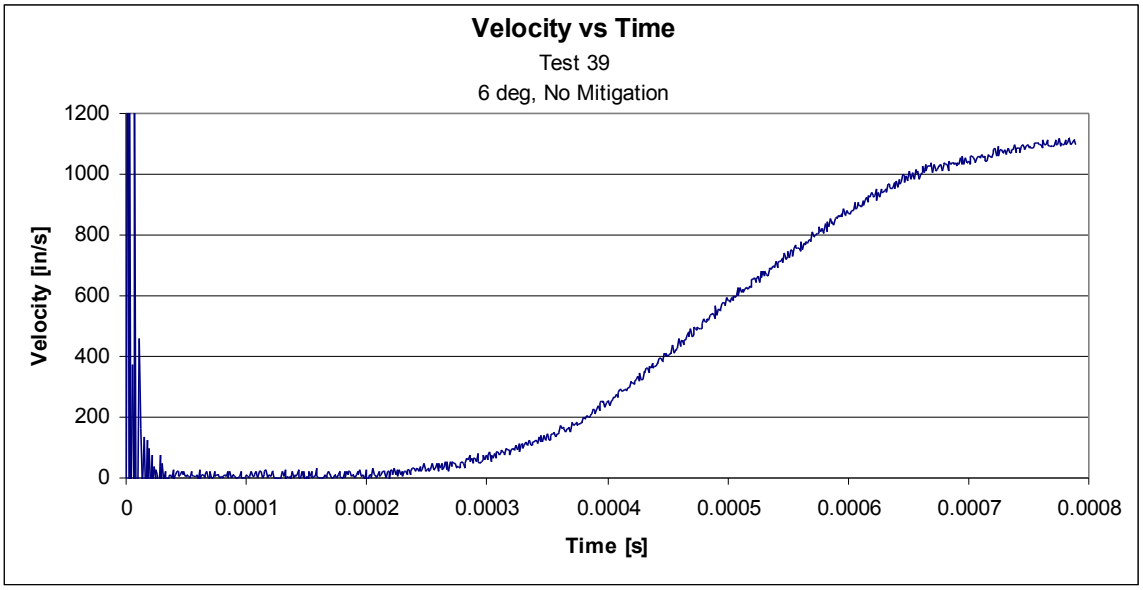

Figure A. 10: Test 39 velocity profile

SoD [in]	DoB [in]	Small Scale Acceleration [g's]	Full Scale Acceleration [g's]
3.19	0.30	8314	633

Table A.10: Test 39 conditions and acceleration

Test 36: 6 deg, 1 L Brace, Foam Filled

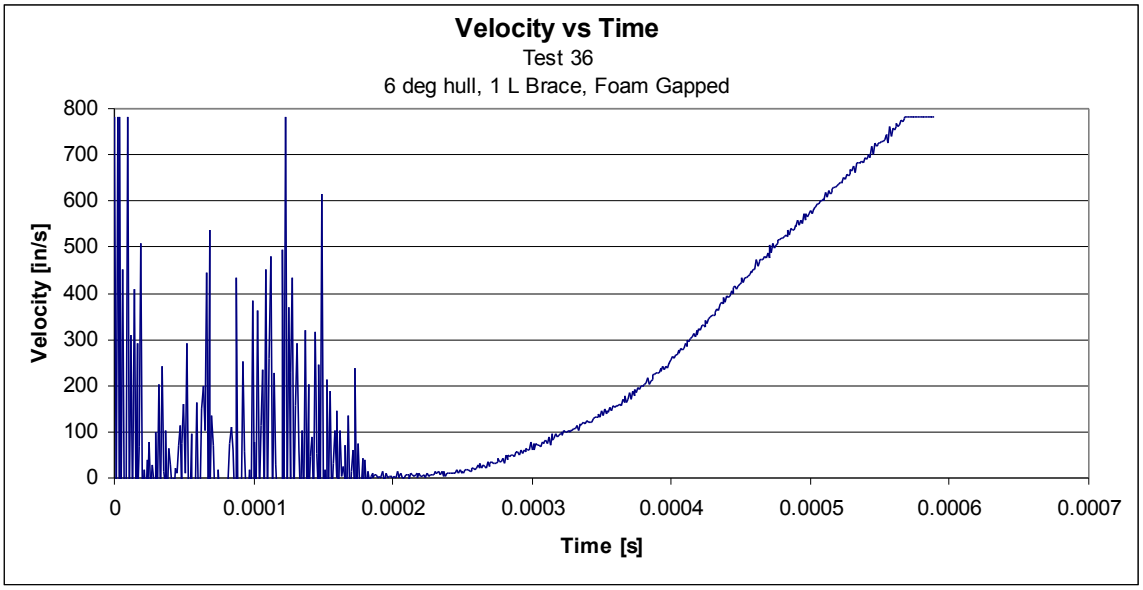

Figure A. 11: Test 36 velocity profile

SoD [in]	DoB [in]	Small Scale Acceleration [g's]	Full Scale Acceleration [g's]
3.19	0.30	8188	623

Table A.11: Test 36 conditions and acceleration

Test 38: 6 deg, Foam Frame

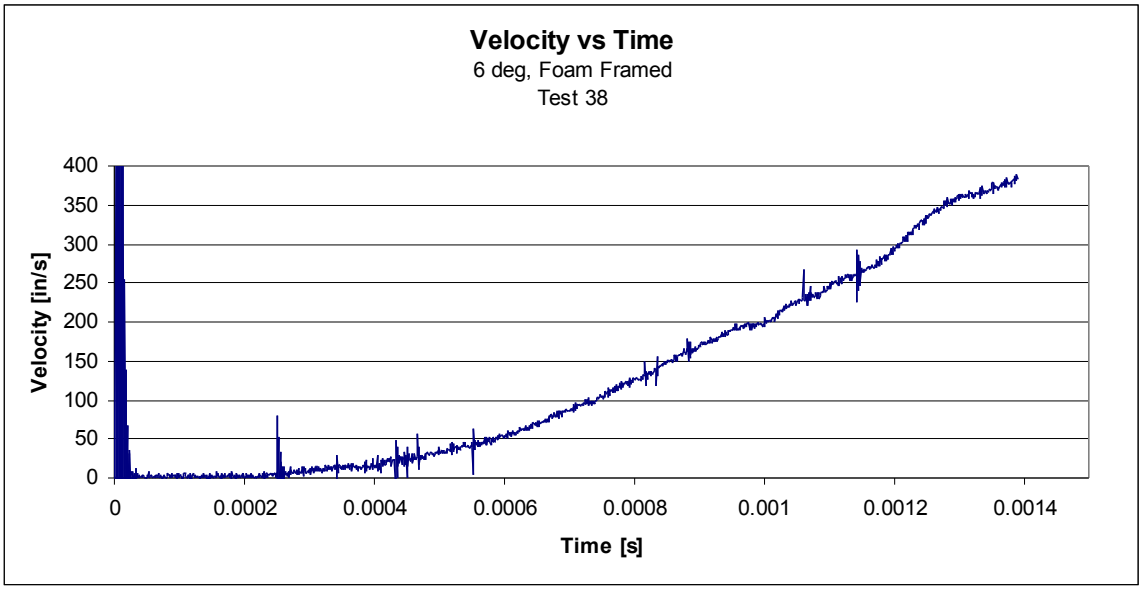

Figure A. 12: Test 38 velocity profile

SoD [in]	DoB [in]	Small Scale Acceleration [g's]	Full Scale Acceleration [g's]
3.19	0.30	1835	140

Table A.12: Test 38 conditions and acceleration

Test 14: 13 deg, No Mitigation

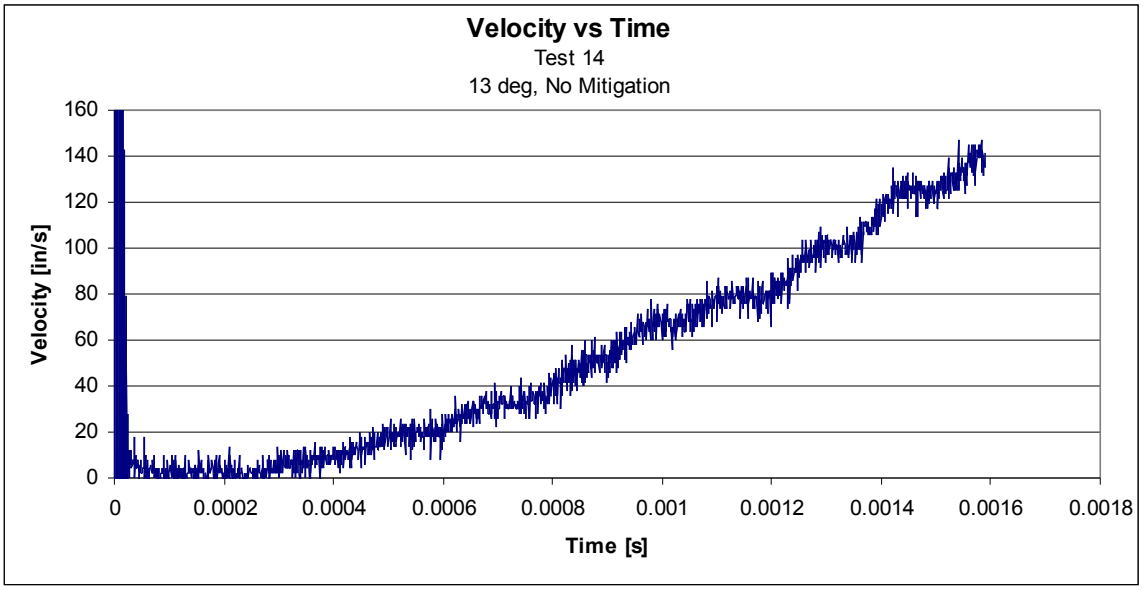

Figure A. 13: Test 14 velocity profile

SoD [in]	DoB [in]	Small Scale Acceleration [g's]	Full Scale Acceleration [g's]
3.19	0.30	384	29

Table A.13: Test 14 conditions and acceleration

Test 40: 13 deg, No Mitigation

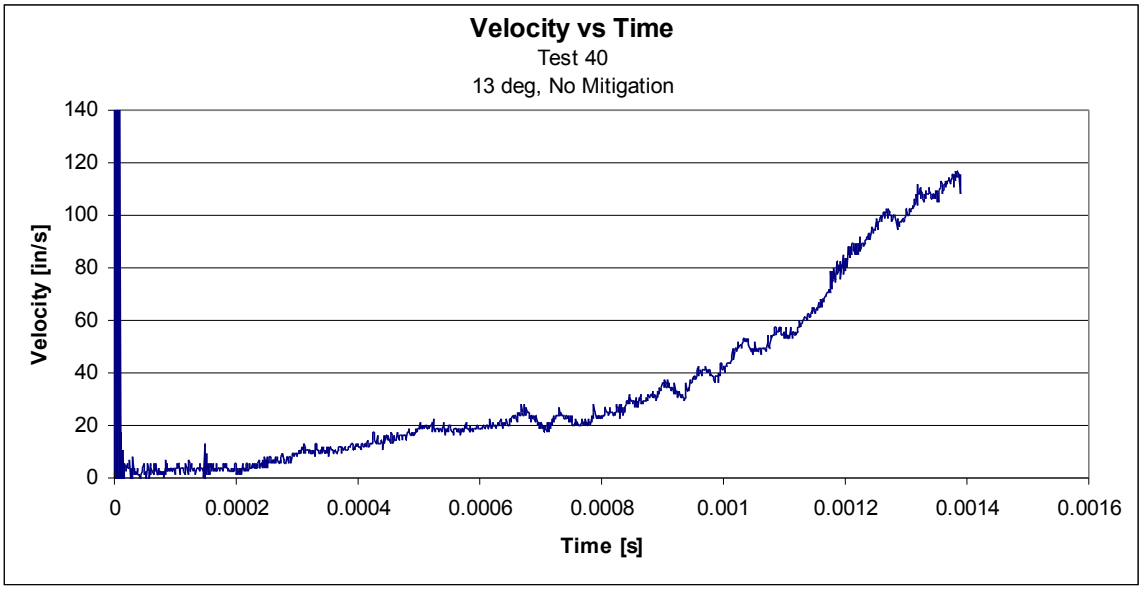

Figure A. 14: Test 40 velocity profile

SoD [in]	DoB [in]	Small Scale Acceleration [g's]	Full Scale Acceleration [g's]
3.19	0.30	1037	79

Table A.14: Test 40 conditions and acceleration

Test 37: 13 deg, 1 L Brace

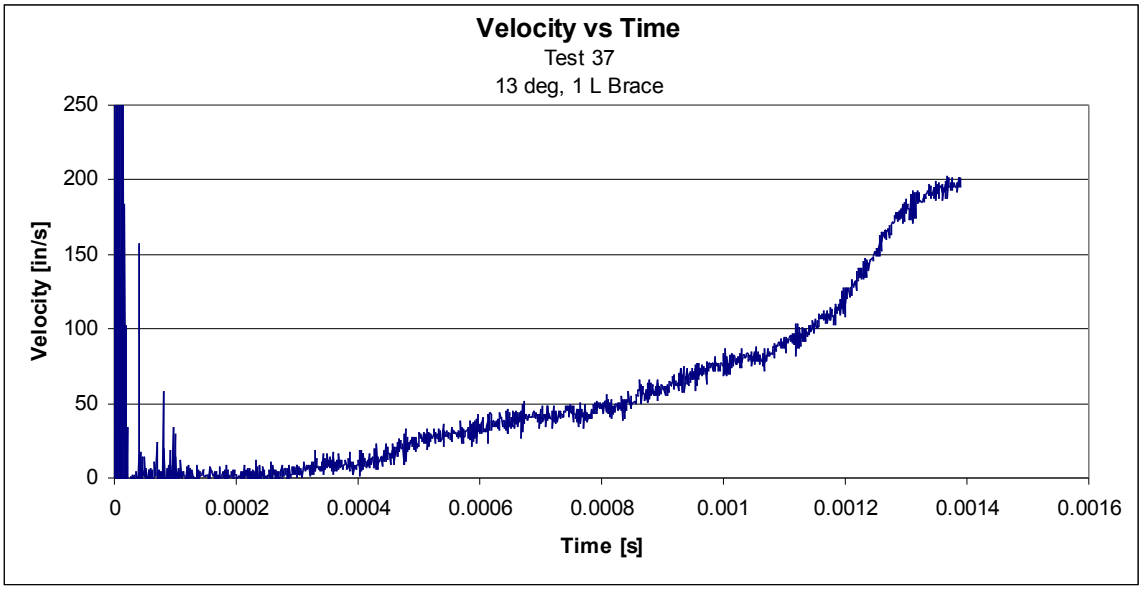

Figure A. 15: Test 37 velocity profile

SoD [in]	DoB [in]	Small Scale Acceleration [g's]	Full Scale Acceleration [g's]
3.19	0.30	1625	124

Table A.15: Test 37 conditions and acceleration

Test 18: 13 deg, 2 ll L Braces

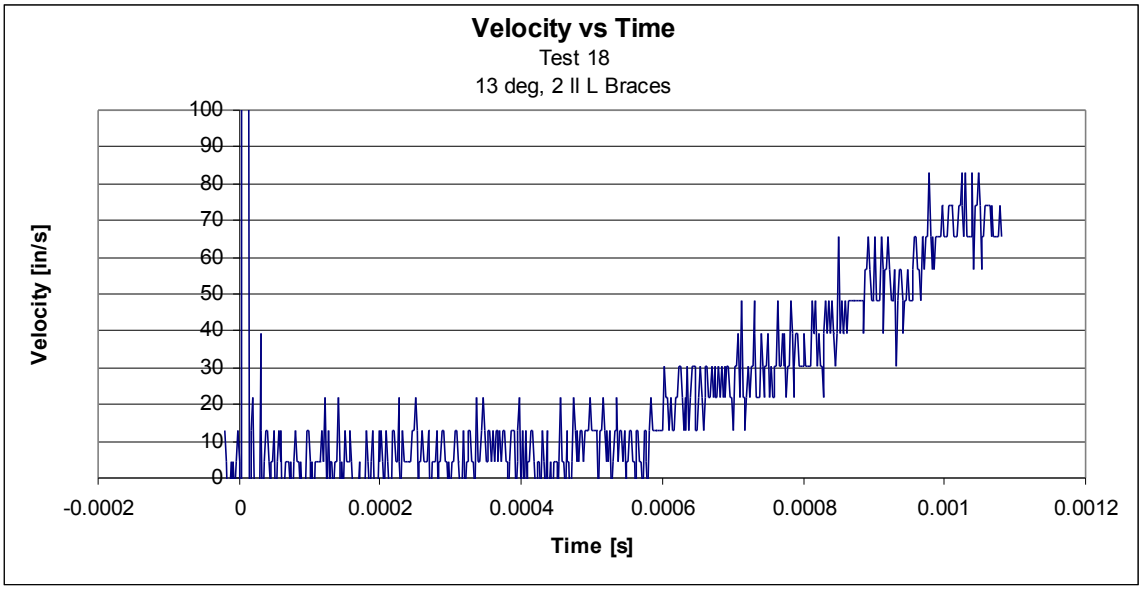

Figure A. 16: Test 18 velocity profile

SoD [in]	DoB [in]	Small Scale Acceleration [g's]	Full Scale Acceleration [g's]
3.19	0.30	292	22

Table A.16: Test 18 conditions and acceleration

Test 21: 13 deg, 2 x L Braces

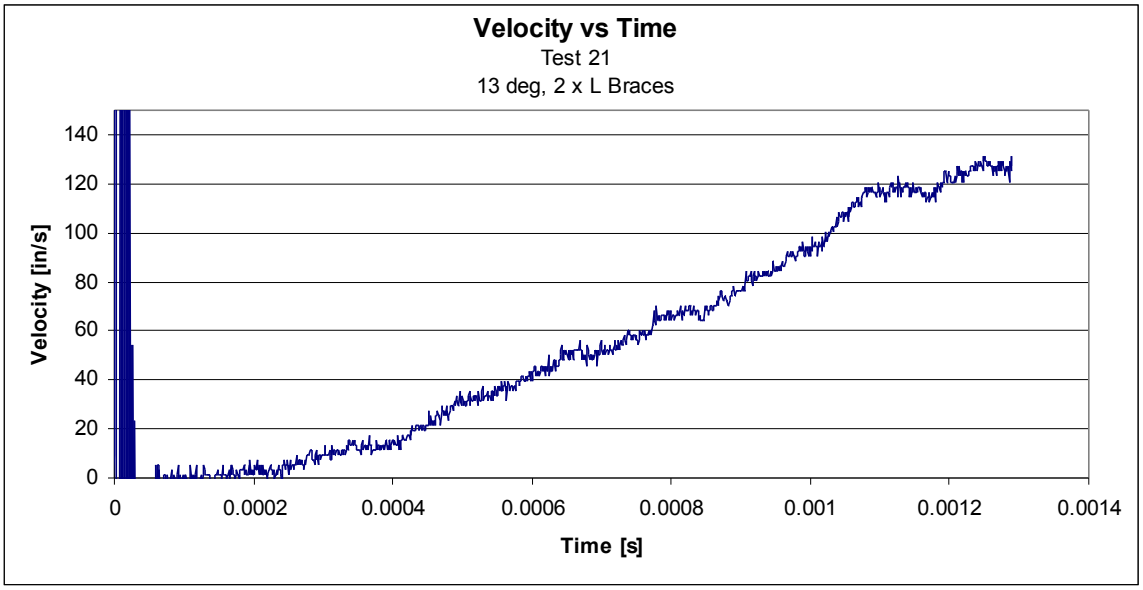

Figure A. 17: Test 21 velocity profile

SoD [in]	DoB [in]	Small Scale Acceleration [g's]	Full Scale Acceleration [g's]
3.19	0.30	813	62

Table A.17: Test 21 conditions and acceleration

Test 15: 13 deg, 1 U Brace

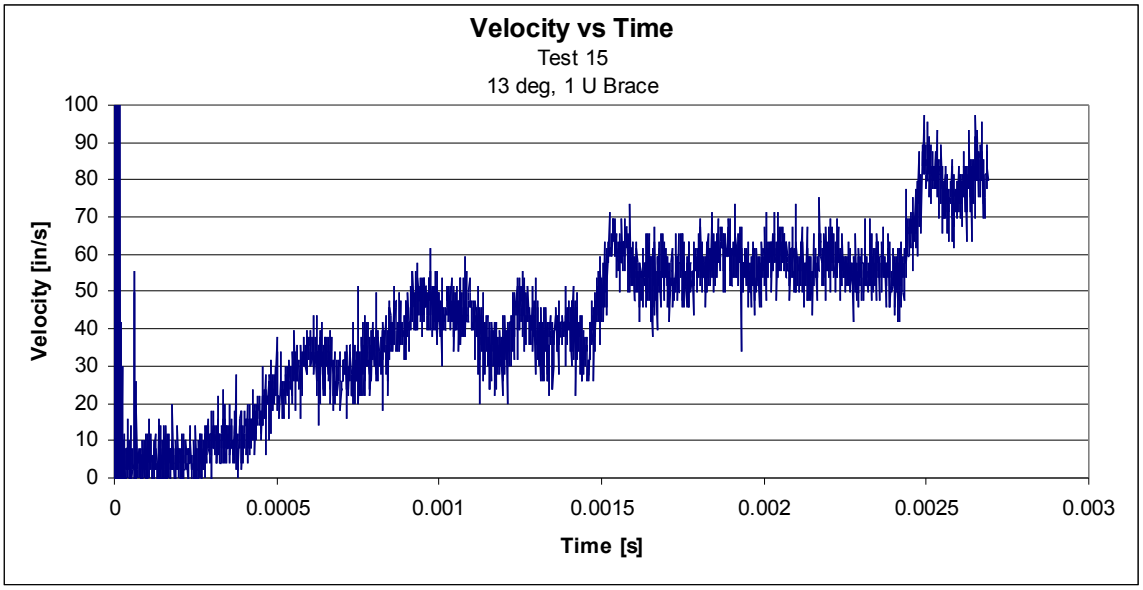

Figure A. 18: Test 15 velocity profile

SoD [in]	DoB [in]	Small Scale Acceleration [g's]	Full Scale Acceleration [g's]
3.19	0.30	63	5

Table A.18: Test 15 conditions and acceleration

Test 27: 20 deg, No Mitigation

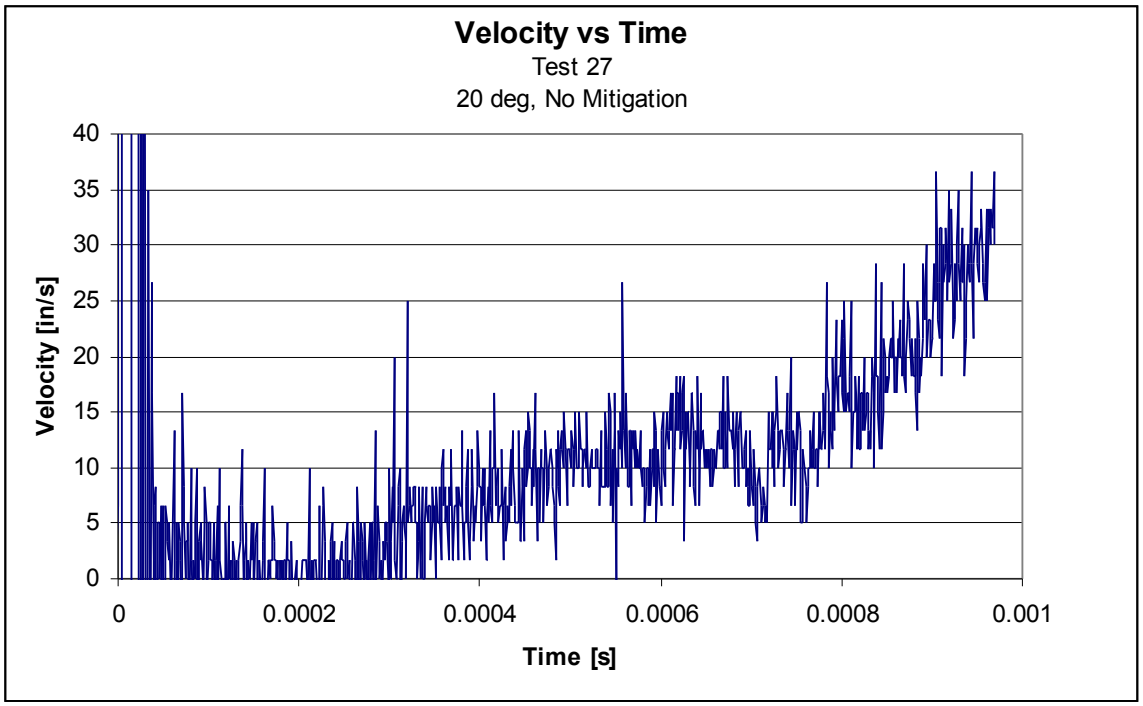

Figure A. 19: Test 27 velocity profile

SoD [in]	DoB [in]	Small Scale Acceleration [g's]	Full Scale Acceleration [g's]
3.19	0.30	721	55

Table A.19: Test 27 conditions and acceleration

Test 28: 20 deg, No Mitigation

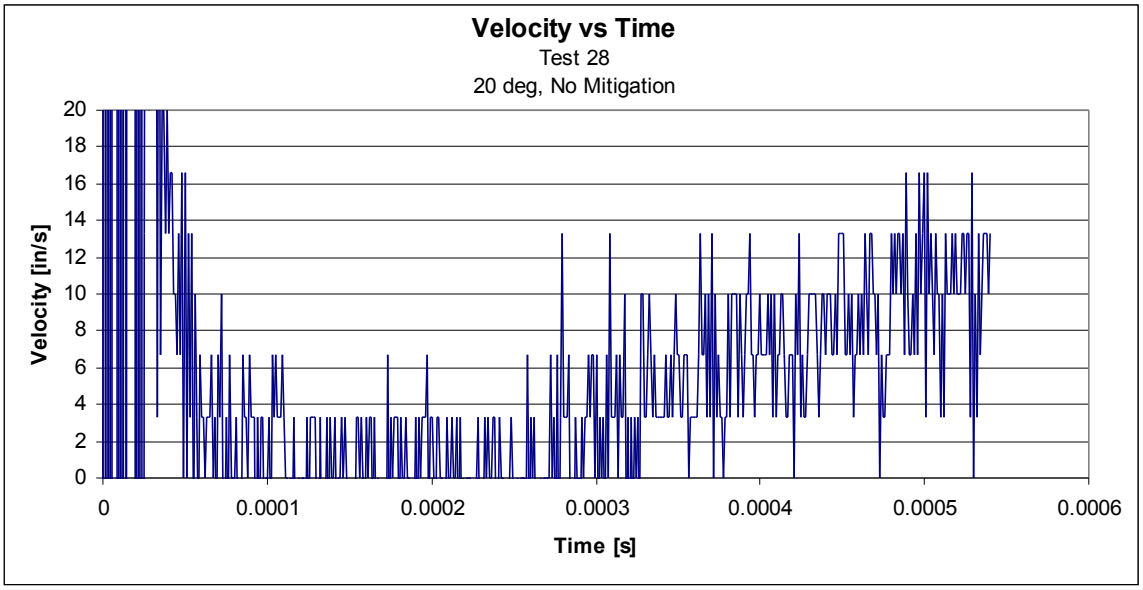

Figure A. 20: Test 28 velocity profile

SoD [in]	DoB [in]	Small Scale Acceleration [g's]	Full Scale Acceleration [g's]
3.19	0.30	414	32

Table A.20: Test 28 conditions and acceleration

Test 33: 20 deg, 1 L Brace

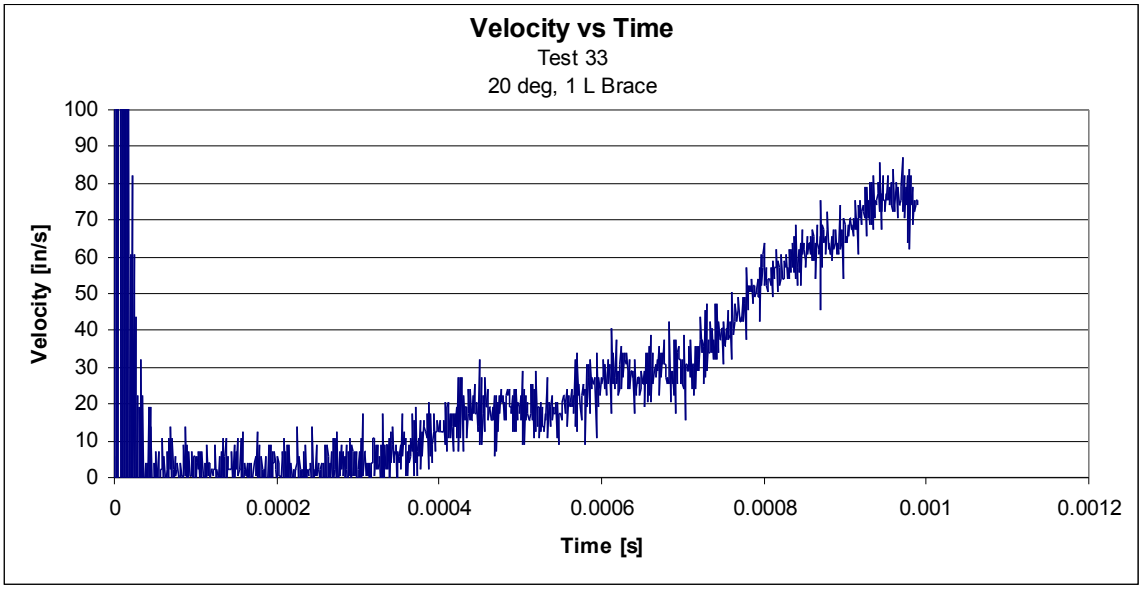

Figure A. 21: Test 33 velocity profile

SoD [in]	DoB [in]	Small Scale Acceleration [g's]	Full Scale Acceleration [g's]
3.19	0.30	449	34

Table A.21: Test 33 conditions and acceleration

Test 35: 20 deg, 2 ll L Braces

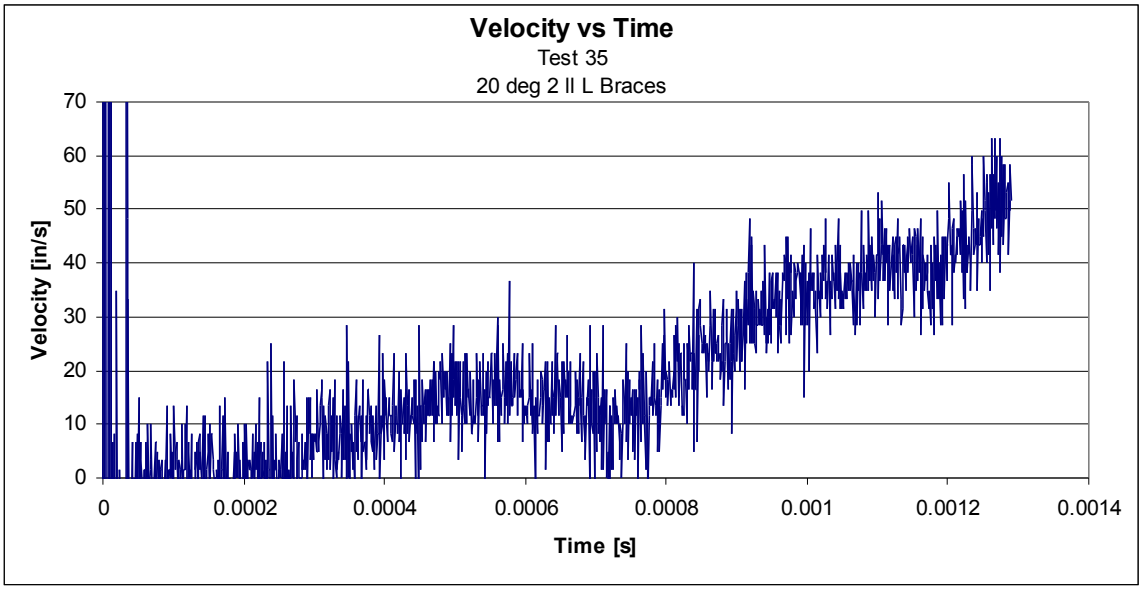

Figure A. 22: Test 35 velocity profile

SoD [in]	DoB [in]	Small Scale Acceleration [g's]	Full Scale Acceleration [g's]
3.19	0.30	274	21

Table A.22: Test 35 conditions and acceleration

Test 12: No Hull, 1.75 in SoD

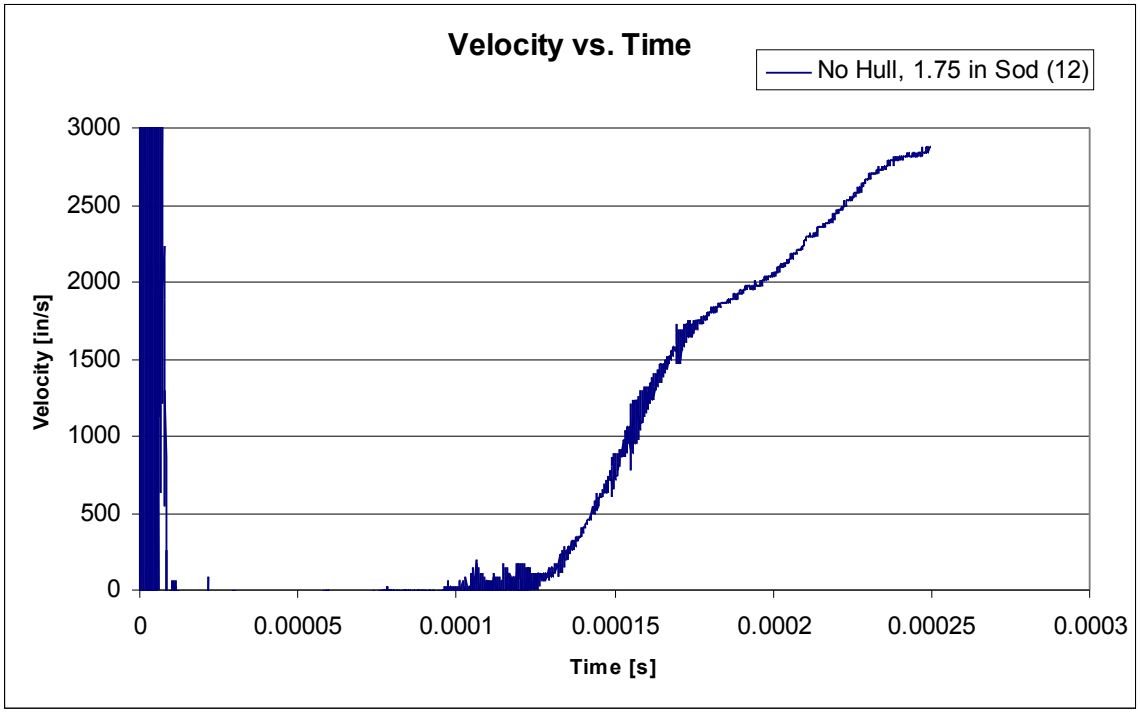

Figure A. 23: Test 12 Velocity Profile

SoD [in]	DoB [in]	Small Scale Acceleration [g's]	Full Scale Acceleration [g's]
1.75	0.30	59465	4526

Table A.23: Test 12 conditions and acceleration

Test 11: 0 deg Hull, 1.75 in SoD

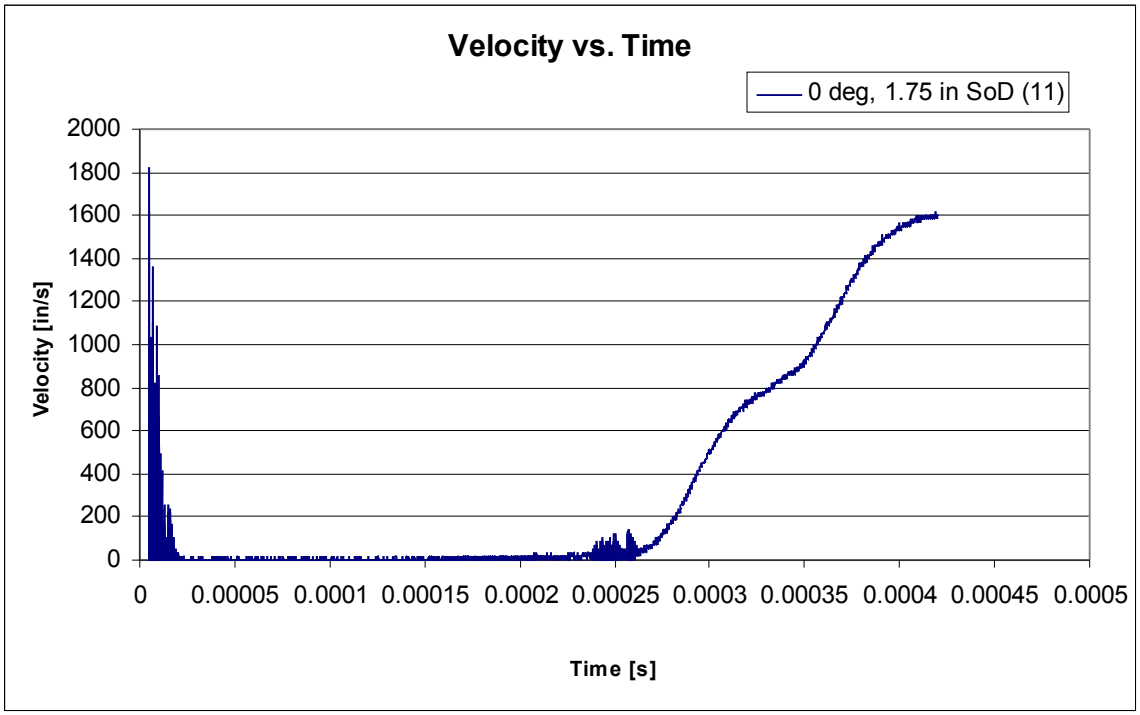

Figure A. 24: Test 11 velocity profile

SoD [in]	DoB [in]	Small Scale Acceleration [g's]	Full Scale Acceleration [g's]
1.75	0.30	49590	3774

Table A.24: Test 11 conditions and acceleration

Test 44: No Hull, 2.55 in SoD

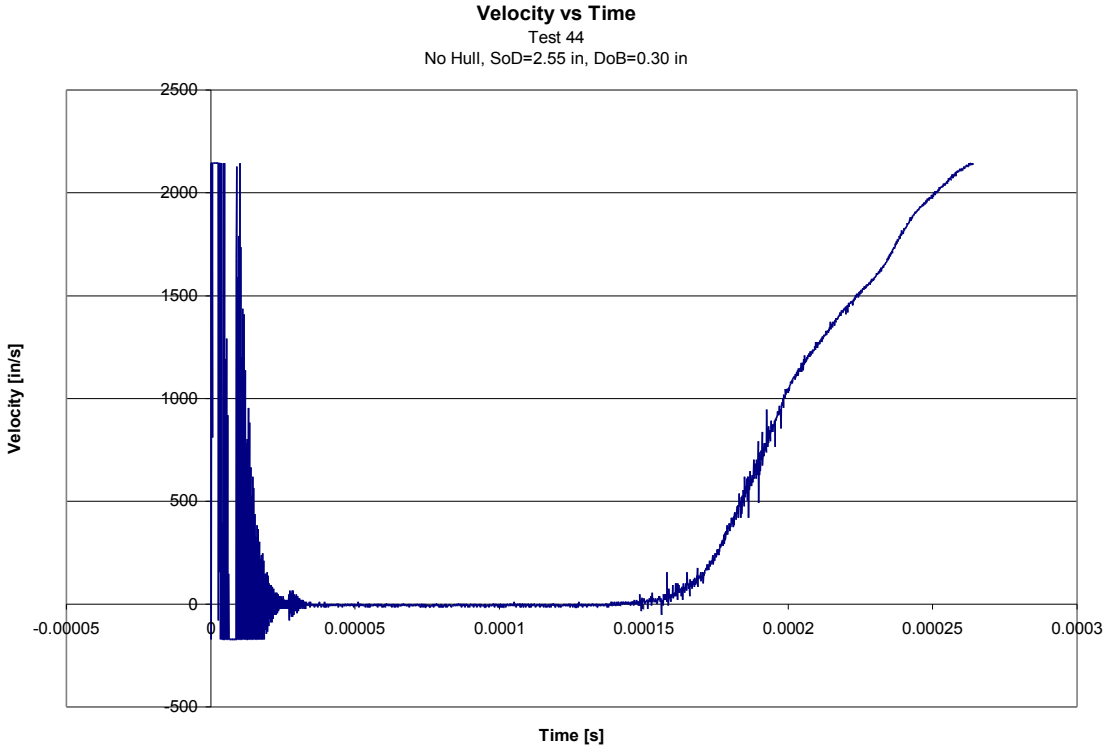

Figure A. 25: Test 44 Velocity Profile

SoD [in]	DoB [in]	Small Scale Acceleration [g's]	Full Scale Acceleration [g's]
2.55	0.30	88146	6708

Table A.25: Test 44 conditions and acceleration

Test 43: 0 deg Hull, 2.55 in SoD

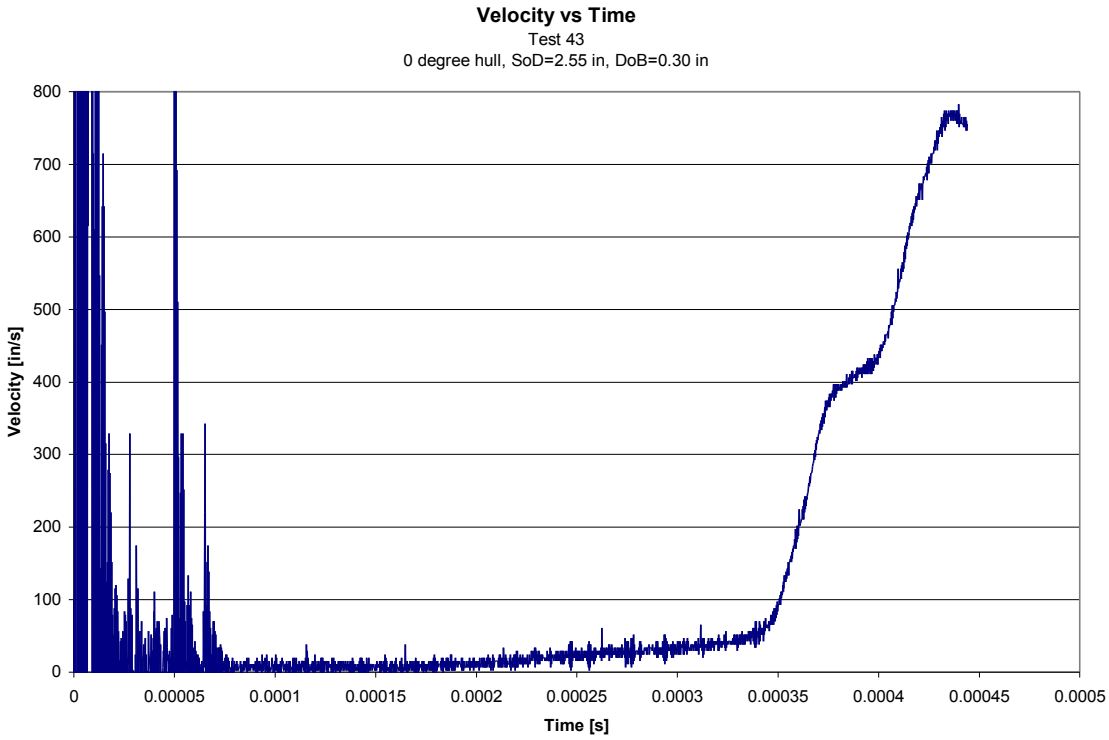

Figure A.26: Test 43 velocity profile in time

SoD [in]	DoB [in]	Small Scale Acceleration [g's]	Full Scale Acceleration [g's]
2.55	0.30	30551	2325

Table A.26: Test 43 conditions and acceleration

Appendix B: Phantom Camera Specifications

v7.2
Specifications

phantom

Features

Auto exposure
"EDR" Extreme Dynamic Range™
High-g configuration
Optional Continuous data streaming to 2,000pps
Range data input
Continuous recording
Pre-trigger recording
Post-trigger recording
On chip global shuttering
Strobe sync
Segmented image memory
Continuous color video output
IRIG-B timing capture with phase shift
10/100/Gigabit Ethernet

Sensor: 800 x 600 pixel SR-CMOS monochrome, or 24 bit color array

Sensitivity: 4800 ISO/ASA monochrome, 1200 ISO/ASA color

Pictures per Second (pps): Full sensor resolution: to 6,688pps

Allocated formats: to 190,476pps with "CAR" (Continuously Adjustable Resolution) feature

Exposure Time: Variable, independent of sample rate (pps), to 2 microsecond (1 microsecond sec. option)

Trigger: Continuously variable pre/post

Imager Control: 10/100/Gigabit Ethernet, or RS232 serial interface

Preview and Focusing: Via computer monitor or continuous video out

Lens Mounts: Nikon mount standard. Many other lens mounts available, including C-mount

Inputs/Outputs: (via integrated quick-release connector):

Trigger: Rising/falling TTL pulse w/filter, or switch closure

Sync Image: TTL pulse

Event Marker: TTL pulse or switch closure

Ready Signal: TTL pulse

IRIG-B Timing: IRIG-B code, modulated or unmodulated input, with IRIG-B output, lock, and variable phase shift

Range Data Input

Strobe Sync: TTL pulse

RS232

Network: 10/100/Gigabit Ethernet

Video out: NTSC, or PAL

Power: 24VDC/1.5 Amp

MEMORY

Standard: 1024 Megabytes integral image memory. Records 2,210 images for .35 second of continuous recording at 6,688pps, full format. Longer recording times for lower sample rates and allocated formats. (example: 22.1 seconds at 100pps)

Optional: 2048 Megabyte integral image memory continuously records 4,421 images (.7 sec.) at 6,688pps full frame, and the 8192 Megabyte option will record 17,684 full frame images (2.8 sec.) at 6,688pps full frame.

Optional: Non-Volatile Flash Memory, up to 6 GB.

ENVIRONMENTAL

100g up to 10 millisecond
50g up to 100 millisecond
Three axis

SOFTWARE

Phantom® operates in a Windows™ environment with familiar commands found in familiar places. Standard functions include:

Acquisition: Image capture, IRIG-B timing capture & standard time annotation. Field of view & focus. Sample rate & aspect ratio selection. Shutter speed. Histogram. Brightness & contrast, gamma adjust. Trigger modes. Continuous record. Save & recall setups.

Analytical playback: Immediate playback of ciné. Variable playback speeds in forward or reverse, including freeze frame & endless loop. Random Go-to-Image. View single images at random from any ciné. Tile/cascade multiple images on one screen. Timing data displayed with each image. Ciné editor. Multi Ciné Viewer.

Measurements: Linear or angular measurements. Displacement. Velocity. RPMs. 100 data points per image. English and metric units. Generate measurement reports. Report files & images are compatible with spread sheet software, and image analysis software such as TrackEye®, Image Express®, or Falcon®.

Image processing: Smooth, sharpen, pseudocolor, negative image, and edge detection. Brightness, contrast & gamma adjust. 3x3 and 5x5 filter matrix for custom image processing.

File management: Organize, save, compress and export cinés, or single images. File formats are compatible with most word processing, desktop publishing, and presentation software.

DIMENSIONS

Size: 4.3 x 4.0 x 9.5 inch (HWD) (12.5 x 11 x 25 cm) (HWD)

Weight: 7 lbs (3.2kg)

Power: 24VDC/ 1.5Amp

Mounting: 1/4-20 inch and four 10-32 threaded hole pattern in base and top

Mounting Axis: Any position

Material & Finish: Machined aluminum housing, powder coat finish

Country of Origin: The United States of America

STANDARD ACCESSORIES

Phantom® software. Single user license*

1024 Megabyte integral image memory*

Ethernet. Sync output pulse, trigger, pretrigger, video out, and IRIG-B

110/220VAC-28VDC International Power Adapter. 12 foot (3.7 m) power cord

One year warranty.

QUESTIONS?

For technical assistance, systems integration, custom options, or information on imaging techniques, please call us toll free:

1 .800.RESOLUTION

(USA & Canada 1.800.737.6588)

For the most up-to-date information, specifications and options, please visit our website:
www.visionresearch.com

vision
research

Specifications and features subject to change without notice.

*(*Other options available.) Phantom is manufactured in the USA under US patent Number 5625412 and patents pending. Phantom®, EDR®, and Memory Gate® are registered trademark of Vision Research Inc. Windows™ and the Windows logo are trademarks of MicroSoft Corporation.*

Vision Research, Inc. • 100 Dey Road • Wayne, New Jersey 07470 USA • (973) 696-4500 Fax (973) 696-0560

Figure B. 1: Phantom V7.2 Specifications [B.1]

References

[1.1] "Global War on Terrorism by Reason," United States Department of Defense. <http://siadapp.dmdc.osd.mil/personnel/CASUALTY/gwot_reason.pdf>, accessed April 29, 2008.

[1.2] Chabai, Albert J. "On Scaling Dimensions of Craters Produced by Buried Explosives." Journal of Geophysical Research Vol. 70, No. 20. October 1965.

[1.3] Fu, Raymond, Allen Lindfors, Jeffery Davis. "Scaling for Internal Blast." AIP Conference Proceedings 2004, Vol. 706 Issue 1, p1440-1443.

[1.4] Baker, W.E. Similarity Methods in Engineering Dynamics: Theory and Practice of Scale Modeling, Rev. Ed., Elsevier. 1991.

[1.5] Taylor, L.C., R.R. Skaggs, W. Gault. "Vertical Impulse Measurements of Mines Buried in Saturated Sand." Fragblast, Vol. 9, No. 1, March 2005.

[1.7] Fourney, W.L., U. Leiste, R. Bonenberger, D. Goodings. "Explosive impulse on plates." Fragblast Vol. 9, No. 1, March 2005.

[1.8] Bretall, Damien. "Inverse Hybrid Method for Determining Explosive Loading on Plates Due to Buried Mines." M.S. Thesis, University of Maryland, 2007.

[1.9] Fourney, W.L., U. Leiste, R. Bonenberger, D. Goodings. "Mechanism of Loading on Plates Due to Explosive Detonation." Fragblast, Vol. 9, No.4. December 2005.

[2.1] "RP-87 EBW Detonator." Teledyne Technologies, Inc. <http://www.teledynerisi.com/products/0products_1ebw_page27.asp>, accessed Feb 25, 2008.

[2.2] "FS-17 Firing System." Teledyne Technologies, Inc. <http://www.teledynerisi.com/products/0products_2fs_page49.asp>, accessed Feb 25, 2008.

[2.3] Perls, Thomas A. and Erich Buchmann. "A Bar-Magnet Velocity Meter." The Review of Scientific Instruments, Vol. 22, No. 7. July 1951.

[2.4] " North Star Light with Clamp Base." Vision Research. <http://visionresearch.com/store/index.cfm?fuseaction=product.display&product_ID=4>, accessed Feb 26, 2008.

[4.1] Genson, Kevin. "Vehicle Shaping for Blast Damage Reduction." M.S. Thesis, University of Maryland, 2006.

[6.1] Reitz, John R., Frederick J. Milford, Robert W. Christy. "Foundations of Electromagnetic Theory." Addison-Wesley Publishing Company, 1980.

[B.1] "V7.1Spec." Vision Research, Inc. <http://www.visionresearch.com/uploads/docs/Discontinued/V7/v7.1spec.pdf>, Accessed 22 May 2008